



University of  
Stavanger

Faculty of Science and Technology

## BACHELOR'S THESIS

Study program/Specialization:  Chemistry and environmental engineering/Chemistry	Spring semester, 2021  <u>Open</u> / Restricted access
Writer: Camilla Undheim	<i>Camilla Undheim</i> ..... (Writer's signature)
Faculty supervisor: Malcolm A. Kelland  External supervisor(s):	
Thesis title:  An established manual for corrosion testing and corrosion inhibitor analysis	
Credits (ECTS): 20	
Key words:  Manual, assembly, corrosion, corrosion inhibitor, bubble testing, LPR measurement, corrosion rate, inhibition efficiency	Pages: ..113.....  + enclosure: .....  Stavanger, ..15/6-21.... Date/year



# AN ESTABLISHED MANUAL FOR CORROSION TESTING AND CORROSION INHIBITOR ANALYSIS

BUBBLE TESTING AND LINEAR POLARIZATION RESISTANCE MEASUREMENT

Bachelor's Thesis by Camilla Undheim

Faculty of Science and Technology  
Department of Chemistry, Bioscience and Environmental Engineering

# TABLE OF CONTENTS

ACKNOWLEDGEMENT .....	5
ABSTRACT .....	6
Chapter 1 – Introduction .....	7
1.1 – Corrosion in the Oil and Gas industry .....	7
1.2 – Corrosion Management .....	9
1.2.1 – Corrosion Inhibitor .....	9
1.2.2 – Environmental risks and restrictions.....	10
1.3 – Quantitative analysis .....	11
1.3.1 – Bubble Testing Method.....	11
1.4 – Electrochemical measurement .....	12
1.4.1 – Linear Polarization Resistance measurement .....	13
Chapter 2 – Assemble the Gamry Instruments Multiport Electrochemical Cell Kit and performing LPR measurement with the Gamry Framework.....	18
2.1 – Equipment and Assembly.....	19
2.1.1 – The Main Cell.....	21
2.1.2 – The Reference Bridge Tube .....	23
2.1.3 – The Reference Electrode.....	25
2.1.4 – The Counter Electrode .....	26
2.1.5 – The Working Electrode.....	27
2.1.6 – The Gas Dispersion Tube.....	31
2.1.7 – Connection Clamps .....	34
2.2 – The Testing Sequence.....	36
2.2.1 – Input values.....	37
2.2.2 – During testing.....	43
2.2.3 – Output values/Experimental results .....	45
2.3 – Troubleshooting .....	55

2.3.1 – Leakage in Working Electrode.....	55
2.3.2 – Overload Errors .....	55
2.3.3 – Rust deposits on Connection Clamps.....	56
2.3.4 – Choosing “vs. E <sub>ref</sub> ”.....	57
2.3.5 – Clogging of the Glass Frit Tip.....	57
2.3.6 – Damaged Metal Sample .....	58
2.3.7 – Bubble accumulation .....	60
Chapter 3 – Methods and procedures .....	62
3.1 – Selected Parameters and conditions.....	62
3.1.1 – Testing Sequence .....	62
3.1.2 – Stirring.....	63
3.1.3 – Gas Flow .....	63
3.1.4 – Parameters Input values and Methods used .....	63
3.1.5 – Metal Sample .....	64
3.1.6 – Brine Solution.....	64
3.1.7 – Hydrocarbon Mix.....	65
3.1.8 – Corrosion Inhibitor .....	65
3.2 – Experimental Procedures .....	68
3.2.1 – Brine .....	68
3.2.2 – Brine with added CO <sub>2</sub> gas.....	70
3.2.3 – Brine with added CO <sub>2</sub> gas and Corrosion Inhibitor .....	74
Chapter 4 – Experimental Results and discussion.....	78
4.1 – Experimental Results.....	79
4.1.1 – Corrosion Rate.....	79
4.1.2 – Inhibition Efficiency.....	81
4.1.3 – Effect of adding Hydrocarbon Mix .....	84
4.1.4 – Effect of adding Oxygen Scavenger.....	85

4.1.5 – Effect of adding CO <sub>2</sub> gas.....	87
4.1.6 – Leak Observation.....	88
4.3 – Overall Discussion .....	90
Chapter 5 – conclusion and further recommendations .....	93
5.1 – Conclusion .....	93
5.2 – Further Recommendations .....	93
References.....	95
Appendix A – Detailed data results, Blank Testing.....	99
Appendix B – Detailed data results, CI’s Testing .....	103
Appendix C – Additional Pictures .....	109

## ACKNOWLEDGEMENT

As a high amount of my interest and previous experience comes from working as a service mechanic on subsea equipment in the Oil and Gas industry, it was early in the start of my bachelor's degree that I was determined to continue on this pathway and combining it with another deep interest: inorganic chemistry. This thesis can be considered as a final endpoint in completing my bachelor's degree in chemical and environmental engineering in 2021.

One of my first lectures I attended at the University of Stavanger was lectured by Professor Malcolm Andrew Kelland. Because of his good teaching methods presented in that course and broad experience, I had a hope that he would be able to be my supervisor when I was going to take on my bachelor thesis. I would like to give him a big thank you for making this possible, and for being a very good supervisor with thorough guidance and support.

I would also provide a thank you to my co-supervisor Tor Hemmingsen for supplying with the testing equipment used in this thesis and necessary information.

Furthermore, I would like to thank Utsav Raj Dotel for making time to teach me about the equipment and testing procedures used through this thesis and for being available for questions when they presented themselves.

In addition, I would like to thank Sumit Ganguly, Erik Dirdal and Radhakanta Ghosh for being available for consult and providing with advises through my time at the laboratory at UiS.

Lastly, I would like to thank my love Ole and my sister Randi for the endless amount of support, consults and huge amount of help in many different situations.

## ABSTRACT

In the Oil and Gas industry the risk arising because of corrosion is very well known. As harsh conditions present themselves on the equipment on the rigs, the conditions from the reservoirs and up into the pipe production lines presents can be even harsher. As the search for new reservoirs is moving towards more challenging regions, reservoirs classified as High Pressure and/or High Temperature (HTHP) are frequently encountered, bringing with them a numerous amount of risks and challenges [1], [2]. One of these challenges is the presence of CO<sub>2</sub> gas, as the chemical behaviour of this gas has been mostly depending on the pressure and temperatures of the environment it is presented in.

Since one of the chemical behaviours of CO<sub>2</sub> gas is to diffuse into water and create a weak carbonic acid, it can provide a corrosive environment for the subsea equipment and accelerate the corrosion process of the subsea equipment. Because corrosion caused by the presence of CO<sub>2</sub> in the production fluid is known for being one of the most prevalent types of corrosion induced in the Oil and Gas industry, a huge amount of time and effort has been made into the study of corrosion caused by CO<sub>2</sub>, to find the best strategy for managing or preventing it [3]–[5].

Using various testing methods and procedures researchers has come up with a range of different corrosion management strategies, such as injecting low dosage corrosion inhibitors. In order to evaluate the corrosion inhibitors, their performance and inhibition efficiency needs to be analysed.

The goal for this thesis was to establish a manual on how to perform this type of quantitative analysis for corrosion inhibitors, by using The Bubble Test method with the Gamry MultiPort Electrochemical Cell Kit and linear polarization resistance (LPR) measurement with Gamry Framework program.

The final manual presented contains in-depth explanations on how to assemble and use the equipment, perform LPR measurements and troubleshooting, experimental procedures used, and experimental data results collected.

In addition to making a manual that have an in-depth assemble procedure of the equipment and description on how to perform an LPR measurement, it was computed test procedures and methods with detailed description of preparations done.

Three corrosion inhibitors were studied through multiple individual experiments through individual LPR measurements. The measurements were performed on C1018 mild steel in the presence of 500ppm Imidazoline, Luvicap EG and an experimental corrosion inhibitor synthesised at the UIS, and the impact was compared to a blank and corrosion inhibition efficiency was calculated.

# CHAPTER 1 – INTRODUCTION

As metals are mostly obtained from ores as low energy oxides, it requires a high amount of energy to convert them to usable pure metal compounds. While much of the required energy supplied is lost to the environment as a byproduct, much of it is also absorbed and stored within metal atoms in the final metal structure. Corrosion occurs when this stored-up energy within the metal atoms is spontaneously released, making the metal atoms to convert back to its natural oxidised state [2], [6].

For corrosion to happen, 3 elemental factors needs to be present: a metallic surface, a conductive electrolyte and an electron acceptor [7]. The combination of these factors creates a potential difference to arise that serves as a driving force, with the degree of potential difference often indicating how severe the corrosion will be [8], [9]. This potential difference makes a set of electrochemical reactions known as redox reactions to be initiated simultaneously. These reactions are in general composed of two half reactions, known as oxidization and reduction half-reactions. The oxidization half-reaction causes neutral metal atoms to leave some of their negative charged electrons behind in the metal surface and diffuse into the environment as positively charged ions. The electrons left behind in the metal surface can then migrate to another part of the metal surface, where an electron acceptor undergoes a reduction reaction and thus removes the electrons from the metal surface. In general, these coupled electrochemical reactions are responsible for the corrosion, or rust, that we see in our ordinary life.

But since there exists a high variety of challenging environments, there is also a high risk of challenging corrosion problems, such as the corrosion caused by the presence of CO<sub>2</sub> gas known as “sweet corrosion” [10]. Today the challenge with “sweet corrosion” is a continuously never-ending story, with researchers working on the better combat strategies for controlling, managing, or even preventing it to happen.

## 1.1 – Corrosion in the Oil and Gas industry

In the oil and gas industry a large amount of time, effort, and costs is focused on maintaining fluid flow from the wells to the processing equipment. This is called flow assurance. In this field most of the potential risks that can take place within the offshore pipelines and subsea systems are being identified, evaluated, and managed [2]. A very important topic in the field of flow assurance is the constant and ongoing problem with corrosion, where the corrosion caused by the presence of CO<sub>2</sub> gas is one of the most prevalent corrosion issues [2], [5], [11].



As corrosion caused by dissolved CO<sub>2</sub> gas in the production fluid has been proposed to manifest itself in various of ways depending on the pressure, temperature, kinetics, and pH level in the pipelines systems, these factors combined or alone can strongly affect the degree and severeness of the CO<sub>2</sub> corrosion and may need to be crucially evaluated [12]–[14]. Also, changes in the fluid composition such as gas-oil ratio (GOR), addition to that the production fluid is mostly composing of hydrocarbons, seawater (brine), hydrogen sulphide (H<sub>2</sub>S), carbon dioxide (CO<sub>2</sub>), can alone or together contribute differently under each factors presented [2], [15].

While gasses are normally getting more soluble with increasing pressure, there has been suggestions that an increase in temperature and salt concentrations can contribute to an overall decrease in the CO<sub>2</sub> gas solubility [16], [17].

Dry CO<sub>2</sub> gas alone does not make corrosion to occur, but when the CO<sub>2</sub> gas get dissolved into the brine water it interacts with water molecules through multiple reactions and produces a weak carbonic acid. This makes the pH level to decrease to a more acidic region at around 4-5, which creates a more corrosive environment and speed up the corrosion process [2], [3], [9], [18].

The production of carbonic acid and how it affects the corrosion of iron can be described through the following general reactions [12], [14], [19]:

- 1)  $\text{CO}_{2(g)} \rightarrow \text{CO}_{2(aq)}$
- 2)  $\text{CO}_{2(aq)} + \text{H}_2\text{O}_{(l)} \leftrightarrow \text{HCO}_3^-(aq) + \text{H}^+(aq)$
- 3)  $\text{HCO}_3^-(aq) + \text{H}^+(aq) \leftrightarrow \text{H}_2\text{CO}_{3(aq)}$
- 4)  $\text{H}_2\text{CO}_{3(aq)} \leftrightarrow 2\text{H}^+(aq) + \text{CO}_3^{2-}(aq)$

With the oxidisation of iron at the anodal site and reduce the hydronium ions on the cathodal site trough the following reactions [14]:



This reflects only a small portion of the challenging situations towards evaluating, estimating, and determining how severe the corrosion may be and what type of corrosion is most likely to occur. A general categorization of the types corrosion to occur is uniform corrosion or localized corrosion: with localized corrosion being pitting-/crevice corrosion, galvanic corrosion, stress cracking corrosion, intergranular corrosion (SCC), microbially influenced corrosion (MIC), erosion corrosion, and hydrogen embrittlement [13], [14].

## 1.2 – Corrosion Management

In order to understand how CO<sub>2</sub> corrosion appears and what can be done to manage or prevent it, several different testing equipment's and techniques have been used [13], [14].

By using trustworthy testing equipment and procedures to simulate the environmental conditions as close to real conditions as possible, researchers have come up with a range of strategies for corrosion management. This includes cathodic protection, using corrosion resistant alloys, water removal, or using corrosion inhibitors [13], [14], [20].

### 1.2.1 – Corrosion Inhibitor

Since the usage of low-dose corrosion inhibitors has been determined to be a highly effective corrosion management strategy when it comes to combatting CO<sub>2</sub> corrosion, it has been a high priority for many researchers to develop new inhibitors, optimize their system performance and make them as green as possible [3], [11].

The corrosion inhibitor compounds can be arranged into groups based on their corrosion inhibition combat strategies, such as anodic, cathodic passivating, neutralizing and active, vapor phase and film forming [12]. The film-forming corrosion inhibitor (FFCI) is mostly the type being used when protection of oil and gas production lines is necessary [3], [13], [14], [21].

The FFCI's can function as a surface-active chemical commonly called surfactant, which means that they can interact with a metal surface through selective chemical properties and create a protective barrier between the metal surface and the corrosive environment [14], [22], [23]. This generally happens because of the overall molecular structure have amphipathic properties: A polar hydrophilic part and a non-polar hydrophobic part.

The polar hydrophilic part, called a headgroup, can be adsorbed to the metal surface and reject interactions with fatty carbon chains such as hydrocarbons. The non-polar hydrophobic part of the molecule can therefore provide the barrier, as this hydrophobic part mostly contains fatty carbon chains which rejects water molecules and charged ions present in the environment [3], [13], [21], [22]. The overall explanation is also illustrated in *Figure 1* [24].

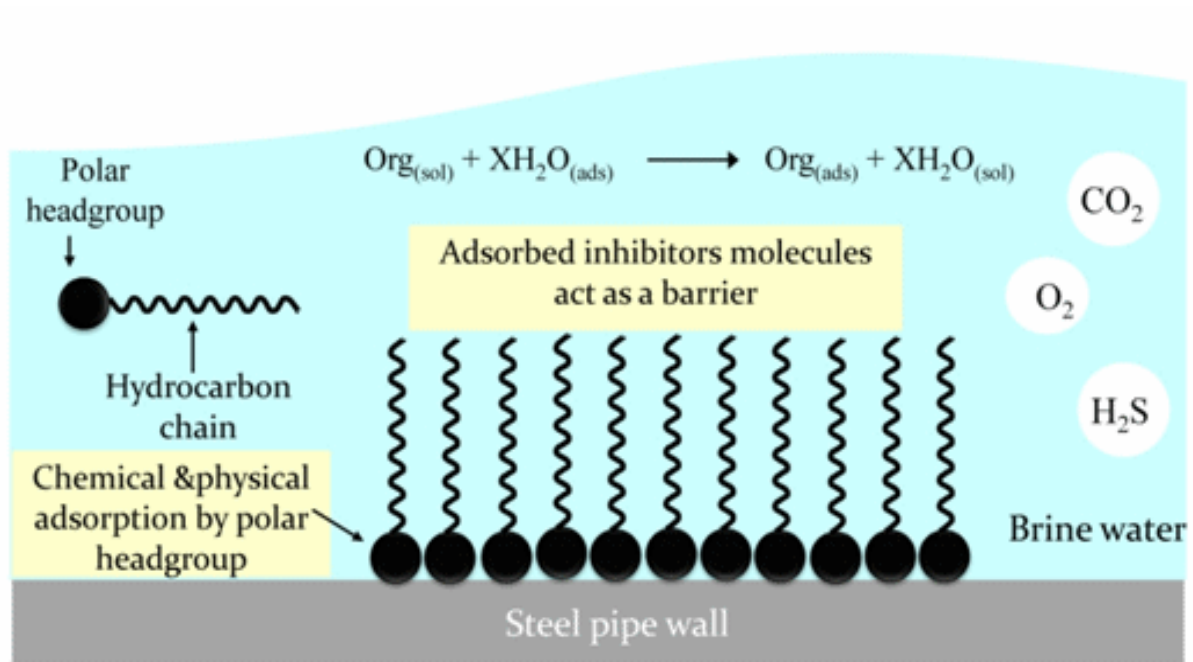


Figure 1: Illustration of the mechanism behind FFCI's [24].

### 1.2.2 – Environmental risks and restrictions

But even though the FFCI's seems to be a very solid combat strategy when dealing with corrosion, they can still bring with them some undesired side-effects such as foam formation in pipelines, high toxicity to living organism, low combability in specific environmental conditions or when combined with other chemicals [13], [14], [23].

The foaming may sometimes be an intentional ability for many chemicals but can also be an undesired side-effect for many other chemicals. Because of foam formation inside pipeline systems may further result in high costs, logistic restrictions and additional operational requirements, the foam formation trait should be kept to a minimum if this trait is not intentional [2].

Researchers has also seen through studies that inhibition efficiency can sometimes increase with an increase of corrosion inhibitor concentration, and some are effective only at high concentrations [4], [25]. Since the cost can also be a determining factor the price tag should also be kept at the lower range to make it cost effective, given that many compounds are expensive alone or gets expensive when a large amount is needed [23].

But even though many compounds can show a good ability when it comes to inhibition properties, they can further show a large negative impact on the ecosystems because of its toxicity. The overall

chemical structure of the corrosion inhibitors has been suggested to have a major impact on the toxicity level and bioaccumulation, with both the size and chemical species playing a role [13]. The toxic trait can be through a reversible or irreversible impact in the organ system, or disturb a biochemical process in parts or whole processes [23].

Compatibility is an additional factor that researchers may need to consider when it comes to creating or optimize corrosion inhibitors. The presence of calcium ions, iron ions, other chemicals, and the ability to diffuse into the oil-phase are all factors that can prevent the corrosion inhibitors to function optimally [26].

All the subjects above, and probably many more, are things that may need to be thoroughly considered as the search for greener corrosion inhibitors continues, where green inhibitors is often referred to as inhibitors that are environmentally friendly, cheap to formulate and renewable [25]. Since many of the corrosion inhibitors used in the oil and gas industry are organic based compounds, they can therefore point towards that organic compounds shows the most promising results [3], [13], [23].

## 1.3 – Quantitative analysis

To evaluate the overall degree of corrosion, how different environmental factors influences the corrosion behaviour and the degree of corrosion inhibitor performance, a high amount of testing may be needed under several different circumstances. With testing methods such as static testing, jet impingement, rotating cylinder electrode, rotating disc electrode, wheel test, flow loop test, bubble test, kettle test and many others being available a high amount knowledge can be gathered [13], [14].

### 1.3.1 – Bubble Testing Method

The bubble testing method used in this thesis can be used for simulating the flow conditions in the production pipelines in a very small scale, which makes this a widely used testing technique when corrosion inhibitor characteristics and performance needs to be quickly analysed [27]. This testing method is performed inside a small kettle at the laboratory, which makes it a testing method that does not require a large and time-consuming set up procedure.

Since it is a small-scale simulation of the environment occurring inside the oil production pipelines, the testing conditions should be as close to real situation as possible to get the most reliable data result. One of these situations is that the corrosion process often happens in the absence of oxygen, or anaerobic conditions, which can make the corrosion process to happen through more specific sets of reactions [14]. By saturating the brine solution with CO<sub>2</sub> gas through continuous bubbling it in, most

of the oxygen inside the brine solution should get removed, and the CO<sub>2</sub> gas dissolved into the brine solution will furthermore create the corrosive environment encountered inside the production pipelines.

To simulate the flow kinetics as much as possible this a magnetic stirrer can be used, and where done in this thesis. Higher flow kinetics can make it possible for a higher amount of reactants to be induced to the metal surface and from there increase the overall corrosion rate [14].

## 1.4 – Electrochemical measurement

As earlier mentioned, in a general corrosion process there is a current of electrons flowing from the anodal site to the cathodal site. A metal that undergoes a natural corrosion process often has the anodal side and cathodal site on the same surface in the presence of an electrolyte, which makes an overall complete corrosion cell to be present in an open electrical circuit [28]–[30]. By taking advantage of this natural occurring current and forcing it to happen through a closed electrical circuit, quantitative electrochemical analysis such as linear polarization resistance (LPR) can be performed.

In this thesis, this was performed by using a three-electrode system that was coupled to a potentiostat and performing linear polarization resistance (LPR) measurement. As the LPR measurement strategy made it possible to collect high amount of data of the corrosion behaviour for a metal species in a selected environment, an estimate the corrosion rate within a short time period could be done [4].

The three-electrode system used consisted of a Working Electrode, Counter Electrode and Reference Electrode, which together with the conducting electrolyte inside the kettle presented as the overall closed electrical circuit. The Working Electrode holds the metal sample where the corrosion is being analysed, the Counter Electrode introduces or removes excess current (A) in the closed electrical circuit, and the Reference Electrode measures the Working Electrode potential (V). All the electrodes are furthermore coupled to a potentiostat that controls the current through the electrochemical cell and measure it between the Counter Electrode and Working Electrode relative to the metal samples open circuit potential [31], [32]. An illustration of the overall system is presented in *Figure 2* [33].

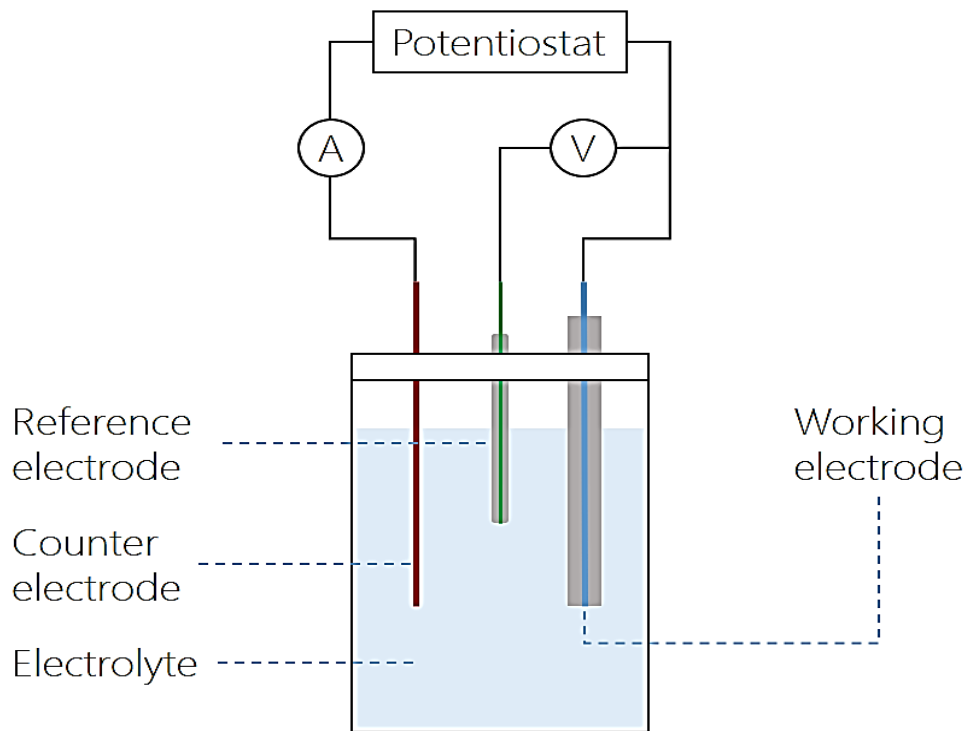


Figure 2: Illustration of a three-electrode system [33].

### 1.4.1 – Linear Polarization Resistance measurement

The LPR measurement is furthermore originally based on numerous theories and underlying mathematical equations [28], [34], [35]. As the purpose of this thesis was to make a manual on how to perform the LPR measurement, a thoroughly in-depth explanation on each theory and equation contributing was considered to lie beyond the scope of this thesis. The following theory is therefore put together in a more general and simplified manner to give a general understanding of the LPR measurement strategy.

If a metal is exposed to a conductive environment with both oxidization and reduction half reaction happening in a steady and constant pace relative to each other, then the metal can be said to be in an equilibrium with its environment in an open circuit. This is when no external electrical force is applied to the metal, and the largest driving force is mostly the metals electrochemical behaviour towards the environment it is exposed to. Furthermore, as the number of electrons left in the metal surface due to the oxidisation being equal to the electrons removed by the reduction reaction, the overall net current is said to be equal to zero [28], [34].

The situation is illustrated in *Figure 3*, with the oxidization/corrosion of iron in an conductive corrosive environment [29]:

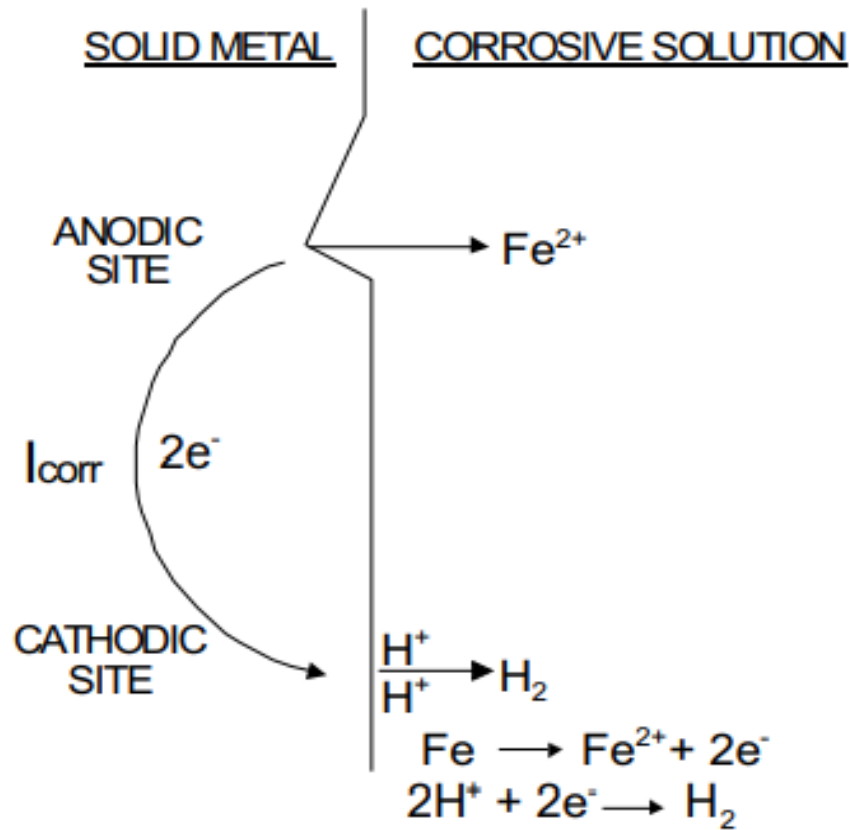


*Figure 3: Illustration of the corrosion process of iron in a corrosive environment [29].*

But even though the overall net current is said to be zero at the equilibrium situation, an electron flow from the anodic site to the cathodic site will be present as the corrosion process proceeds in a steady pace. This electron flow, known as the corrosion current ( $I_{corr}$ ), cannot be measured directly as it is dependent on properties within each of the individual oxidization ( $\beta_a$ ) and reduction ( $\beta_c$ ) half reaction [29], [34]. But this current makes a potential to be present during the steady equilibrium process, which can be measured in voltage (V), and is often noted as the open-circuit potential ( $E_{oc}$ ) or in some cases of electrochemical measurements the corrosion potential ( $E_{corr}$ ) [34].

When an external electrical potential (V) is introduced to the conductive environment by a counter electrode, this would make the metal's potential to alternate towards a more positive or negative

potential relative to its initial  $E_{oc}$  potential, and thus make it to undergo a polarization process [28], [31], [32], [34].

During this process one of the electrochemical half-reaction increases in pace relative to the other, with a corresponding increase in electron current ( $I$ ) measured in amperes (A) and direction (positive or negative) relative to the “zero net current” at  $E_{oc}$ . If the added potential ( $V$ ) makes the metal’s potential to be more negative relative to its  $E_{oc}$  potential, it will stimulate the reduction reaction to proceed in a higher pace with a negative current ( $I$ ). If the added potential ( $V$ ) makes the metal’s potential to be more positive relative to its  $E_{oc}$  potential, it would make the oxidation reaction to proceed in a higher pace with a positive current ( $I$ ) [28], [34], [35].

Since the degree of applied potential ( $V$ ) in the polarization process can be seen to determine which of the electrochemical half-reactions is going to be the most dominant with a corresponding degree and direction of increase in current ( $I$ ), the amount of increase in current (A) can furthermore in general reflect how much resistance ( $\Omega$ ) the electrons have towards migrating in the polarization process, and thus the metal’s polarization resistance ( $R_p$ ). This means that if a metal has a high resistance towards polarization ( $R_p$ ), then the electrons has a high resistance to migrate, and thus metal has a low ability to corrode. If a metal has a low resistance towards polarization, then the electrons has a low resistance to migrate, and thus the metal has a high ability to corrode [29]. By using these general assumptions, the metal’s polarization resistance ( $R_p$ ) can from there be used to estimate the metal’s  $I_{corr}$  value, and from there approximate an overall corrosion rate that can illustrates the metal degree of corrosion in the environment it is exposed to [28], [32], [34], [35].

These explanations and assumptions are a brief and short version of the general theory that the LPR measurement is based on. Through highly more detailed explanations and numerous of theories, such as Faraday’s law and the Butler-Volmer equation (1), researchers and scientists has put lots of work into establishing an overall mathematical relationship that connects all the parameters together, through a version of the Stern-Geary equation (2) presented below [28], [34], [35].

(1) Butler-Volmer equation: 
$$I = I_{corr} * \left( e^{\frac{2,303*(E-E_{corr})}{\beta a}} - e^{\frac{-2,303*(E-E_{corr})}{\beta c}} \right)$$

(2) Stern-Geary equation: 
$$R_p = \frac{\Delta E}{\Delta i} = \frac{\beta a * \beta c}{2,303 * I_{corr} (\beta a + \beta c)}$$



The Stern-Geary equation above (2) mainly holds if the applied voltage during the polarization process is close to the metal's  $E_{\text{corr}}$  value. At this point, it implies that if a small potential range ( $\Delta E$ ) were to be introduced to the metal, a corresponding current ( $\Delta i$ ) would appear, which approximates to a linear trend close to the metal's  $E_{\text{OC}}$  potential. The slope in this linear trend would represent the metal's  $R_p$  value, and from there the metal's corrosion rate can be approximated [28], [34], [35]. In *Figure 4* below is a visual illustration of these correlations [36].

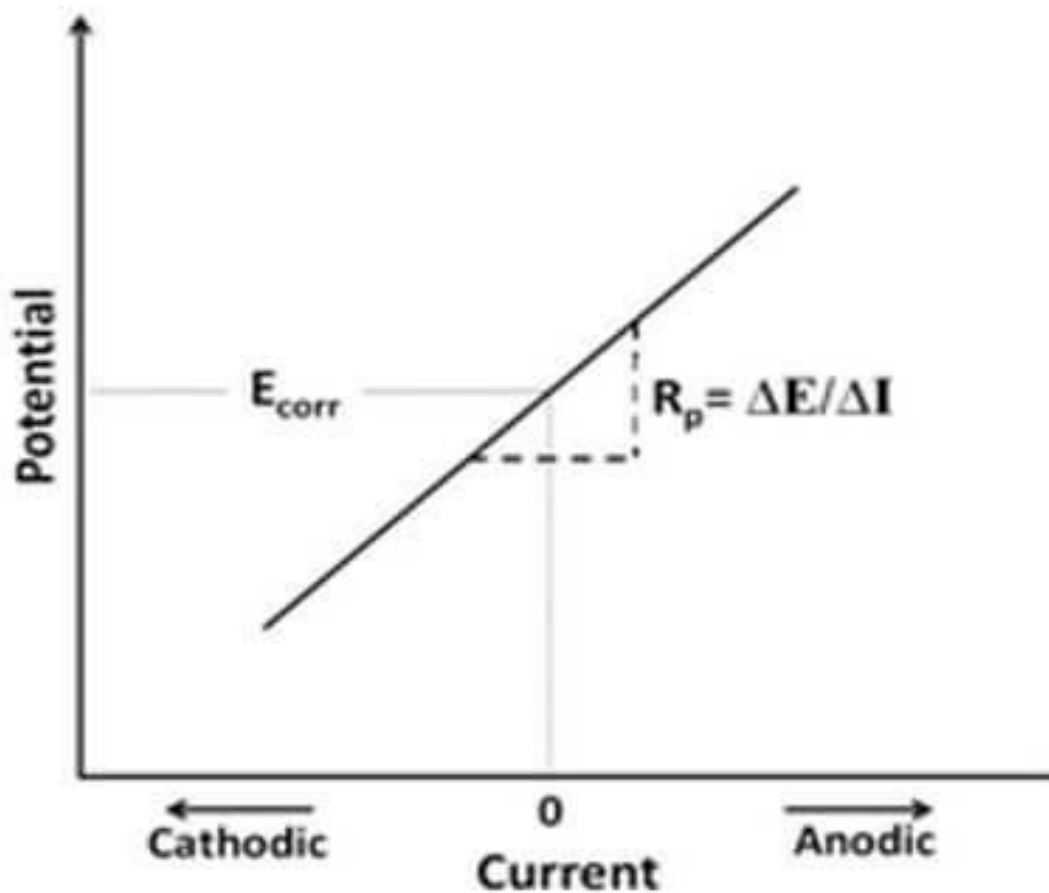


*Figure 4: An illustration of the relationship between  $R_p$ ,  $\Delta E$  and  $\Delta i$  [36].*

Given that the LPR measurement does not provide any information of the  $\beta_a$  and  $\beta_c$  coefficients for each individual electrochemical half-reactions, the values for these coefficients needs to be determined through either a Tafel plot or through general experience with the given system [34].

As earlier mentioned, when performing the LPR measurement a high amount of information on the corrosion behaviour of selected metal species in the given environment can be gathered. Illustrated in *Figure 4*, the corrosion current ( $I_{corr}$ ) value can be estimated at the measured corrosion potential ( $E_{corr}$ ) when the metal is said to be in equilibrium with its environment, by taking advantage of the assumption that the net current is equal to zero at this point. If the area of metal surface exposed to the corrosive environment is also taken in to account, the amount of current measured (A) converts to current density ( $A/cm^2$ ) and the unit of polarization resistance becomes area dependent ( $\Omega \cdot cm^2$ ), which gives a more specified and accurate data result.

## CHAPTER 2 – ASSEMBLE THE GAMRY INSTRUMENTS MULTIPOINT ELECTROCHEMICAL CELL KIT AND PERFORMING LPR MEASUREMENT WITH THE GAMRY FRAMEWORK

The benefit of using the Gamry MultiPort Electrochemical Cell Kit is that it has a high variety of applications within the field of corrosion testing. It is a very user-friendly equipment that gives large quantities of data within each of the tests performed. For this thesis the focus was mainly on the Bubble Testing method together with Linear Polarization Resistance (LPR) measurement, as this gives a good general assessment regarding the corrosion behaviour of a metal sample when introduced to the selected environment.

Because of the following procedures presented is solely based on the Gamry Instruments MultiPort Electrochemical Cell Kit and Gamry Framework, the following procedures has been put together by using a combined collection of information from the instruction manual that followed with the equipment: Gamry Instruments – MultiPort Electrochemical Cell Kit – Operator’s Manual [37], instruction manual for the software: Gamry Instruments – Echem Analyst™ Software Manual [38], YouTube videos from the producer [39], [40], application notes from the producer [31], [32], [34], [41], [42], and communication through e-mail with the producer [43]. In addition to detailed guidance from an experienced corrosion engineer at UiS named Utsav Raj Dotel, and good guidance from supervisor. Different techniques can be used and modified, but this was not explored in this thesis due to time limitation.

## 2.1 – Equipment and Assembly

When assembling the equipment, it must be strongly emphasized that the glassware and measurement equipment are very prone to damage. The glass ground-joints do not need any greasing on the sealing surface as this is not necessary for the MultiPort equipment. Doing so may cause contamination of the test solution and may also give inaccurate data reading. The equipment must be kept clean, and gloves should be worn to keep the risk of contamination is at its lowest.

All the parts shown in *Figure 5* are described in the following sub-chapters.

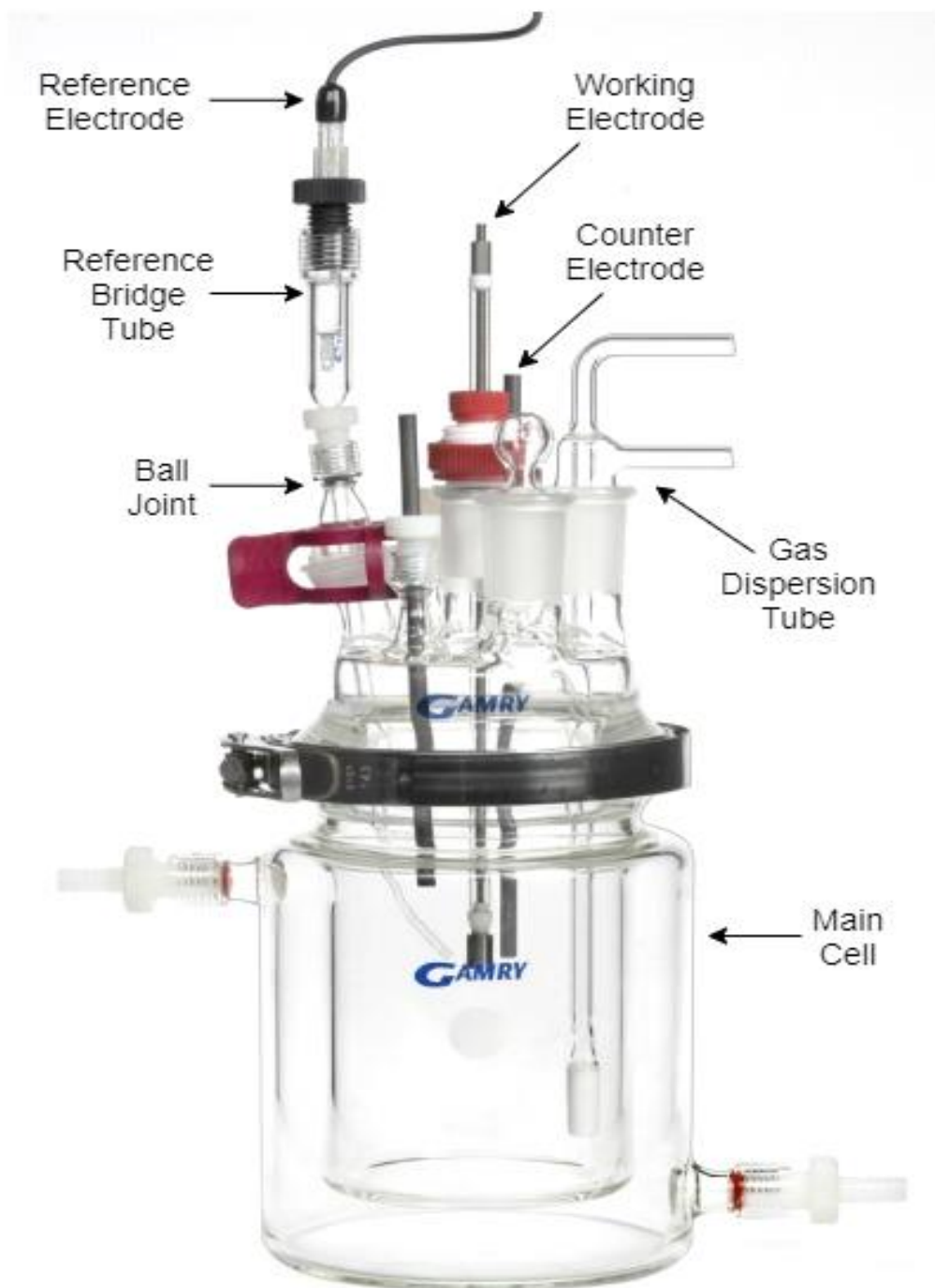


*Figure 5: A complete assembled Gamry MultiPort Electrochemical Cell with added name tags and location of the parts [37].*

## 2.1.1 – The Main Cell

Assembling the Main Cell with all its necessary parts is the first thing to start with. An illustration of the Main Cell, with the necessary notations and locations, is presented in *Figure 6*. The Main Cell can contain up to 1000ml solution in total, which must always be taken into consideration when the experiment requires a mix of solutions. Therefore, performing calculations of ratio with respect to the maximum allowed volume of solution in the cell is crucial.

### **Preparations and Assembly**

- It is necessary to perform a thoroughly visual check of the Cell Bottom, Cell Top, and the O-Ring seal gasket for any signs of damage or contamination before assembling the Main Cell. A proper laboratory cleaning procedure with distilled water or acetone is therefore recommended.
- When this is done, ensure that the Cell Bottom stands firmly on a flat area with no danger of falling. The Flange Clamp is then opened and put over the flange at the Bottom Cell compartment and left in an open position.
- The O-Ring seal gasket is placed into the O-Ring groove that is located at the Bottom Cell flange before putting the Cell Top on.
- The Cell Top and Cell Bottom are sealed together by closing the open metal Flange Clamp at the Cell Bottom securing the combined flanges.

The purpose of the Flange Clamp is to prevent the Cell Top from sliding off the Cell Bottom, so a minimal amount of force should be needed when closing it [37]! If the Flange Clamp is too tight, it can break the glassware. To loosen or tighten the Flange Clamp grip, use the Set Screw located on the opening/closing mechanism.



Figure 6: The Main Cell with added name tags and location [37].

## 2.1.2 – The Reference Bridge Tube

### **The Reference Bridge Tube**

The Reference Bridge Tube is a thin glass tube, with its main purpose to shield the Reference Electrode from potential damaging factors that may take place during testing [37]. It works by supplying a stable connection between the Reference Electrode and test solution through a conductive solution within the glass tubing. At the tip of the Reference Bridge Tube there is a small porous Glass Frit Tip. This Glass Frit Tip serves as a liquid junction, which provides the Reference Electrode with a stable connection to the solution with no rapid changes caused by flow or temperature [37], [43].

An illustrative picture of the Reference Bridge Tube accompanied with added name tags of components and their selected location is presented in *Figure 7*. The Reference Bridge Tube fits any of the #7-ports, but it is specially designed to fit in the SJ28-Ball-Joint-Port with the SJ28 Male and SJ28-to-#7 Teflon Adapter [37][*Figures 6-8*].

To keep the Ball-Joint secured and stable at the Cell Top, a rubber/plastic Clamp is needed. This gives the benefit of moving the Bridge Tube inside the cell to the desired position close to the Metal Sample surface without making a direct contact with the Metal Sample surface.

Before doing any further preparations, the Ball Joint must be assembled with the SJ28-Male presented in *Figure 8* and a rubber/plastic clamp.

### **Preparations and Assembly**

- Before putting the Reference Bridge Tube to use, it is necessary to do a thoroughly visual check for any damage or contamination. The Glass Frit Tip must be checked for clogging, cracks, or any other unwanted damage. Proper rinsing with distilled water inside and outside should be performed even though no visible contaminations were located. Acetone can be used for washing the outside if necessary.
- Injecting liquid into the Reference Bridge Tube is done manually by using a small pipette. If small air pockets occur on the tube wall or at the Glass Frit Tip, they can be removed by gently tapping on the sidewalls or by the help of a small wire [43]. Before inserting the Reference Bridge Tube to the Main Cell for testing, it must be filled with a conductive solution, preferable the test solution if possible.



- After the Reference Bridge Tube is filled with the conductive solution, the threaded SJ28-to-#7 Teflon Adapter is slid on, followed by the O-Ring gasket, and then the assembly is inserted into the Main Cell through the SJ28 Male on the Ball-Joint.

It is crucial to keep in mind that the Reference Bridge Tube is a very fragile glassware so inserting it through the Ball Joint needs to be done gently. This should be done by gently wiggling the tube in through the Ball Joint and tightening the Teflon adapter to the Bridge Tube when it is all the way down. If the Reference Bridge Tube position needs to be adjusted within the Main Cell, it should be done by moving the SJ28 Male on the SJ28-Ball-Joint manually after inserting [37], [39].



Figure 7: The Reference Bridge Tube with added name tags and locations [37].



*Figure 8: The SJ28 Ball-Joint-Port Male with added name tags and locations [44].*

### 2.1.3 – The Reference Electrode

The Reference Electrode that is used is an Ag/AgCl electrode saturated with KCl, with a potential of 199mV vs. a normal hydrogen electrode supplied by Gamry, and is presented in *Figure 9* [45]. The black tip is a protective rubber seal, which must be removed before use.



*Figure 9: The Ag/AgCl Reference Electrode supplied by Gamry [45].*

#### **Preparation and Assembly**

- The Reference Electrode should be rinsed with distilled water before inserting the Reference Electrode into the Reference Bridge Tube.

- To ensure a secure fit of Reference Electrode inside the Reference Bridge Tube, a threaded #11-Bushing slides over the Reference Electrode, followed by an O-Ring seal.
- The Reference Electrode is then inserted into the Reference Bridge Tube at the top end marked with #11-Port.
- Secure the Reference Electrode in place by tightening the #11-Bushing. Make sure that the tip of the Reference Electrode is fully submerged into the conductive solution inside the Reference Bridge Tube.

## 2.1.4 – The Counter Electrode

The Counter Electrode is a porous graphite rod, and is needed to complete the overall electrical circuit within the Main Cell [37], [46]. A fully assembled Counter Electrode with added name tags and location is presented in *Figure 10*.

It is important to make sure that the Counter Electrode has a larger surface area submerged compared to the submerged Metal Sample surface area in order to avoid overloads [46]. Having the Counter Electrode surface submerged at least twice the size of the submerged Metal Sample surface has been recommended in literatures [28].

### **Preparation and Assembly**

- Before the Counter Electrode is used a thorough visual check for any damage or contamination must be performed. Since the graphite rod is made out of a very porous material it can adsorb several unwanted chemical species [37]. Therefore, a proper laboratory cleaning procedure is needed. Acetone can be used for washing if necessary.
- Start by sliding on a #7-Bushing, followed by an O-Ring for a secure fit of the Counter Electrode to the Main Cell.
- After this is carried out, the Counter Electrode is inserted into one of the #7-Ports on the Cell Top and secured into place by tightening the #7-Bushing. A small tilt on the Counter Electrode can happen but is not of any concern [37].

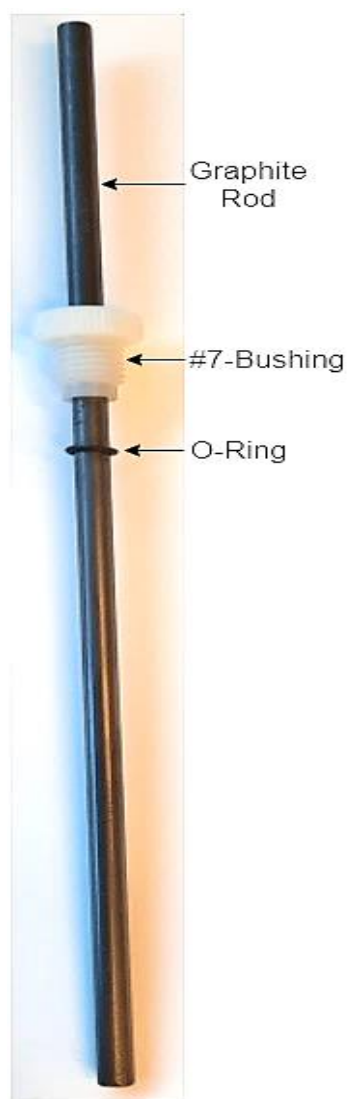


*Figure 10: Assembled Counter Electrode at the laboratory, with added name tags and location [37], [39].*

### 2.1.5 – The Working Electrode

Electrochemical experiments often have its focus at the Working Electrode as this is where the Metal Sample that is being analysed is positioned. The Stainless-Steel Rod within the Working Electrode holds the Metal Sample and provides a direct connection, which makes it is possible to apply and adjust an external potential to the given Metal Sample and measure the responding current as it arises.

Since the Metal Sample is positioned on the Working Electrode, it makes the Working Electrode one of the more sensitive parts within the experiment. If complications such as leakage into the Pyrex Tube,

damage or localized corrosion happen, it may result in significant errors during testing. Thus, proper preparations and assembling is crucial to get the most accurate and reliable data reading as possible.

The Working Electrode is also the last electrode to enter the Main Cell. If deoxygenating or gas flushing of the solution within the cell is necessary, this must be done before inserting the Working Electrode [37].

The fully assembled Working Electrode is presented in *Figure 11* with added name tags and locations.

### **Preparation and Assembly**

- Before the Working Electrode is assembled, all the parts must be visually checked for any damage and/or contaminations. Proper laboratory cleaning procedure with distilled water and acetone is highly recommended.
- The Working Electrode can be assembled by using different strategies, but it was experienced that by starting with preparing the Pyrex Tube made the rest of the steps easier [37], [39]. When preparing the Pyrex Tube, start off by un-screw the Top-Nut on #24/40-Port Adapter and separate the two parts. Slide #24/40-Port Adapter without the small Top Nut about halfway down on the Pyrex Tube, followed by an O-Ring seal and the small Top-Nut.
- All the parts for the Pyrex Tube are now on, but not connected. Connecting the Top Nut to the #24/40-Port Adapter is the last step to do after inserting the Working Electrode into the Cell Top, as this secures the Pyrex Tube in its place inside the #24/40-Port Adapter.
- With the Pyrex Tube prepared, the rest of the Working Electrode can be assembled. Do this by first locating on the Threaded Rod tip end that has the smallest threads, as this is where the Metal Sample is being mounted on. The Threaded Rod is then inserted into the Pyrex Tube, with the smallest threads facing the opposite direction of the Top-Nut.
- Next step is to take the cone-shaped Teflon Compression Gasket and apply a small O-Ring at the end with the biggest surface area to ensure a proper sealing. The cone-shaped Teflon Compression Gasket slides over the tip end of Threaded Rod containing the smallest threads, with the O-Ring facing the Pyrex Tube for sealing. The Metal Sample is screwed onto the smallest threads, leaving this end finished.

- The Teflon Centering Washer slides over the Threaded Rod in the opposite end of the Metal Sample, with the smallest cross section towards the Pyrex tube. To keep the whole Working Electrode together a Standoff Hex Nut is screwed on the Threaded Rod right above the Teflon Centering Washer. When tightening the Hex nut, hold onto the Metal Sample at the opposite end and tighten it finger-tight. Tightening it further may result in the O-Ring being squeezed out of position and can cause leakages. Cracking/breaking of the Pyrex tube can also be a consequence of overtightening the Hex nut [37], [39].
- The whole Working Electrode is now assembled and ready to be inserted into the Main Cell through the Cell Top. The #24/40-port Teflon Adapter fits any of the #24/40-ports on the Cell Top, but is preferable to be inserted in the centre port [39].
- When the Working Electrode is inserted into the Cell Top, it can be adjusted to the desired position by gently pulling or pushing it up or down through the #24/40-Port Teflon Adapter. When the desired position is achieved, the small Top Nut is screwed together with the #24/40-Port Adapter to lock it in place.

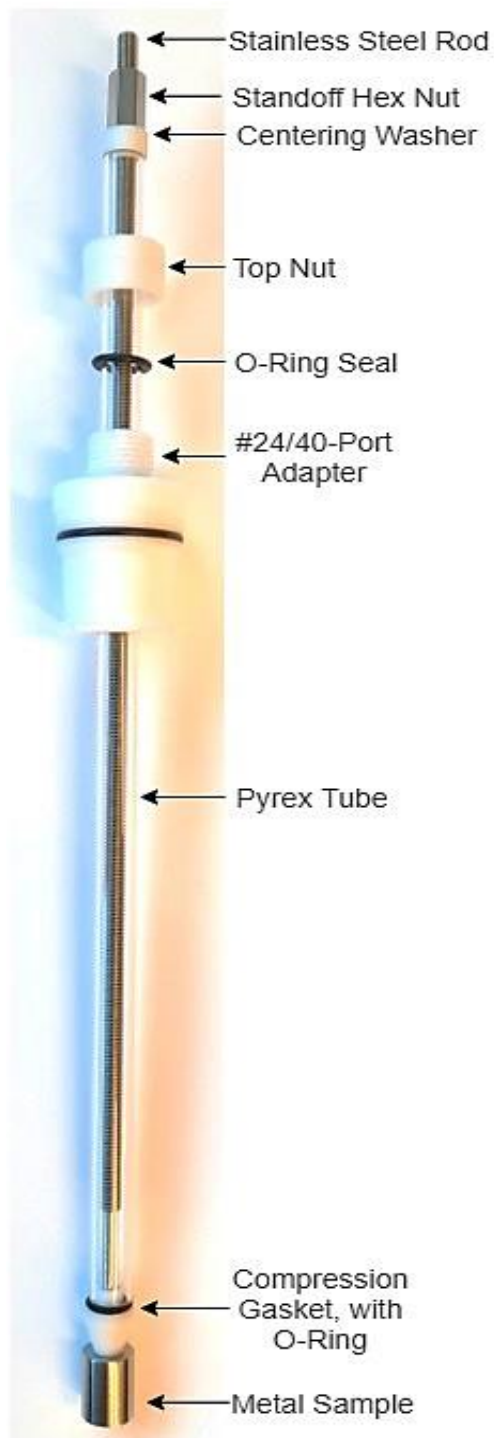


*Figure 11: Assembled Working Electrode at the laboratory, with added name tags and location [37], [39].*

## 2.1.6 – The Gas Dispersion Tube

The Gas Dispersion Tube is used when the addition of gas to the test solution is necessary, such as the addition of CO<sub>2</sub> gas done in this thesis. The Gas Dispersion Tube is presented in *Figure 12* with added name tags and locations. The Gas Dispersion Tube is made of a double compartment glass cylinder that supplies an Inlet and Outlet for the applied gas. It is crucial to keep the Outlet open to prevent pressure build-up within the Main Cell, as this can lead to severe and unpleasant consequences [37].

On the side of the Gas Dispersion Tube there are two hose barbs that are used for Inlet and Outlet when gas is applied.

If Purge Gas is applied, it is recommended to use the hose barb located at the highest point for Inlet and the hose barb located at the lowest point for Outlet or venting, as seen in *Figure 12* [37].

### **Preparation and Assembly**

- The Gas Dispersion Tube must be thoroughly visually checked for any damage or contamination before being used. Since the tip end of the Gas Dispersion Tube is very porous it can have a high amount of contamination, and thus need a thoroughly cleaning with proper laboratory cleaning procedure.
- The Gas Dispersion Tube is inserted into the Main Cell through one of the #24/40-Ports after the Main Cell is filled with solution and secured. Connecting the Gas Hoses to the hose barbs on the Gas Dispersion Tube is done after inserting it into the Main Cell.
- Note that vacuum can occur inside the Gas Dispersion Tube when the gas flow is shut off, which can make solution to be sucked into the gas hose tubing. To prevent this, it is recommended to connect a Water-Trap between the Gas Dispersion Tube and the Outlet Needle Valve.
- If the solution needs to be saturated with gas before testing, it was experienced that it is best to keep the gas flow as high as possible without splashing the solution accompanied by good stirring. When the test is set to start, the gas flow and stirring needs to be lowered to get the best data reading.





*Figure 12: Gas Dispersion Tube, with added name tags and locations [37].*

Regulating the gas flow through the Gas Dispersion Tube is done by manually adjusting the Needle Valve on the Gas Regulator illustrated in *Figure 13*, while visually observing the amount of gas entering the solution.

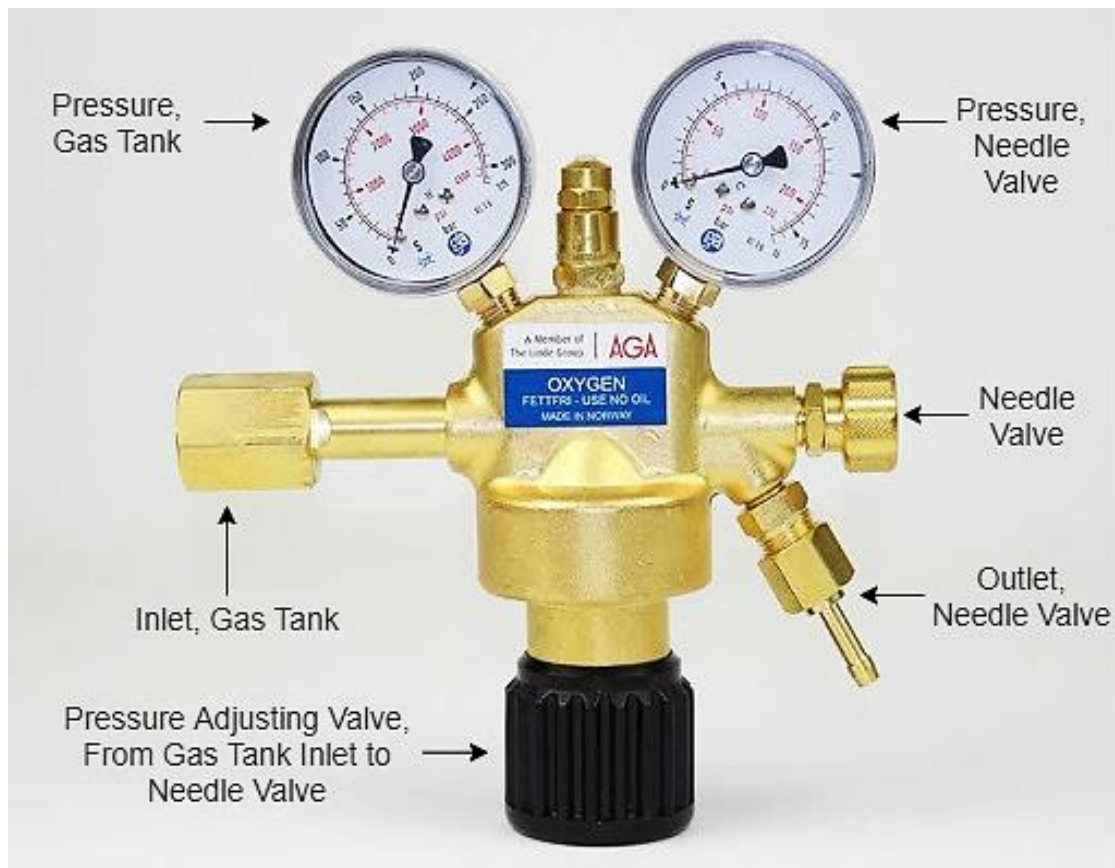


Figure 13: Illustration picture of a gas regulator, with added name tags and locations [47].

When opening the Main Valve on the CO<sub>2</sub> gas tank and the other valves presented in *Figure 13* to insert CO<sub>2</sub> gas into the test solution, it should be done in the following order.

1. Open slightly the Main Valve located on the gas tank. The gauge named "Pressure, Gas Tank" in *Figure 13* will show a pressure increase, which is the pressure present inside the gas tank.
2. Open the "Pressure Adjusting Valve, From Gas Tank Inlet to Needle Valve" located in *Figure 13* until the gauge named "Pressure, Needle Valve" in *Figure 13* shows approximately 50psi, which is the pressure at the "Needle Valve" in *Figure 13*.
3. Open slightly the "Needle Valve" in *Figure 13* while observing the amount of gas entering the solution inside the Main Cell. This valve can have a small delay, meaning that the amount of gas flow through the Needle Valve may take some time to present itself inside the solution. Because of this, the Needle Valve must be slowly open with small amounts until the desired amount of gas flow is observed.

When the gas is to be shut off, repeat the order presented but close instead of open.

## 2.1.7 – Connection Clamps

Make sure that the Connection Clamps are clean and free of severe rust deposits before connecting them to the electrodes. If severe rust deposits are located, these Connection Clamps must be cleaned or replaced to ensure the best connection with no overload error. Ensure that the Connection Clamps have a solid grip onto the electrode, as the loose connections can also result in an undesirable amount of overload errors. The Connection Clamps located on each individual electrode must not touch each other!

The Connection Clamps illustrated in *Figure 14* are clamped directly onto the given electrodes. External wiring from the electrodes to the Connecting Clamps can be used if necessary. By using external wiring, the risk of the Connection Clamps of touching each other or falling off is lowered and also prevents the Connection Clamps of getting in contact with moisture from the Main Cell.

As depict in *Figure 14*, the following connections must be made:

- Blue Clamp (Working) and Green Clamp (Working Sense) to the Working Electrode.
- Red Clamp (Working) and Orange Clamp (Working Sense) to the Counter Electrode.
- White Clamp to the Reference Electrode.
- Black banana plugs are Ground and have no connections to any electrodes.

The Black banana plugs can be used if reducing noise within the data reading is necessary, by connecting them to a ground source such as water pipes or a Faraday's cage [37]. Otherwise, these must be kept away from any other Connection Clamps!

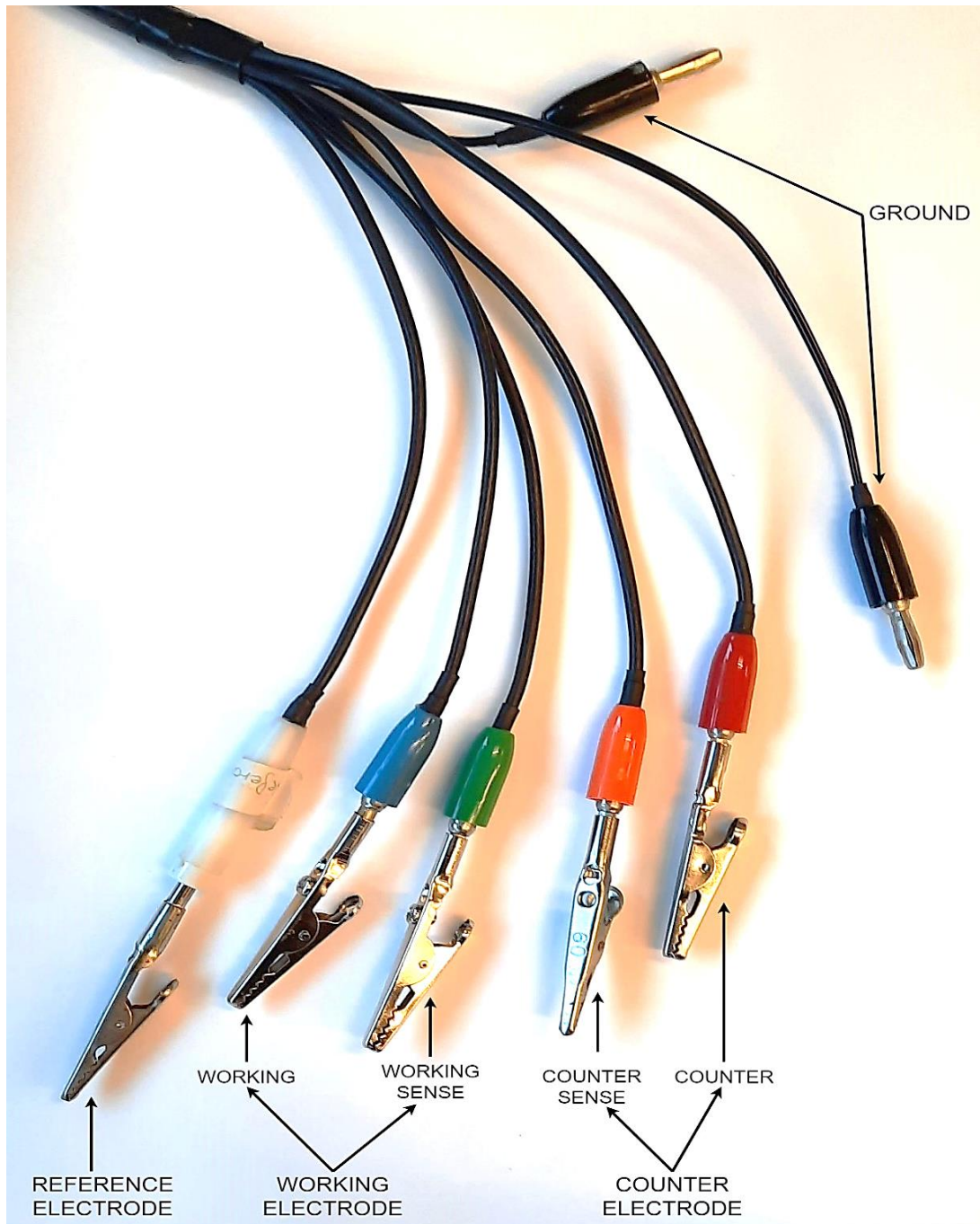


Figure 14: Picture of the Connection Clamps taken at the laboratory, with added name tags for each and what electrode they must be connected to [48].

## 2.2 – The Testing Sequence

The following explanations has been put together by consulting an experienced corrosion engineer named Utsav Raj Dotel, literatures from producer, user manuals, YouTube videos and performing excessive testing under many different situations. As many advises was given through verbal conversations with Utsav, these have been referred to by using a star (\*) to acknowledge his advises.

The following testing sequence focuses on how to perform a Linear Polarization Resistance (LPR) measurement by using the Gamry Framework program package, and to use the Output data results for further analysis. In the Gamry Framework the LPR measurement is notated as Polarization Resistance but is the same measurement method. The LPR measurement always starts with analysing the Metal Samples Open Circuit Potential, which is often noted as “Open Circuit (V)” or  $E_{OC}$ . When a stable  $E_{OC}$  value is achieved the LPR measurement starts, where a potential is being linearly applied relative to the measured  $E_{OC}$  value and the responding occurring current is analysed [34].

The time it takes to perform a LPR measurement is mainly determined by the Scan Rate, Initial E(V), and Final E(V), and can be estimated through:  $\text{Measuring time} = (|\Delta E|) / (\text{Scan Rate})^*$ . If the absolute potential difference between the Initial E(V) and Final E(V) is 40mV and Scan Rate is set to be 0.125mV/s, this results in a testing time of 320 seconds, or around 5-6 minutes. This time calculation is just for the LPR measurement alone. When taking into consideration the time it takes for measuring the OCP, the overall time will be increased by the time it takes for getting a stable OCP value.

To perform the LPR measurement the programs illustrated as shortcuts in *Figure 15* is necessary, with an in-depth clarification table in *Table 1*.



Figure 15: Screenshot taken at the laboratory of the shortcuts of the Gamry Framework programs for performing LPR measurement and analysing the experimental results.

Table 1: Clarifications of the Gamry Framework program package presented in Figure 15.

<b>Gamry Framework</b>	The main operating program package and is where all the desired tests are selected performed.
<b>Gamry Echem Analyst</b>	The analysing program where tests are analysed.
<b>My Gamry Data</b>	The program where all experimental files is stored.

### 2.2.1 – Input values

The Input values are in general the LPR measurement limitations. By selecting the Scan Rate, Initial- and Final Potential, and Sample Period the Potentiostat applies this potential and measures the responding current through continuous data sampling. The experimental result is a potential versus current plot which illustrates the overall corrosion behaviour of the Metal Sample in the selected environment.

#### **The Gamry Instruments Framework**

When opening the Gamry Instruments Framework, the program presents its working platform as in *Figure 16*. By clicking on “Experiments” in the toolbar menu all the available tests are presented, and LPR measurement can be selected [*Figure 16-17*].

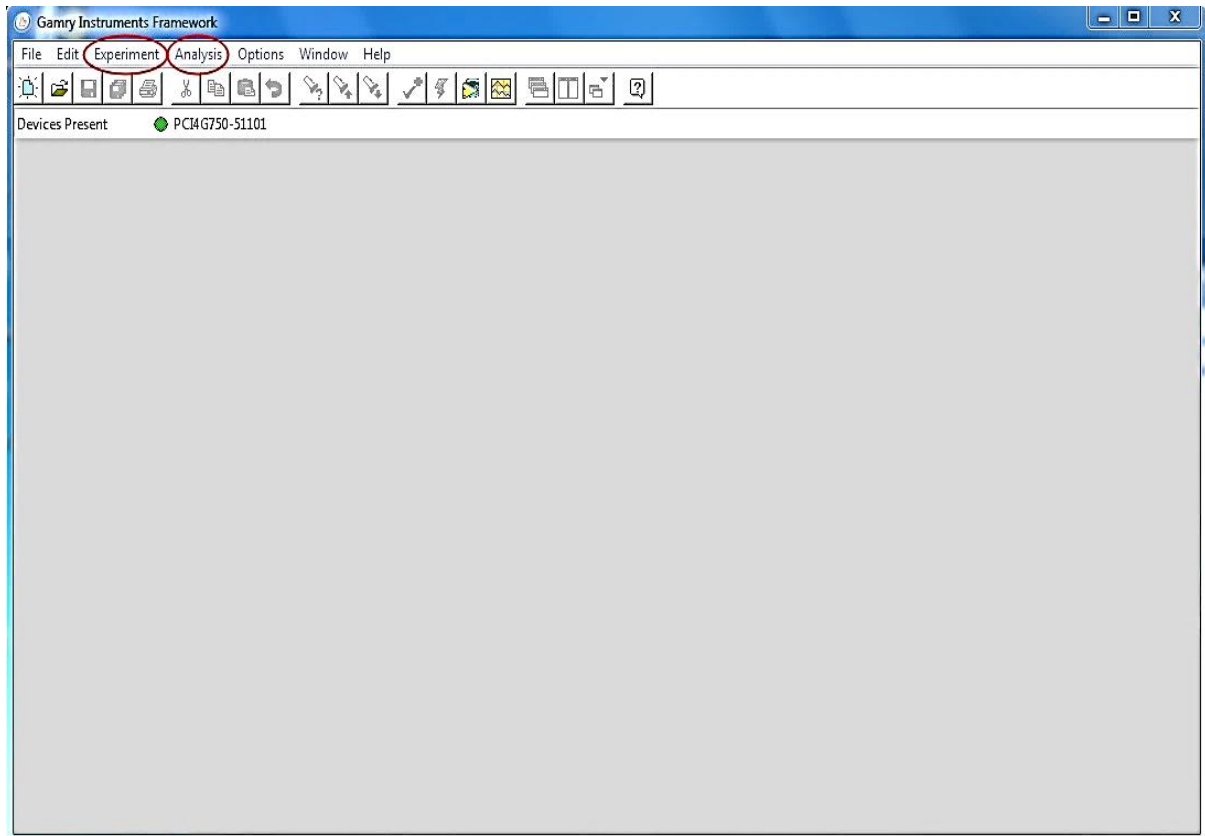


*Figure 16: Screenshot taken in the laboratory of the Gamry Instruments Framework working platform.*

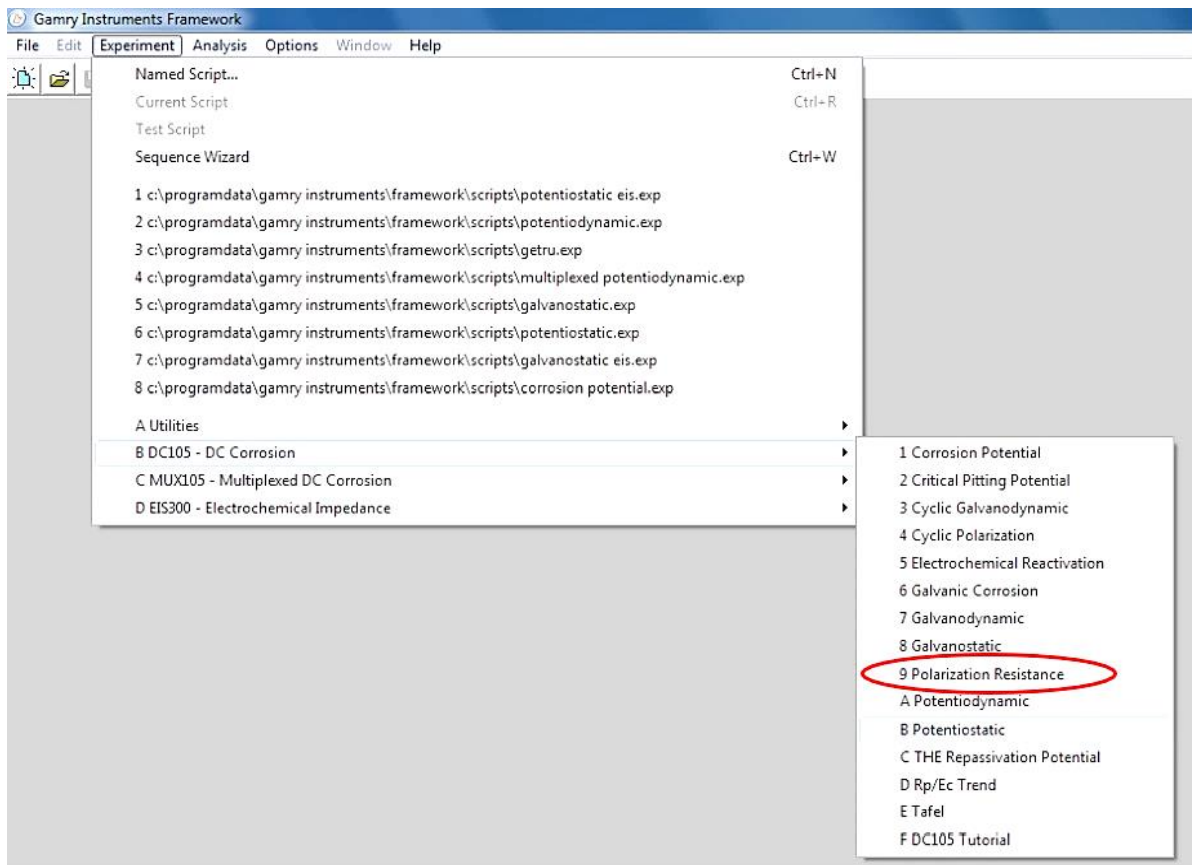


Figure 17: Localising the Polarization Resistance (LPR) measurement in the toolbar [49].

When the LPR measurement is selected, the window in Figure 18 is presented where all the Input values are selected. An in-depth clarification of each parameter in Figure 18 can be found in Table 2.



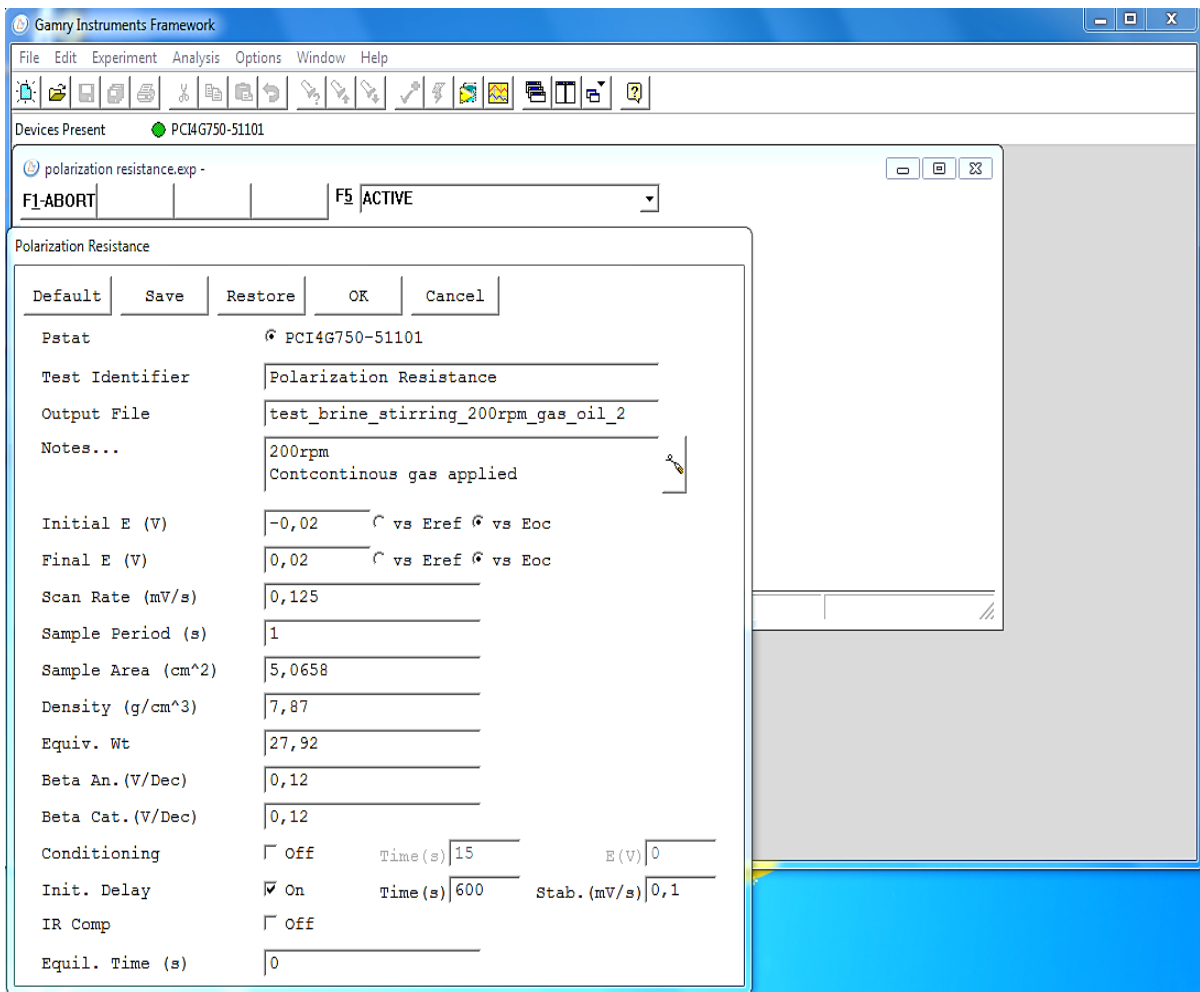


Figure 18: Screenshot taken at the laboratory of the window where selecting the Input values for LPR measurement is done.

Table 2: Clarification of parameters in Figure 18 [32], [34], [38].

<b>Pstat</b>	Shows the connected potentiostat.
<b>Test identifier</b>	Tells what type of test is selected.
<b>Output File</b>	The desired file name for the Output file.
<b>Notes...</b>	If any details related to the test performed such as the conditions, the concentrations, the stirring rate etc. are necessary, it can be entered here.
<b>“vs E<sub>ref</sub>”</b> <b>“vs E<sub>oc</sub>”</b>	Selects what the applied voltage range/potential sweep is relative to. It is highly recommended* to use “vs. E <sub>oc</sub> ” as this ensures that the LPR test performed are based on the Metal Sample’s properties. If the “vs. E <sub>ref</sub> ” is selected, then the measured E <sub>oc</sub> value for given Metal Sample needs to be added into the “Initial E(V)” and “Final E(V)” values*.
<b>Initial E(V)</b>	This is the initial applied voltage and can be regarded as the LPR measurements “starting point”. This is often the most negative potential within the selected potential range. The allowed range is ±10V with a resolution of 1/8 <sup>th</sup> mV. Its accuracy depends on the settings selected. Usually this is less than -20mV “vs. E <sub>oc</sub> ” [32].
<b>Final E(V)</b>	This is the final applied voltage and can be regarded as the LPR test “end point”. It is often the most positive potential within the selected potential range. The maximal allowed range is ±10V with a resolution of 1/8 <sup>th</sup> mV. Its accuracy depends on the settings selected. Usually this is less than +20mV “vs. E <sub>oc</sub> ” [32].
<b>Scan Rate (mV/s)</b>	This is where the rate/speed of the scan is determined by selecting the amount of voltage applied per second. A low voltage per second will result in a longer time span of the test performed, and too high voltage per second can result in unreliable data [32].
<b>Sample Period (s)</b>	This determine how often the potentiostat will take a measurement, and thus determines how well defined the resulting graph will be. The minimum and maximum Sample Period recommended is between 0,2 seconds and 600 seconds [32].
<b>Sample Area (cm<sup>2</sup>)</b>	This is where the surface area of the metal sample that is exposed to the test solution is selected. It is crucial to get this value as accurate as possible so that the resulting data from the test will be as highly reliable as possible.
<b>Density (g/cm<sup>3</sup>)</b>	The density of the metal sample.

<b>Equiv. Wt.</b>	This is the mass of the metal species that will react with one Faraday of charge. For an atomic species equivalent weight = $AW/n$ , where $AW$ is the atomic weight of the metal species [34].
<b>Beta An. (V/Dec) and Beta Cat. (V/Dec)</b>	These are constants related to the anode and cathode half reactions and is dependent of many factors. To obtain the exact values for these constants a Tafel test must be performed. The values in <i>Figure 18</i> is the built-in default values in the Gamry Instruments Framework [32], [34].
<b>Conditioning</b>	Whether on or off, for how long, and under what potential. This potential is vs. Reference [38].
<b>Init. Delay</b>	Whether on or off, this is when the $E_{OC}$ is measured. The last point taken here is where the Open Circuit Potential is regarded to be [38].
<b>IR Comp.</b>	This is selected if IR compensation was used [38].

By using a combination of the Gamry Instrumental Framework built-in Default values, calculations, advises\*, and performing a numerous testing with different Input values, it was observed that the parameter values presented in *Figure 18* usually gave a relatively stable measurement. These values are based on metal samples composed of C1018 Mild Steel with consistent area, which makes values such as "Density", "Equiv. Wt" and "Sample Area" to be constant for this specific metal species.

If any uncertainties towards what Input values, the Default values can be selected by clicking on the "Default" button showed in *Figure 18*. Note that when using this setting, the Sample Area is set to be  $1\text{cm}^2$  and is highly recommended to be changed. This is because of the LPR measurement technique is very area depended in order to get the most accurate data results, and hence an inaccurate surface area can result in an unreliable data result.

Since the exact values for the  $\beta_a$  and  $\beta_c$  constants required a high amount of knowledge on the Tafel measurement it was not explored in this thesis, and thus the impact of changing these values was not explored [32]. The built-in default values for these constants presented in *Figure 18* was used in every LPR measurement performed.

## 2.2.2 – During testing

### The Open Circuit Potential ( $E_{OC}$ ) measurement

After the Input values have been selected, the LPR measurement is initiated by clicking “OK”.

At first, the Metal Sample’s  $E_{OC}$  is analysed as in *Figure 19*. This measurement is also being saved, making it possible to evaluate the stability of the  $E_{OC}$  measurement. The better the stability the more accurate the LPR measurement will be, as the  $E_{OC}$  value should be relatively close to the  $E_{corr}$  value in the resulting data [34]. If  $E_{OC}$  measurement varies a lot, then the test results may over- or underestimate the corrosion rate behaviour. The Reference Electrode measures the  $E_{OC}$  potential relative to its own known potential and samples the data as illustrated in *Figure 19*. This measuring will continue until it reaches a certain stability, which is determined by the Input value “Init. Delay” in *Figure 18*.

When a stable  $E_{OC}$  is achieved, the final value is registered and used as a reference point for the LPR measurement if the “vs.  $E_{OC}$ ” is selected.

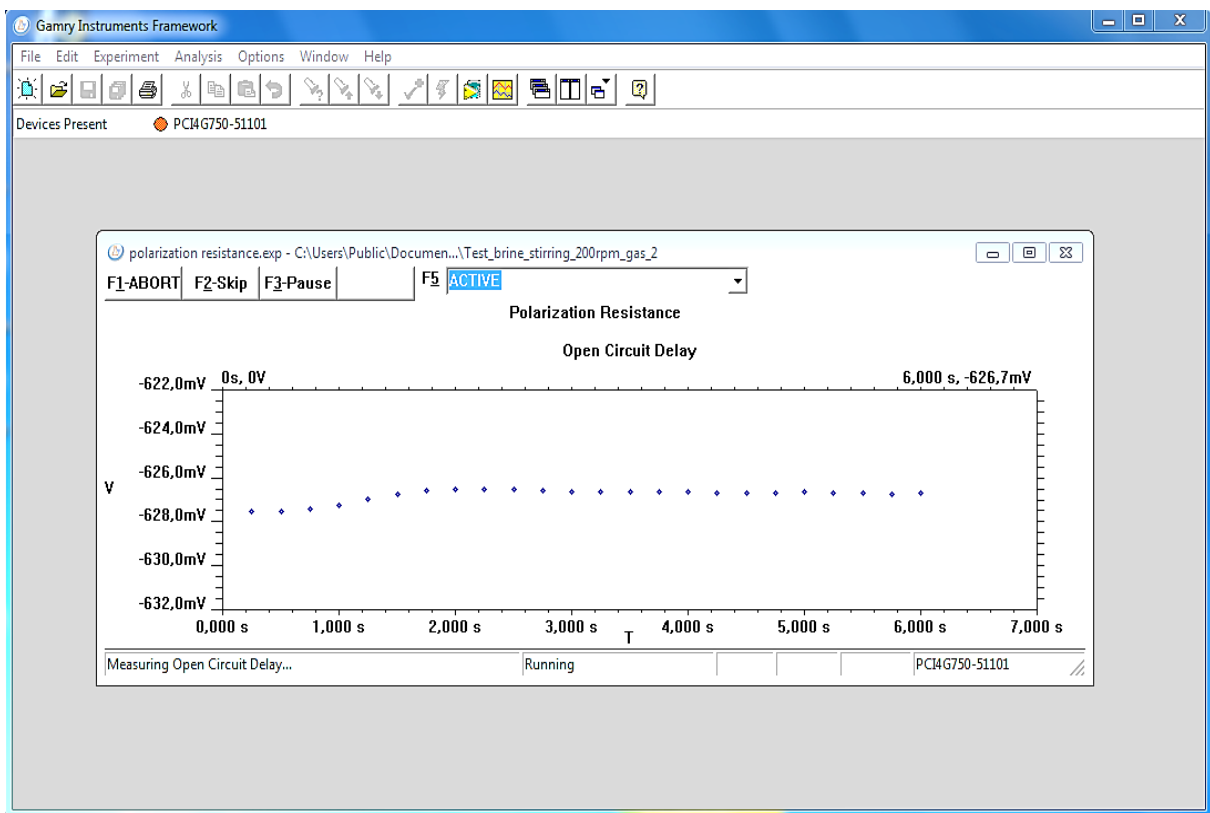


Figure 19: Screenshot of an Open Circuit Potential measurement performed in the laboratory.

## The LPR measurement

When the LPR measurements starts, the initial E(V) potential is applied relative to the measured  $E_{OC}$  value and increasing to the Final E(V) potential, with continuously data sampling as illustrated in *Figure 20*. During the data sampling, the data points will frequently alternate between a more positive and a more negative current ( $I(\mu A)$ ) as the applied potential (E(V)) increases towards a more positive region. This is normal due to the anodic and cathodic half-reactions are frequently “switching” [29]. The data will appear very scattered in the beginning because of the small potential ( $10^{-3}$ ) and resulting current ( $10^{-6}$ ), nevertheless, as the measurement continues the data collection will show a more distinct trend.

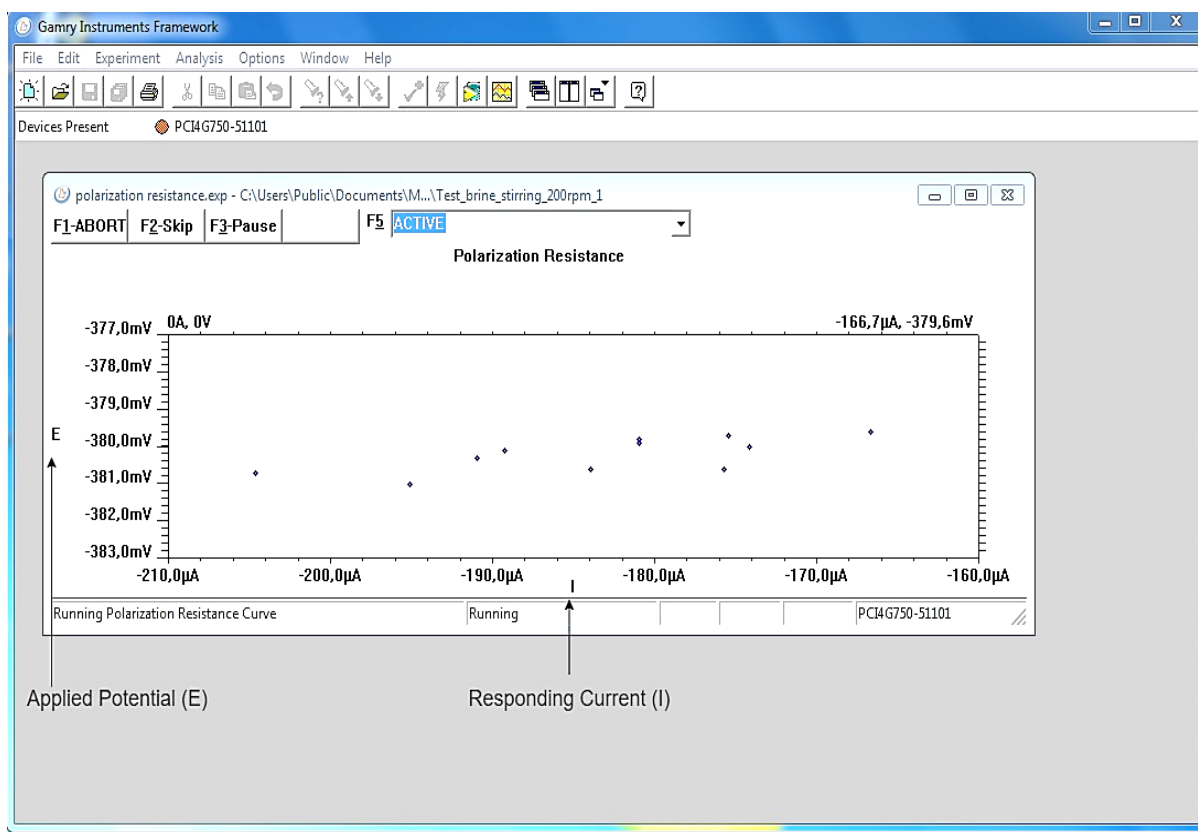


Figure 20: Screenshot of a running LPR measurement performed in the laboratory.

### 2.2.3 – Output values/Experimental results

After the test is done the Potentiostat stops and gives a command “Experiment – done”. By clicking on “F2 – Skip”, the results are saved, and a new test can be initiated if desired. If the “F1 – ABORT” is pressed the data will not be saved and cannot be restored.

#### **The Gamry Echem Analyst**

The Gamry Echem Analyst sub-program is used when the collected data from an experiment needs to be analysed\*. This can be done by clicking on “Analysis” in the open “Gamry Framework” program as presented in *Figure 16* and selecting the desired test to analyse.

In the Gamry Echem Analyst, a plot model of the raw data collected from the performed experiment is presented as illustrated in *Figure 21*. An in-depth clarification of the parameters in *Figure 21* can be found in *Table 3*. The potential versus current plot shows all the data sampling that has been collected during the LPR measurement, where the trend and shape of the plot is depending on the Input values and the environmental conditions in the experiment performed.

If the data seem to have a high deviation between each point, it can often be seen that the measurement is in micro amperes, and therefore makes the deviation not so significant after all or alarming\*. A linear trend of the corrosion behaviour can still be very well-defined and give a good illustration of the corrosion behaviour.

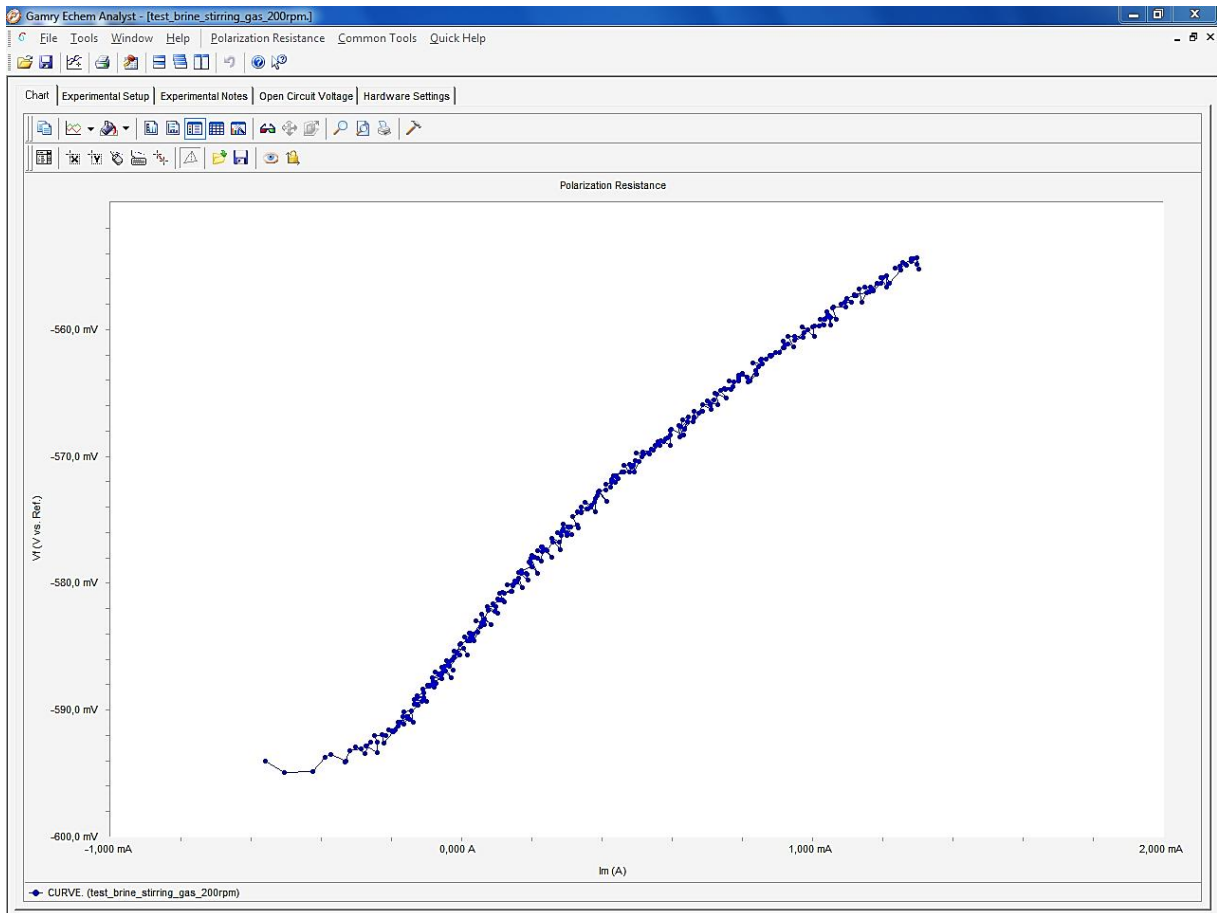


Figure 21: Screenshot of a potential versus current plot from a performed LPR measurement at the laboratory.

Table 3: Clarification of Axis in Figure 21.

<b>Y-axis: Vf (V vs Ref.)</b>	Shows the potential applied relative to the selected reference point. Here the reference point is the measured $E_{OC}$ value. The scaling is a result of the Input values chosen in Initial E(V) and Final E(V).
<b>X-axis: Im(A)</b>	Shows the responding current to the applied potential. The $E_{OC}$ value can be found at $I_m(A) = 0,000$ A, and therefore a zero current is measured.

### Toolbox menu

In Figure 22 the Toolbox menus is presented with some the different commands available in the Gamry Echem Analyst sub-program.

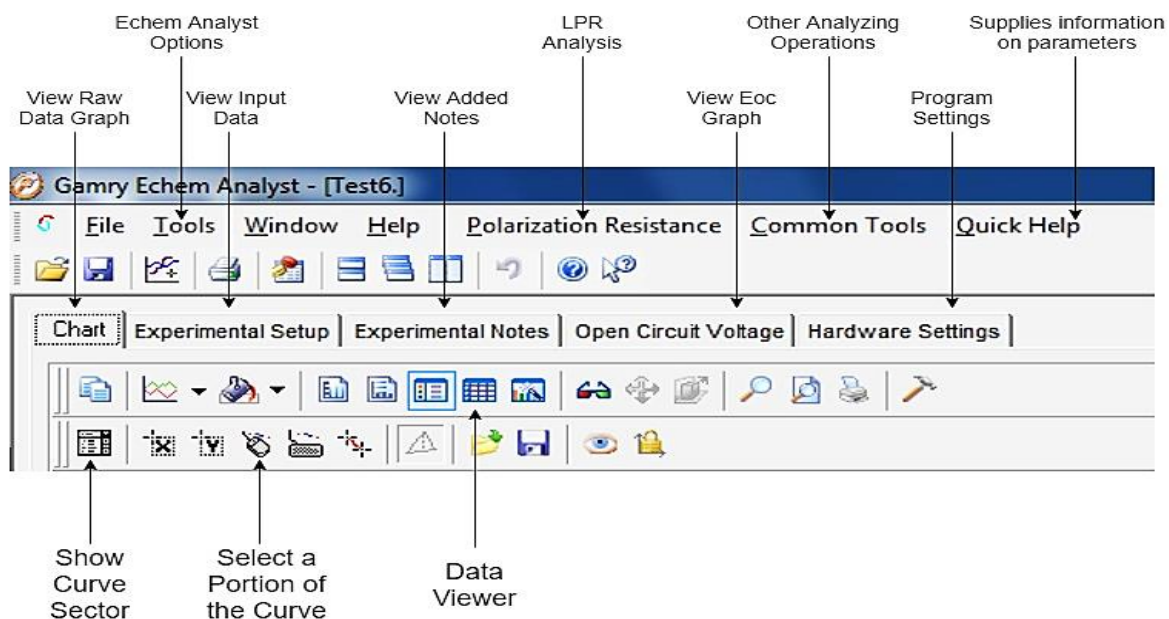


Figure 22: Screenshot of Toolbox menus in Gamry Echem Analyst with nametags and locations taken at the laboratory.

### Open Circuit Potential

By clicking on the "Open Circuit Voltage" in the toolbox menu in Figure 22, the measured  $E_{OC}$  and its behaviour is presented as in Figure 23. In Figure 23 it can be observed that the desired degree of stability is achieved at around 10 seconds. The degree of stability of the Open Circuit Potential can be evaluated and determined if it is acceptable or not.

The  $E_{OC}$  value which has been used as a reference point during LPR measurement can be observed by clicking on the "Experimental setup" in Figure 22, which is presented as illustrated in Figure 24. In addition, all the selected Input values that has been used are also presented as in Figure 24.



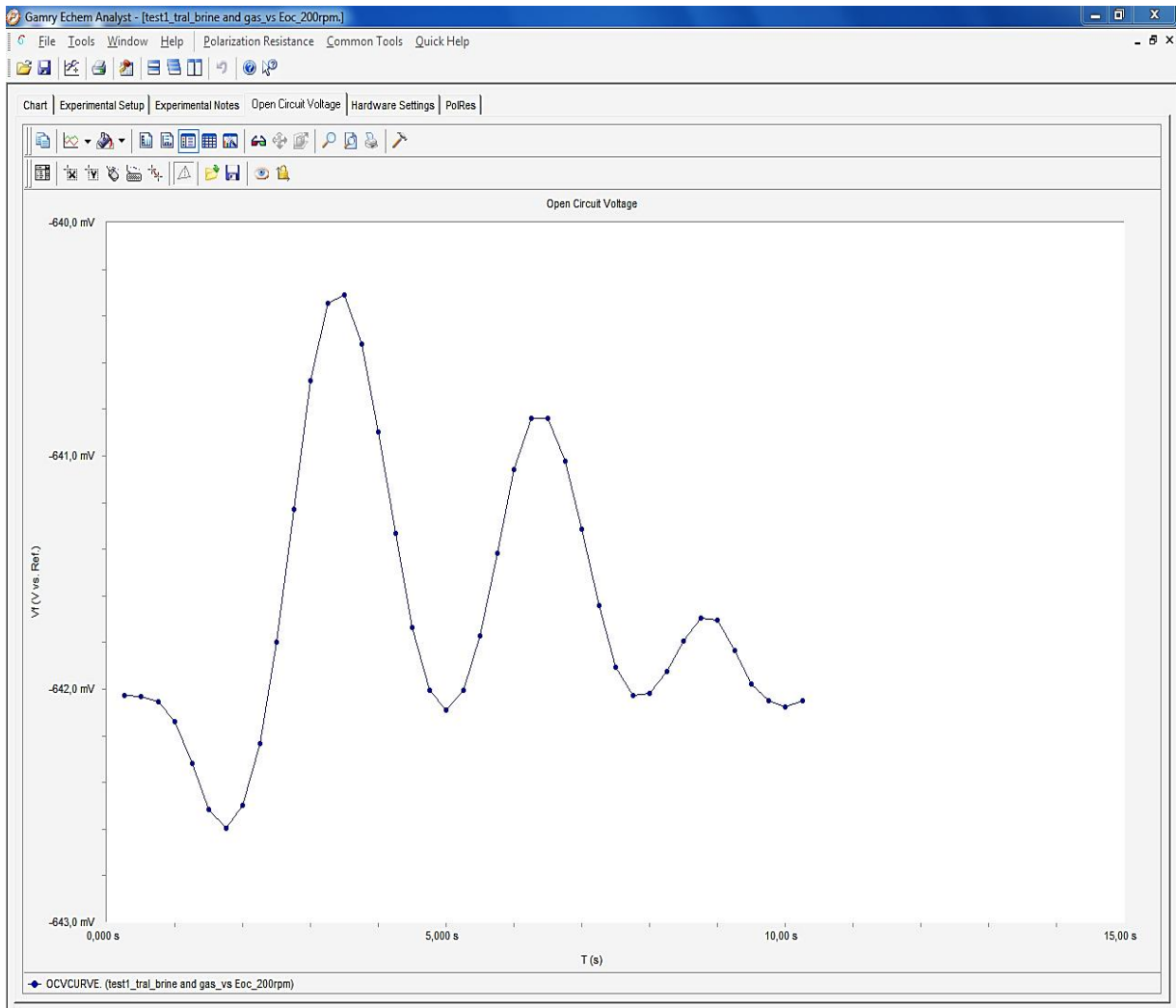


Figure 23: Screenshot of a  $E_{oc}$  measurement over a time period done in the laboratory.

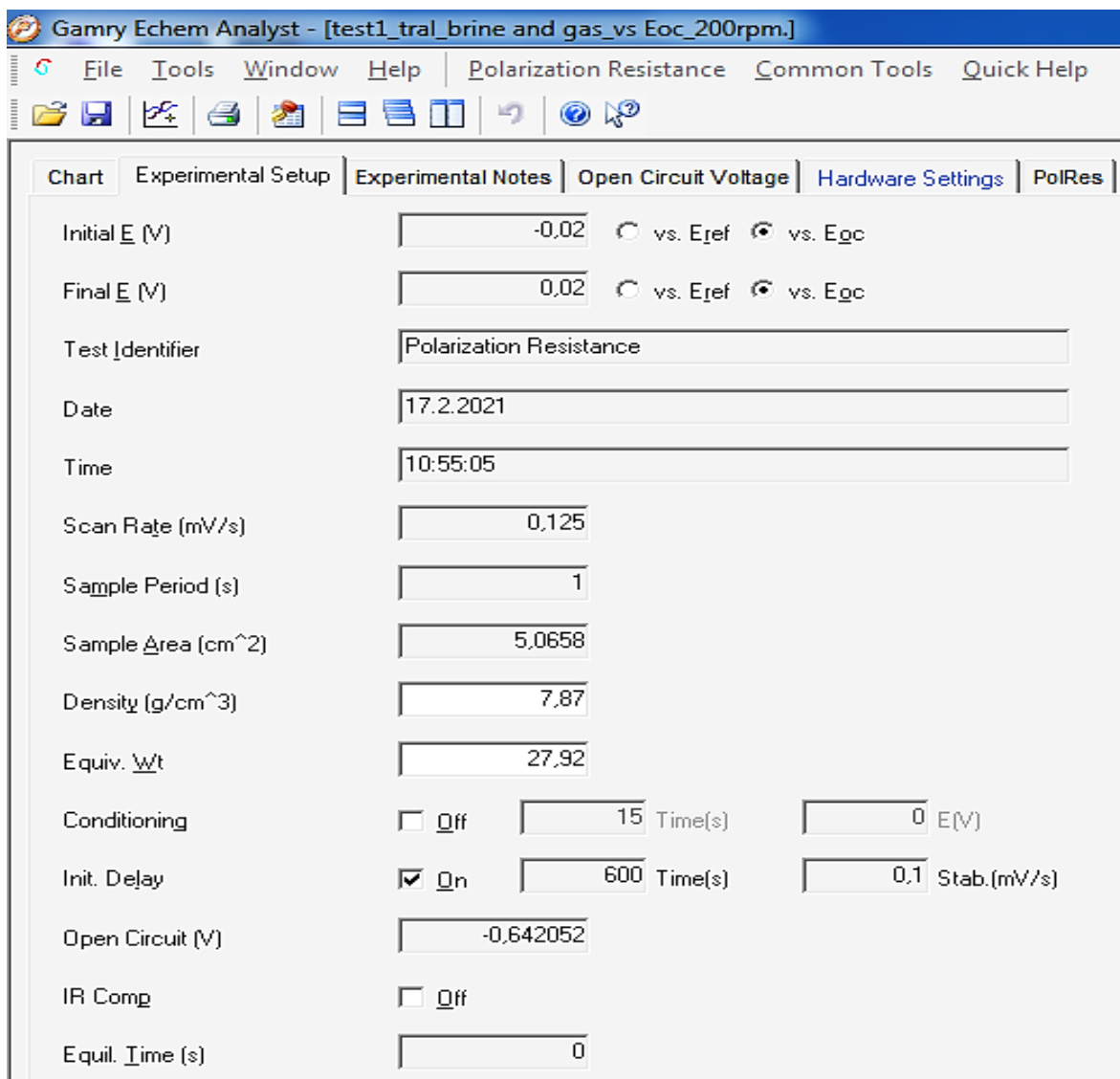


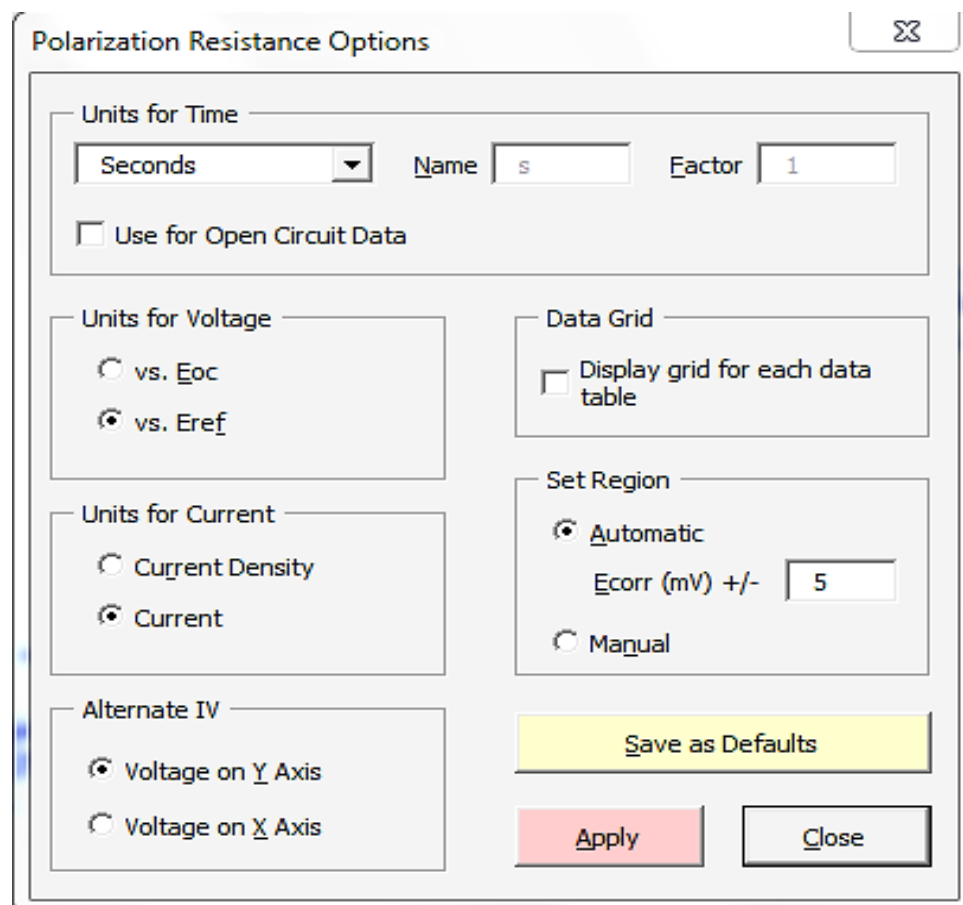
Figure 24: Screenshot of the Experimental Setup values used during a LPR measurement performed in the laboratory. The  $E_{oc}$  value measured can be observed as "Open Circuit (V) = -0,642052".

## Linear Polarization Resistance

The corrosion rate can be determined in two ways when using LPR measurement. By “freehand” with manually selecting the desired voltage region to analyse or using the “Automatic Set Region” were the Gamry Echem Analyst uses a selected consistent voltage region to analyse over [38].

Using “The “Automatic Set Region” was seen to be the most preferable, as this ensured an exact voltage region to analyse over in every test performed. This also ruled out the trouble of achieving the precise analysing region manually.

When using the “Automatic Set Region” the desired region to perform the analysis over can be selected when clicking on “Polarization Resistance” at the toolbox-menu in *Figure 22*, and further clicking on “Option” in the roll-down-menu. The window illustrated in *Figure 25* is then presented, were an in-depth clarification of the parameters can be found in *Table 4*. These clarifications can be presented when placing the mouse arrow pointer over each parameter in the “Option” menu.



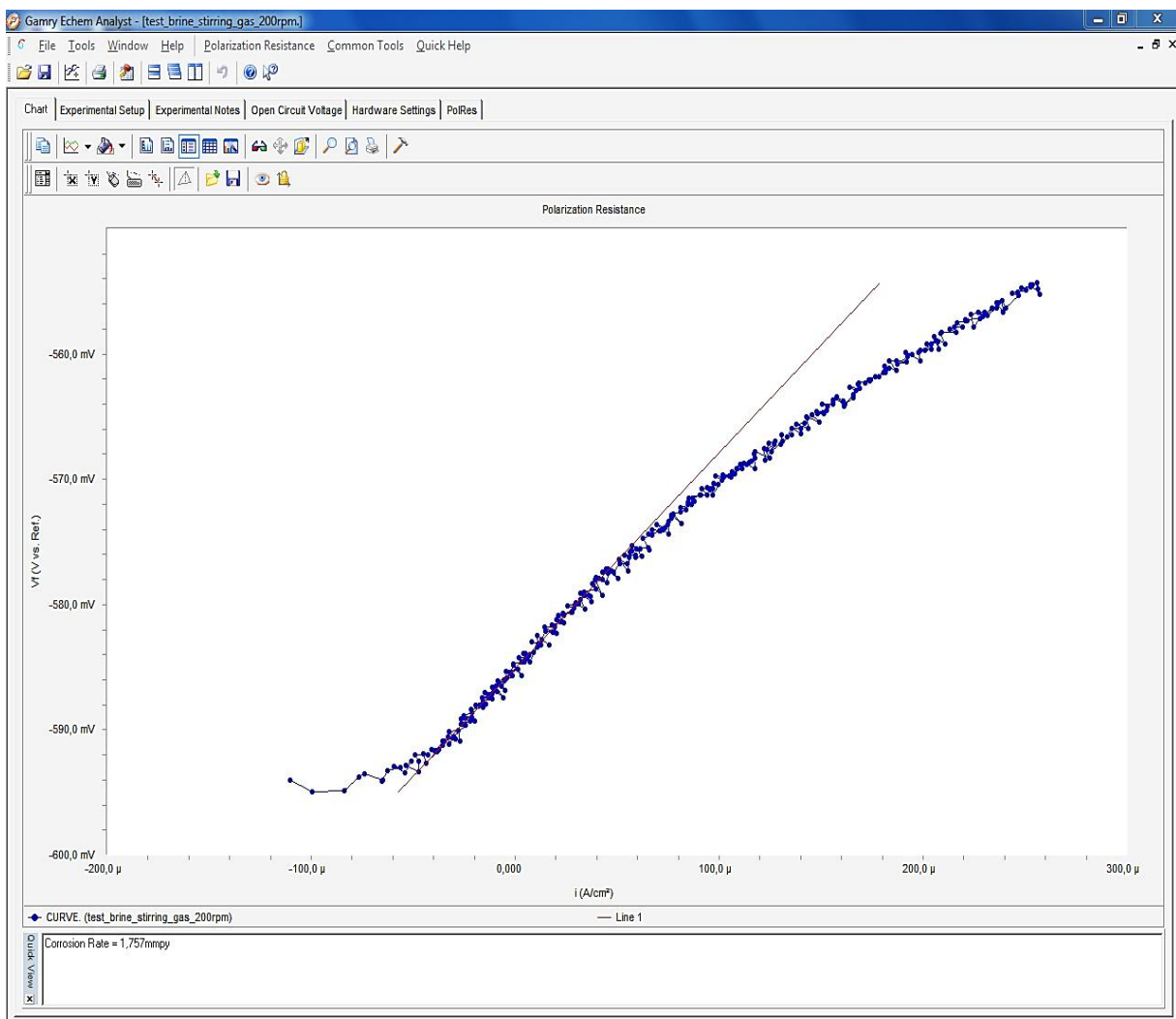
*Figure 25: Screenshot taken at the laboratory of the “Option menu” presented in the Gamry Echem Analyst program.*

Table 4: Clarification of parameters in Figure 25 [38].

<b>Units for Time</b>	The unit of time that is used.
<b>Units for Voltage</b>	How the applied potential is presented in the resulting data plot. When the "vs E <sub>OC</sub> " is selected, the potential is presented as a range is relative to a point zero. When the "vs E <sub>ref</sub> " is selected, the potential is presented as a range relative to the included E <sub>OC</sub> .
<b>Units for Current</b>	How the responding current is presented in the resulting data plot. When the "current" is selected, the current is presented in Amperes (A) without taking account for the Metal Sample's area. When the "current Density" is selected, the current is presented in Amperes per square centimetre (A*cm <sup>2</sup> ), the area of the Metal Sample is taken in account. Since the amount of current measured relative to the exposed metal surface area provided a more realistic data result, the current density was advised to be used*. It is also common to use current density in polarization resistance data [32].
<b>Alternate IV</b>	What parameter is presented in the axis.
<b>Data Grid</b>	If the data grid is preferred or not.
<b>Set Region</b>	At what potential range the Corrosion Rate is being calculated from. This can be changed if desired but is normally equal or less than ±20mV [32], [34].
<b>"Save as Default"</b>	If selected, the changes done is set as default values.
<b>"Apply"</b>	When clicking "Apply" the Gamry Echem Analyst will check if you are sure about the selected changes, followed by asking for the β <sub>a</sub> and β <sub>c</sub> values before performing any calculations.

When LPR measurement is performed, the Gamry Echem Analyst will perform an estimated linear fit of the  $R_p$  over the  $E_{OC}$  reference point within the desired voltage analysing region, and directly calculates the Corrosion Rate by using the  $R_p$  slope. This is illustrated in *Figure 26*, with the red line representing the performed linear fit and Corrosion Rate presented in the “Quick View” right below the plot.

When there is a negative current present relative to “ $i(A/cm^2)=0,000$ ” this indicates that there is mainly reduction occurring, and when the current converts to positive it indicates that mainly oxidation is occurring [28].



*Figure 26: Screenshot of LPR test current measurement and corrosion rate calculated performed in the laboratory.*

By clicking on the “PolRes” in the toolbox menu, a detailed list of the collected data and performed calculation from the LPR measurement is presented as illustrated in *Figure 27*. An in-depth clarification of the parameters presented in *Figure 27* can be found in *Table 5*.

Parameter	Value
Lower Fit Limit	-589,6 mV vs. Ref. (Pt# 35)
Upper Fit Limit	-579,7 mV vs. Ref. (Pt# 120)
Beta A	120,0e-3 V/decade
Beta C	120,0e-3 V/decade
I <sub>corr</sub>	151,3e-6 A/cm <sup>2</sup>
E <sub>corr</sub>	-584,7 mV
R <sub>p</sub>	172,2 ohms*cm <sup>2</sup>
Corrosion Rate	1,757 mmpy
test_brine_stirring_gas_200rpm.	

*Figure 27: Screenshot of “PolRes” data from LPR measurement done in the laboratory.*

*Table 5: Clarification of parameters in Figure 27 [34], [38].*

<b>Lower Fit Limit</b>	This is the lowest point of the analysis region selected for corrosion rate calculation, relative to the selected reference point (“vs. E <sub>oc</sub> ” or “vs. E <sub>ref</sub> ”).
<b>Upper Fit Limit</b>	This is the highest point of the analysis region selected for corrosion rate calculation, relative to the selected reference point (“vs. E <sub>oc</sub> ” or “vs. E <sub>ref</sub> ”).
<b>Beta A and Beta C</b>	This is the beta values for the anodic half-reaction (Beta A) and cathodic half-reaction (Beta C).
<b>I<sub>corr</sub></b>	The estimated corrosion current at E <sub>corr</sub> [34].
<b>E<sub>corr</sub></b>	This is the corrosion potential, and for ideal cases the E <sub>corr</sub> and E <sub>oc</sub> (OCP) are identical, but when performing a corrosion experiment the

	metal surface can alternate and therefore these may not precisely match each other [34].
<b>R<sub>p</sub></b>	This is the resistance the metal has towards undergoing corrosion in the given environment [28].
<b>Corrosion Rate</b>	The estimated rate/amount of corrosion per unit of time, computed from the R <sub>p</sub> slope. The unit can be changed to a desired unit by changing the setting. Here it is in mmpy, which corresponds to millimetres per year.

The Corrosion Rate that is being calculated is only an estimated model of the metal's corrosion behaviour based on the testing environment, uniform corrosion is happening, metal composition and time. It should be highly emphasized that this type of corrosion rate calculation is only valid for uniform corrosion, and can dramatically underestimate the corrosion behaviour if or when localized corrosion occurs [28], [34].

The collected data can be easily inserted into Excel by marking all the desired data, and copy/paste it into the Excel sheet. If each separate datapoints collected in the test is needed, then this can be found by selecting the "Data Viewer" seen in Figure 20 below.

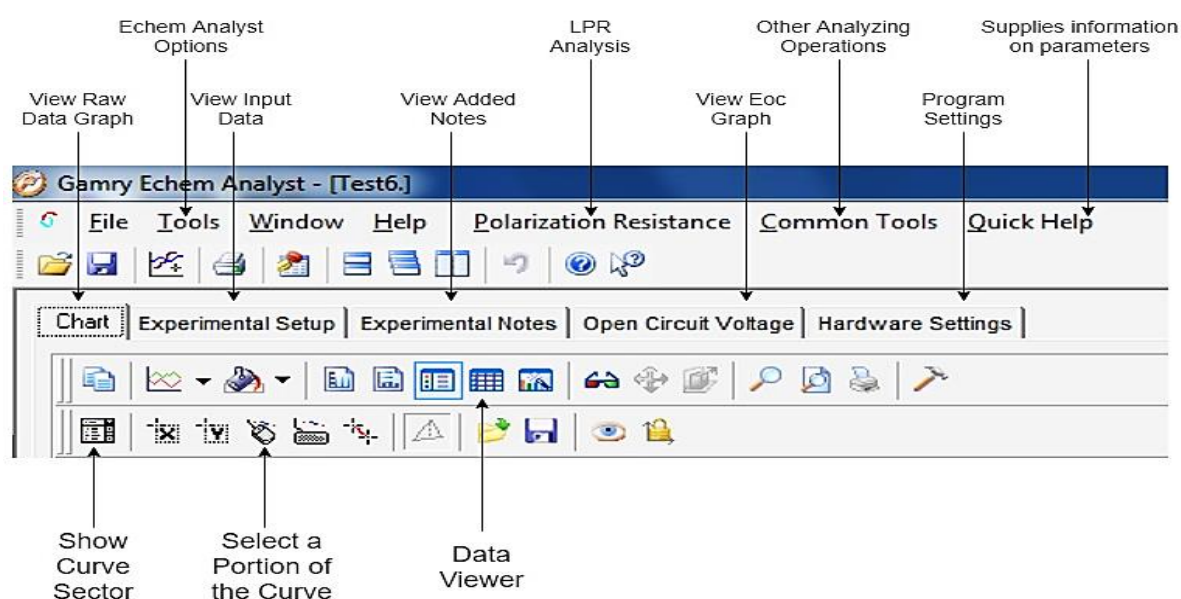


Figure 22: Screenshot of Toolbox menus in Gamry Echem Analyst with nametags and locations.

## 2.3 – Troubleshooting

### 2.3.1 – Leakage in Working Electrode

Leakage within the Working Electrode occurs when either the Metal Sample or Hex Nut is loose, gaskets are moved out of position or inaccurate fitting. This can happen if there is a lot of movement on the Connection Clamps to the electrode or if it is not assembled correctly.

Since the Metal Sample holder is a Stainless-Steel Rod, it will give a significant change in the experimental result collected from the LPR measurement if it receives a connection with the solution. This was observed when testing on C1018 Mild Steel through a high increase in the  $R_p$  value, a very low  $I_{corr}$  and Corrosion Rate, which can be seen in *Picture B-1* and *Picture B-2* in *Appendix C*.

If leakage is suspected, it can be observed through:

- Physical examination, where liquid within the Pyrex tube can be seen.
- Distinct or abnormal change in potential during  $E_{OC}$  measurement.
- Extremely steep exponential trend during LPR measurement.
- Unusual OCP presented in the “Experimental Setup”.
- Unusual high  $R_p$  in the “PolRes”, unusual low  $I_{corr}$  in the “PolRes”, unusual low Corrosion Rate.

If a great number of tests has been performed on the same type of Metal Sample, it possible to compare and evaluate the mentioned factors with good confidence.

### 2.3.2 – Overload Errors

Overload errors can present themselves due to many different factors, such as bad connections to the electrodes, bubble interference, and leakage. An explanation of each overload error is found in *Figure 26*. How the presence of overloads can affect the resulting data plot can be found in *Appendix C* as *Picture C*.



**I OVL** Indicates a **current overload**. Sample area may be too big or the battery/supercap/fuel cell generates too much current for the potentiostat hardware.

**V OVL** Indicates a **voltage overload**. The battery/supercap/fuel cell voltage is too high to measure, or the electrometer is disconnected and has drifted to the rails. Double-check that the white and blue leads are connected properly.

**CA OVL** Indicates a **control amplifier overload**. The potentiostat cannot supply enough current between working and counter leads to reach the desired potential at the working electrode. The blue or white lead could be disconnected, or the cell's uncompensated resistance is so high that the instrument reaches its compliance voltage.

**I ADC** Indicates that the **current channel A/D converter is railed**. Incorrect instrument settings were used during an EIS scan. The state of the cell may be changing too much during the AC measurement to get a valid reading.

**V ADC** Indicates that the **voltage channel A/D converter is railed**. Incorrect instrument settings were used during an EIS scan. The state of the cell may be changing too much during the AC measurements to get a valid reading.

*Figure 28: Screenshot of potential overloads errors that may occur in the Gamry Framework [50].*

### 2.3.3 – Rust deposits on Connection Clamps

Rust deposits on the Connection Clamps are not unusual, but the degree of rust must be evaluated. A severe amount of rust deposits on the Connection Clamps could give bad connection between the potentiostat and the electrodes due to signal disruption.

As experienced, this can be detected through:

- Errors occurring in the program when the experiment is ongoing.
- A distinct high pitch sound when the potential is applied during the testing.
- A high degree of gas bubbles occurs on the Counter Electrode and high amount of precipitate occurs from the Metal Sample at the Working Electrode.

When these factors present themselves, the Connection Clamps were to be taken off and cleaned on the inside of the Female Banana Plug and reattached. Changing the Connection Clamps can be necessary if the rust deposit is too severe.

### 2.3.4 – Choosing “vs. $E_{ref}$ ”

If choosing the “vs.  $E_{ref}$ ” as a reference point in the Input Values before initiating LPR measurement, it must be emphasized how it can affect and influence the whole experiment.

When using the “vs.  $E_{ref}$ ” command, the selected potential is applied relative to the Reference Electrode Potential\*. If the Reference Electrode has a known potential that is higher or lower than the Metal Sample’s  $E_{OC}$  value, it is needed to be taken in to account. The measured  $E_{OC}$  of the Metal Sample must be added to the Initial E(V) and Final E(V), in addition to the desired potential range\*.

If the  $E_{OC}$  potential is not added to Initial E(V) and Final E(V) when selecting the Input Values, extreme cases of corrosion can happen and result in unrealistic data sampling. In *Appendix C Picture E-1* and *Picture E-2* it is showed how the experimental result would look like after performing LPR measurement with “vs.  $E_{ref}$ ”.

### 2.3.5 – Clogging of the Glass Frit Tip

As mentioned before, the Glass Frit Tip on the Reference Bridge Tube contains small canals that ensures a stable connection between the solution and Reference Electrode. If these canals get clogged, the Reference Electrode will struggle to get readings during the LPR measurement and the Glass Frit Tip needs to be thoroughly rinsed or changed [51]. At a point during this thesis the Glass Frit Tip needed to be changed, and by investigation how it has been done by other it was done here in the following order [52].

#### **Changing the Glass Frit Tip**

This is done by first cutting the overlaying Teflon shrinking tube, making it easy to remove. After this is done a new Glass Frit is inserted into a new PTFE sleeve and put over the tip of the Reference Bridge Tube, with the Glass Frit flush with the Teflon shrinking tube.

It must be kept in mind that the purpose of the Glass Fritting is to supply a liquid junction between the solution and the Reference Electrode. Hence, the Glass Frit needs to stand at the very end of the Glass Tip on the Reference Bridge Tube, with the PTFE sleeve properly shrunken tight to hold it in place but not preventing it to function by covering it.

When the Glass Frit is in the optimal position, the PTFE sleeve is heated gently with a heating gun. The Glass Frit must be regularly adjusted to hold the desired position by using the fingertips during heating. After the PTFE sleeve is shrunken tight to the glassware, the Glass Frit is checked for heating damage and that it still is in the optimal position.

In *Figure 29* below is a picture taken at the laboratory of the Glass Frit Tip that was changed at the laboratory.



*Figure 29: Picture taken at the laboratory of the replaced glass frit tip.*

### 2.3.6 – Damaged Metal Sample

Since the Metal Sample is where the corrosion rate is measured, it is crucial to have this in the best condition as possible [37]. Any damage occurring on the Metal Sample can have a certain amount of risk of interfering with the experimental result.

If the Metal Sample is suspected to be a source of errors due to damage, it can be caused by and observed through:

- Visible scratches or rips on the Metal Sample surface.
- Unusual values when the  $E_{oc}$  measurement is performed.

- Unusual experimental results after performing an experiment when comparing to other performed experiments.
- Observed distinct visible lines under the cone-shaped Compression Gasket after performing experiment.
- Extreme localized corrosion.

### **Wet sanding and damage evaluation**

If visible scratches or rips in the Metal Surface is observed, it can be fixed by performing wet sanding. This was explored by using a very fine sandpaper (P1200 or finer) wetted with water and gently rubbing/sanding the Metal Sample surface. The more mirror polished the Metal Sample surface was, the better the experimental result where. When doing this it is possible to sand down the scratches gently without causing more damage. If the scratches are too large or deep this will not work and replacing the Metal Sample is recommended.

If unusual values are occurring during  $E_{oc}$  measurement or when observing the resulting data collected from experiment, it can be caused by visible or non-visible sources. If there are no visible sources for the errors, wet sanding the used Metal Sample as mentioned can reveal severe surface damage that is not easily detected otherwise.

The degree and location of the damage must also be evaluated. It is necessary to observe if the scratches reach from the centre hole and out of the area of the Compression Gasket sealing surface. If they do then this can provide a pathway for the water molecules under the sealing surface and possibly give inaccurate data reading. If they are located only under the sealing surface and not further, then it may not be of any concern. If the scratches are located on an un-sealed surface, then the severeness and depth may need to be thoroughly evaluated. Performing some blank tests to check the stability and behaviour of the Output parameters is therefore recommended.

### **Extreme localized corrosion**

If extreme localized corrosion occurs it can underestimate the corrosion rate enormously [28], [34]! If this is observed, the data collected should be carefully evaluated before a conclusion is to be made. Localized corrosion can be observed as either small holes/cavities or patches with and can lead to difficulty when replicating the experiment is desired. Extreme localized corrosion is difficult to predict as it can be a consequence of many different factors.

In *Figure 30* below is two pictures of a Metal Sample that was used for LPR measurement in this thesis at the laboratory at UiS, which received a severe attack of localized corrosion. At first black patches expanded over the metal sample during testing. When the metal sample was taken out from the solution, these patches turned green (left), that further transformed into brown/yellow patches within a short period of time (right).

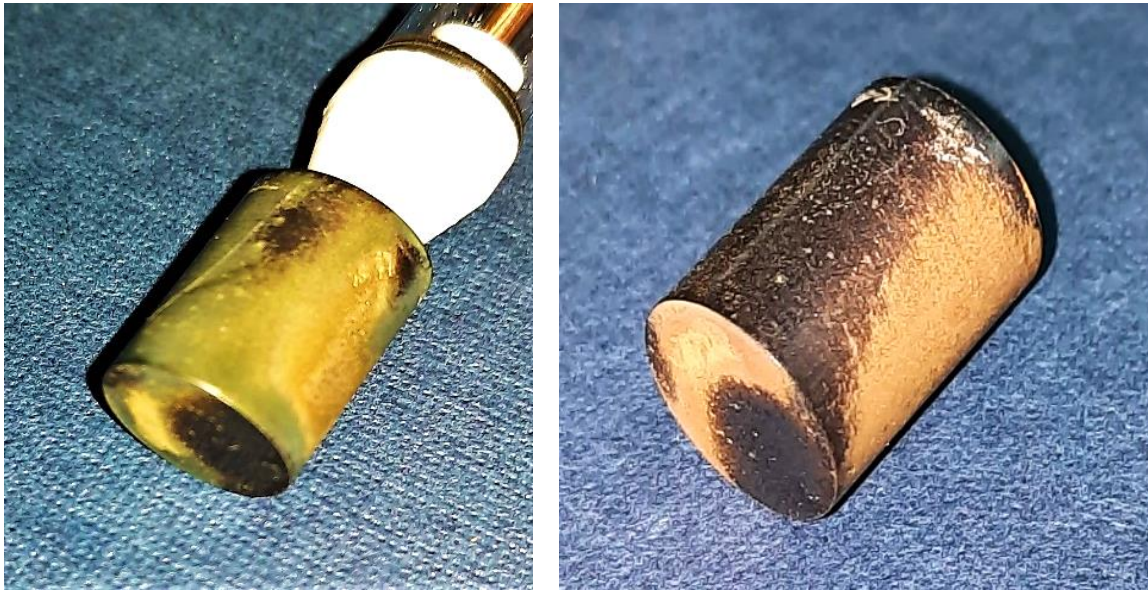


*Figure 30: Pictures taken of a Metal Sample in the laboratory having localized corrosion.*

### 2.3.7 – Bubble accumulation

Bubble accumulations on specific areas can also interfere with the ongoing data reading [37]. If bubbles accumulate on large areas on the Metal Sample surface it can result in poor current reading without any overload errors occurring. This can also give localized corrosion at the surface where the bubble is positioned, and furthermore can result in an inaccurate data reading.

If bubbles accumulate on the Glass Frit Tip at the Reference Bridge Tube, it can result in an inaccurate data reading because of signal blocking to the Reference Electrode. If bubbles occur inside the Reference Bridge Tube, it can interfere with the data reading due to blocking of signals. This can also result in overload errors.

In *Figure 31* below is two pictures of a Metal Sample that was taken before and after a LPR measurement was performed at the laboratory at UiS, where bubble accumulation had occurred. When comparing the Metal Sample before (Left) and after (Right) LPR measurement, the position of each bubble had can be easily seen as they caused localized corrosion to occur at that position.

As also seen in *Figure 31* the Metal Sample had surface damage around the centre hole. This damage was probably caused during the production of this Metal Sample, and the LPR measurement was performed solely to check if it had any influence on the experimental result. The experimental result can be found in *Appendix A – Detailed Data Results, Blank testing as Blank Sample 3*, where it seems that it did not have any influence as the corrosion rate remained in the higher region. This can be because the damage was properly covered by the Teflon Compression Gasket.

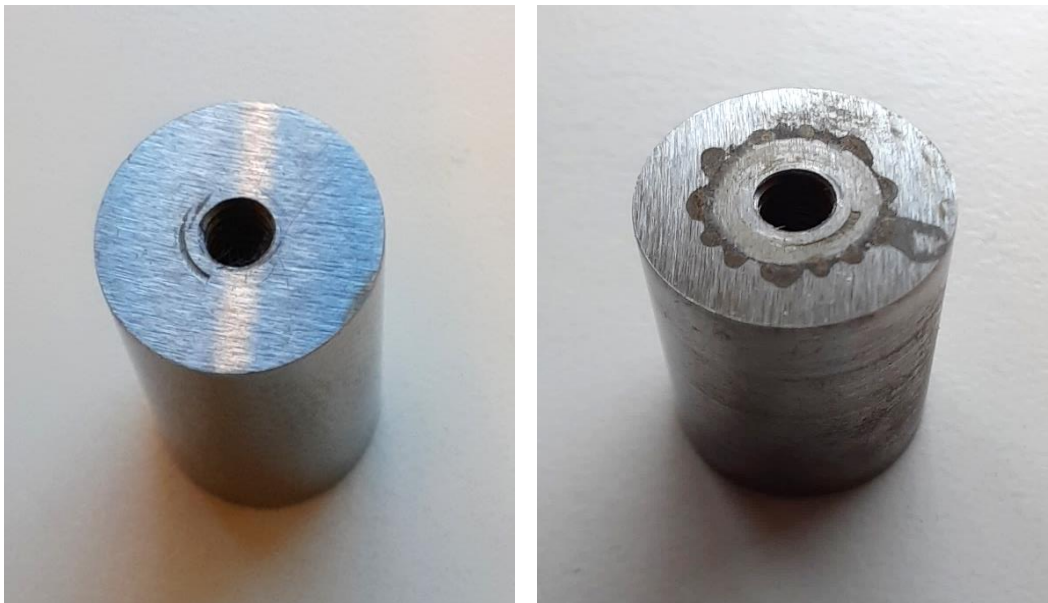


*Figure 31: Pictures taken of a Metal Sample in the laboratory having bubble accumulation during LPR measurement. Left is before LPR measurement, and right is after the LPR measurement.*



## CHAPTER 3 – METHODS AND PROCEDURES

The following methods and procedures presented can be changed if other requirement or factors are desired, but this was not explored in this thesis due to time limitations. The performed tests were done mainly to get an understanding of how the LPR measurement technique operates, investigating what parameters and conditions gave the best result, and to gain enough confidence around the specific testing method that corrosion analysis could be performed.

The following sub-chapters presents the selected testing parameters, conditions, methods, procedures, and preparations consistently used in this thesis.

### 3.1 – Selected Parameters and conditions

When the following situations was tested in this thesis, a set of parameter values and environmental conditions were consistently used which were selected by performing numerous amounts of testing under different conditions. These are presented in the following sub chapters, with some thoughts around why these where considered to be reasonable.

#### 3.1.1 – Testing Sequence

By consulting literatures on how other researchers have performed LPR measurements, it was observed that it was generally performed multiple times within a time range [3], [4], [27], [53], [54]. By taking account for these observations and further recommendation on performing multiple testing, the following testing sequence was put together and used consistently [35].

The number of tests performed per set up were selected to be a minimum of 5 tests, with a 30 minutes time interval in-between. By replicating and repeating this sequential testing procedure on separated days, a higher amount of data was collected with a lower amount of deviation. By using this strategy, it was considered to be possible to exclude the data containing a high amount of deviation as all the testing conditions for each set up were consistent.

If a high amount of deviation was observed in a testing sequence, then the set up and testing sequence was repeated until a consistent trend was observed. The deviation could be such as a suspiciously low corrosion rate when comparing the collected or a high deviation between each individual LPR measurement in the testing sequence. When considering what could be regarded as a suspiciously low corrosion rate where evaluated when the data in *Appendix A – Detailed data results, Blank testing – Blank 1 – Sequence 1* and *Blank 2 – Sequence 1* was compared, and furthermore comparing both of

the data collections to what other researchers as achieved under different environmental conditions as mentioned in the *Chapter 4.3 – Overall discussion*.

### 3.1.2 – Stirring

The stirring was set to 200rpm during testing, as it was desired to simulate the flow conditions inside the pipelines as much as possible. Testing with stirring at 250rpm and 300rpm was examined but resulted in a much higher derivation in-between each data sampling with poor reproductivity. Testing with stirring at 150rpm and lower resulted in a better data sampling but was considered to possibly be an unrealistic representation of the flow conditions within the pipelines.

### 3.1.3 – Gas Flow

The amount of gas flow to have under testing was selected to be in a lower scale, as a high gas flow during testing was observed to result in bubble accumulating on undesired regions. The data sampling was also observed to be poor when having a high gas flow during testing. For CO<sub>2</sub> pre-saturation it was experienced that a high gas flow for minimum 40 minutes accompanied with stirring at 250-300rpm resulted in achieving a pH≈4-5.

The pressurized CO<sub>2</sub> gas used was more than 99% vol. pure CO<sub>2</sub> gas. A picture of more detailed specifications can be found in *Appendix C as Picture D*.

### 3.1.4 – Parameters Input values and Methods used

Each testing parameters with the selected input values used is listed in *Table 6* below, accompanied with the analysing method used. Since these values and methods were observed through multiple testing to give a relatively good result, they were used consistent through all tests presented in the experimental results. Through risk evaluation of possible anomalies that could arise, it was decided that this would also cause this risk to be at a minimum.

*Table 6: selected Input values used in each parameter and analysing method.*

Input values	
<b>Initial E (V)</b>	-0,02 (Default values)
<b>Final E (V)</b>	+0,02 (Default values)
<b>Scan Rate (mV/s)</b>	0,125 (Default values)
<b>Sample Period (s)</b>	1
<b>Sample Area (cm<sup>2</sup>)</b>	5,1756 (Calculated)



<b>Density (g/cm<sup>3</sup>)</b>	7,87 (C1018 Mild Steel)
<b>Equiv. Wt.:</b>	27,92 (C1018 Mild Steel)
<b>Beta An. (V/Dec) and Beta Cat. (V/Dec)</b>	0,12 (Default values)
<b>Conditioning</b>	Not selected
<b>Init. Delay</b>	Selected: T(s) = 600s, Stab. (mV/s) = 0,1
Analysing method	
<b>IR Comp</b>	Not selected
<b>Test Method</b>	Polarization Resistance
<b>Measuring Method</b>	Linear Polarization Resistance measurement
<b>Analysing Method</b>	Automatic Set Region: E <sub>corr</sub> ±5mV

### 3.1.5 – Metal Sample

The Metal Sample used for corrosion analysis was C1018 Mild Steel with the following composition relative to %Fe presented in *Table 7*. This composition was given in the certificate that followed with the Metal Samples received from the producer, which can be found in *Appendix C* as *Picture A*.

*Table 7: Metal Sample Composition relative to the %Fe.*

<b>Chemical Composition (%):</b>	
C	0,18
Mn	0,78
P	0,025
S	0,025
Si	0,20

The Metal Sample was washed with acetone before and after testing to remove surface contaminations.

### 3.1.6 – Brine Solution

The brine solution used was made up of 3,5wt% of NaCl per 100ml distilled water and degassed to remove as much O<sub>2</sub> gas as possible. This was scaled up to 3 L and degassed in a vacuum flask accompanied by a continuous stirring at 200-300rpm.

For each set-up 800ml of brine solution was used. This was because of ratio conditions, as a higher amount of brine solution required more corrosion inhibitor and hydrocarbon mix to be added. A lower

amount of brine solution was observed to result in the Metal Sample Surface being contaminated with hydrocarbon mix on due to the rising vortex from the stirring.

### 3.1.7 – Hydrocarbon Mix

The hydrocarbon mix used was composed of Xylene (mixture of isomers) and n-Decane, with a mixing ratio of 1 part Xylene and 9 parts n-Decane. This was measured out and mixed in a glass flask.

The volume of hydrocarbon mix used in each experiment was 1:19 relative to the amount of brine used, which was in an addition to the brine used.

It was observed that if the volume brine used was 700ml or lower, then droplets of hydrocarbon mix would enter the brine solution and contaminate the Metal Sample surface in the form of a mild protective film. This oil film may furthermore prevent corrosion to happen in a more realistic scale, as it hinders the water molecule to enter the metal sample surface.

### 3.1.8 – Corrosion Inhibitor

Each of the corrosion inhibitors (CI's) that was investigated in the experiments in this thesis are listed below:

- Luvicap EG: A commercial Kinetic Hydrate Inhibitor (KHI) polymer based on vinylcaprolactam presenting some CI abilities. Pre-solved in ethylene glycol from manufacturer, having a concentration of 41,1% KHI. When testing this, it was regarded at 100% pure since it is not a real CI.
- Imidazoline: A fatty acid surfactant used as CI.
- Polymer: An experimental CI polymer made in the laboratory at the UiS.

A concentration of 500ppm in 800ml of brine was used consistently in all the performed tests, with the corresponding weight tabulated as listed below in *Table 8*.

*Table 8: The corrosion inhibitors that was investigated, with percent CI in each compound and weight used to accomplish 500ppm.*

Chemicals Used	Amount CI present (%)	Corresponding weight (g/ml)
Imidazoline	100% CI	0,4g CI/800ml brine
Polymer	25% CI	1,6g CI/800ml brine
Luvicap EG	100% KHI/CI	0,4g CI/800ml

Before the corrosion inhibitors were inserted into the brine solution it was observed that pre-dissolving them in a small separated glass container with 2-5ml brine from the Main Cell often made the CI's easier to insert into the brine solution, as the CI's are often composed of very viscous fluid.

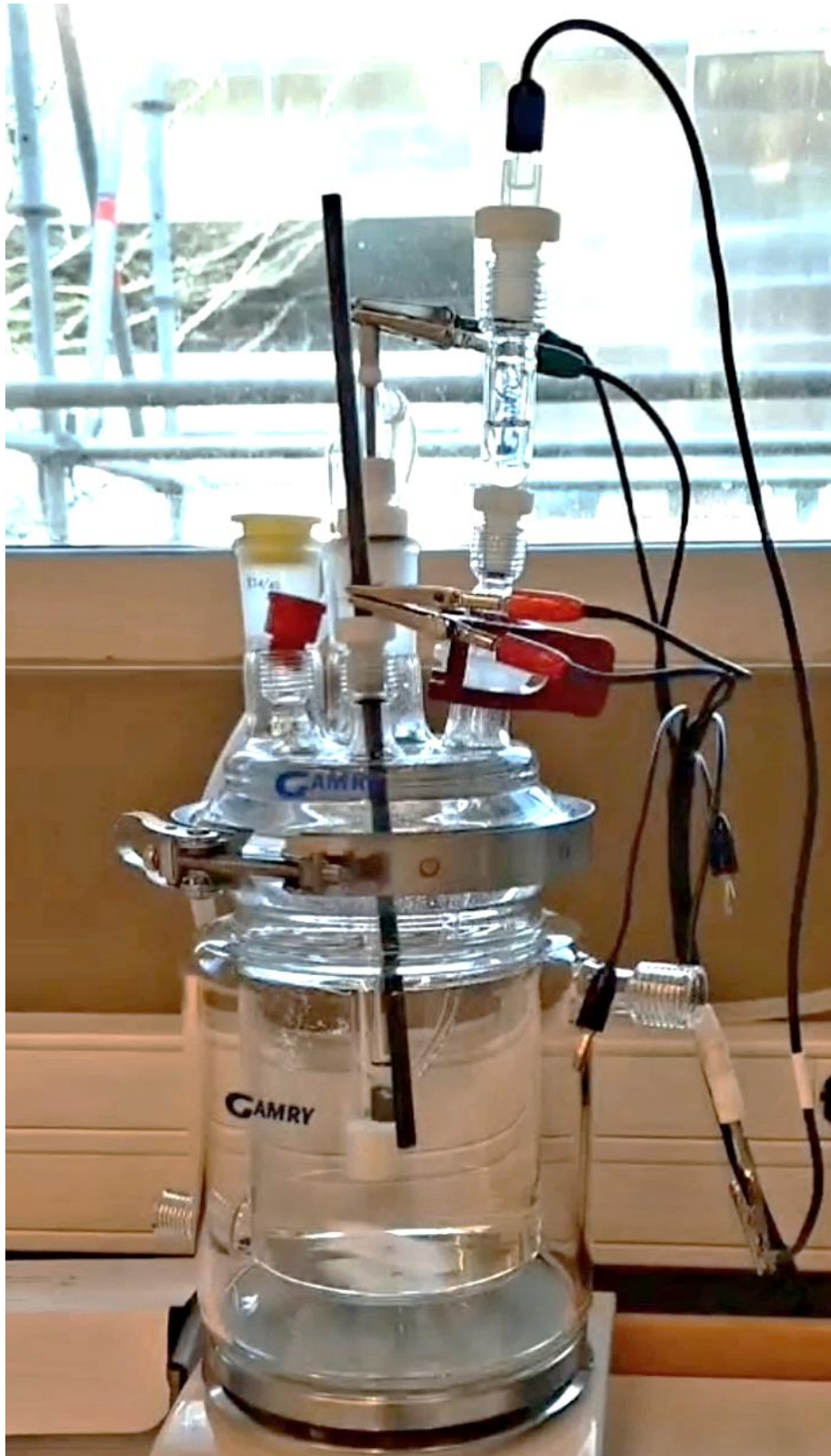


*Figure 32: Picture of a bubble test performed at the UiS laboratory.*

## 3.2 – Experimental Procedures

Each of the individual experimental procedure presented were put together in the following order by using the experience collected when using the equipment and was mainly used in each of the experiments performed in this thesis. The procedures presented can be modified if desired, as they are highly general and based on the assembling procedures presented in Chapter 3.

### 3.2.1 – Brine

#### Requirements:

#### Equipment:

- The Main Cell
- Seals for the open ports
- Reference Bridge tube
- Ag/AgCl Reference Electrode
- Graphite Counter Electrode
- Working Electrode
- Magnetic stirrer with Magnetic Pill
- Pipette

#### Solutions:

- 800-1000ml brine, with a concentration of 3,5wt% NaCl per 100ml distilled water
- Distilled water, for washing

#### Procedure:

1. The preparation started with visually checking, cleaning, and assembling all the required parts as mentioned in “**3.1 – Assembly**”. Consult this section for details.
2. The Main Cell parts were visually checked for contamination and damage, rinsed with distilled water before being filled with 800ml brine and mounted together. The Teflon stirring pill was added trough one of the open ports, and the Main Cell was placed on the magnetic stirrer with “anti-slip” in-between. All the open ports on the Cell Top were sealed until the rest of the preparation was done. The stirrer was set to 200rpm.

3. The Reference Bridge Tube and Glass Frit Tip was visually checked for contamination or damage, thoroughly cleaned multiple times inside and outside before brine was inserted.
4. The Reference Bridge Tube was inserted through the SJ28-to-#7-port in the Ball Joint by gently wiggling and secured by tightening the Teflon seal.
5. The Reference Electrode was rinsed with distilled water before the #11-Bushing and O-Ring was slid on and inserted to the #11-port on the Reference Bridge Tube. When the tip of the Reference Electrode was observed to be fully submerged, the #11-Bushing on the Reference Electrode was tightened.
6. The Counter Electrode was rubbed with a wet paper to remove contaminations and rinsed with distilled water. The #7-Adapter and O-Ring was slid on the Counter Electrode, before being inserted into the #7-port on the Cell Top and secured into place by tightening the #7-Adapter.
7. The parts for the Working Electrode were visually checked for contamination and damage before being cleaned, assembled, and inserted to the #24/40 Centre Port on the Cell Top.
8. After the Working Electrode was inserted, the Glass Frit Tip on the Reference Bridge Tube was adjusted to the right position, about 3-5 millimetres from the Metal Sample surface.
9. The unused ports were left with the sealing on, and the Connection Clamps were properly attached to each Electrode. The distance between the Metal Sample surface and the Glass Frit Tip on Reference Bridge Tube was double checked.
10. The test was initiated as explained in **“3.2 – The Testing Sequence”**.

During testing the electrodes were regularly checked visually for anything that may or may not be desired. This could be for example bubbles trapped between the metal surface and Glass frit Tip, extreme localized corrosion, or leakage.

After testing:

When all the desired tests were done, the equipment were disassembled and cleaned in the following procedure.

1. The Connection Clamps were disconnected from each of the Electrodes.
2. The Reference Electrode was removed from the Reference Bridge Tube and rinsed with distilled water.
3. The Reference Bridge Tube was gently taken out from the Ball Joint at the Cell Top and rinsed with distilled water inside and outside. All the parts on the Reference Bridge Tube were taken off and rinsed with distilled water. The Glass Frit Tip was thoroughly rinsed with distilled water multiple times.
4. The Counter Electrode were taken out of the Main Cell and rubbed with a wet paper to remove any salt deposits. All the parts on the Counter Electrode was taken off and rinsed with distilled water.
5. The Working Electrode was taken out and disassembled. All the parts were rinsed with distilled water. The Metal Sample was cleaned with a brush and acetone.
6. The Main Cell was opened, and brine removed. The Ball Joint was disassembled, and all the parts in the Main Cell were rinsed with distilled water.

### 3.2.2 – Brine with added CO<sub>2</sub> gas

#### Requirements:

#### Equipment:

- The Main Cell
- Seals for the open ports
- Reference Bridge tube
- Ag/AgCl Reference electrode
- Graphite Counter Electrode
- Working Electrode
- Magnetic stirring

- 800-1000ml brine
- Pressurized CO<sub>2</sub> gas tank with Gas Regulator
- Gas Dispersion Tube
- Water trap with 2 hose-barb ports
- 2 hoses for gas
- Pipette

Solutions:

- 800-1000ml brine, with a concentration of 3,5wt% NaCl per 100ml distilled water
- Distilled water, for washing

Procedure:

1. The preparation started with checking, cleaning, and assembling all the required parts as mentioned in “**3.1 – Assembly**”. Consult this section for details.
2. The Main Cell parts were visually checked for contamination and damage, rinsed with distilled water before being filled with 800ml brine and mounted together. The Teflon stirring pill was added through one of the open ports, and the Main Cell was placed on the magnetic stirrer with “anti-slip” in-between. All the open ports on the Cell Top were sealed until the rest of the preparation was done.
3. The Reference Bridge Tube and Glass Frit Tip was visually checked for contamination or damage and cleaned multiple times inside and outside with distilled water before brine was inserted.
4. The Reference Bridge Tube was inserted through the SJ28-to-#7-port in the Ball Joint by gently wiggling and secured by tightening the Teflon seal.
5. The Gas Dispersion Tube was thoroughly rinsed inside and outside with distilled water and inserted into the #24/40-Port on the Cell Top.
6. A gas hose was connected to the Inlet on the Gas Dispersion Tube, and to one of the hose-barb ports on the Water Trap. A second hose was connected at the other hose-barb port on the Water Trap, and to the Needle Valve Outlet on the Gas Regulator at the pressurized CO<sub>2</sub> tank.



7. The Main Valve on the CO<sub>2</sub> tank was opened slightly. The Pressure Adjusting Valve was opened until the pressure at the Needle Valve gauge showed 50psi. The Needle Valve was slightly opened until gas bubbles were seen inside the Main Cell. The gas flow was regulated manually to as high flow as possible, without having the solution splashing. The stirrer was set to 250rpm.
8. The solution was pre-saturated with CO<sub>2</sub> gas for at least 40 minutes to ensure no O<sub>2</sub> present and that a pH of 4-5 were achieved. This was checked with pH-paper strips.
9. The Reference Electrode was rinsed with distilled water before the #11-Bushing and O-Ring was slid on and inserted to the #11-port on the Reference Bridge Tube. When the tip of the Reference Electrode was observed to be fully submerged, the #11-Bushing on the Reference Electrode was tightened.
10. The Counter Electrode was rubbed with a wet paper to remove contaminations and rinsed with distilled water. The #7-Adapter and O-Ring was slid on the Counter Electrode, before being inserted into the #7-port on the Cell Top and secured into place by tightening the #7-Adapter.
11. The parts for the Working Electrode were visually checked for contamination and damage before being cleaned, assembled, and inserted to the #24/40 Centre Port on the Cell Top.
12. The stirring was lowered to 200rpm and the gas flow was lowered to a reasonable amount. Bubble accumulation on undesirable places were removed by tapping on the glassware.
13. After the Working Electrode was inserted, the Glass Frit Tip on the Reference Bridge Tube was adjusted to the right position, about 3-5 millimetres from the Metal Sample surface.
14. The unused ports were left with the sealing on, and the Connection Clamps were properly attached to each Electrode. The distance between the Metal Sample surface and the Glass Frit Tip on Reference Bridge Tube was double checked.
15. The test was initiated as explained in "**3.2 – The Testing Sequence**"

During testing the electrodes were regularly checked visually for anything that may or may not be desired. This could be for example bubbles trapped between the metal surface and Glass frit Tip, extreme localized corrosion, or leakage.

After testing:

When all the desired tests were done, the equipment were disassembled and cleaned in the following procedure.

1. The Connection Clamps were disconnected from each of the Electrodes.
2. The Main Valve at the gas tank was closed. The Pressure Adjusting Valve was closed. The Needle Valve was closed.
3. The hose from the Needle Valve to the Water Trap was disconnected at the Water Trap, followed by the hose from Water Trap to the Gas Dispersion Tube was disconnected and taken off.
4. The Reference Electrode was removed from the Reference Bridge Tube and rinsed with distilled water.
7. The Reference Bridge Tube was gently taken out from the Ball Joint at the Cell Top and rinsed with distilled water inside and outside. All the parts on the Reference Bridge Tube were taken off and rinsed with distilled water. The Glass Frit Tip was thoroughly rinsed with distilled water multiple times.
5. The Counter Electrode was taken out of the Main Cell and rubbed with a wet paper to remove any salt deposits. All the parts on the Counter Electrode were taken off and rinsed with distilled water.
6. The Working Electrode was taken out and disassembled. All the parts were rinsed with distilled water. The Metal Sample was cleaned with a brush and acetone.
7. The Main Cell was opened, and brine removed. The Ball Joint was disassembled, and all the parts in the Main Cell were rinsed with distilled water.

### 3.2.3 – Brine with added CO<sub>2</sub> gas and Corrosion Inhibitor

#### Requirements:

#### Equipment:

- The Main Cell
- Seals for the open ports
- Reference Bridge tube
- Ag/AgCl Reference electrode
- Graphite Counter Electrode
- Working Electrode
- Magnetic stirring
- 800-1000ml brine
- Pressurized CO<sub>2</sub> gas tank with gas regulator
- Gas Dispersion Tube
- Water trap with 2 hose-barb ports
- 2 hoses for gas
- Pipette
- Small container for weighing, and weighing equipment

#### Solutions:

- 800-1000ml brine, with a concentration of 3,5wt% NaCl per 100ml distilled water
- Corrosion Inhibitor, 500ppm relative to the volume brine used
- Hydrocarbon mix, with an addition ratio of 1:19 relative to the volume brine used
- Distilled water, for washing
- Acetone, for washing

#### Procedure:

1. The preparation started with checking, cleaning, and assembling all the required parts as mentioned in “**3.1 – Assembly**”. Consult this section for details.
2. The Main Cell parts were visually checked for contamination and damage and rinsed with distilled water before being filled with 800ml brine and mounted together. The Teflon stirring pill was added through one of the open ports, and the Main Cell was placed on the magnetic

stirrer with “anti-slip” in-between. All the open ports on the Cell Top were sealed until the rest of the preparation was done.

3. The Reference Bridge Tube and Glass Frit Tip was visually checked for contamination or damage and cleaned multiple times with distilled water before brine was inserted.
4. The Reference Bridge Tube was inserted through the SJ28-to-#7-port in the Ball Joint by gently wiggling and secured by tightening the Teflon seal.
5. The Gas Dispersion Tube was thoroughly rinsed inside and outside with distilled water and inserted into the #24/40-Port on the Cell Top.
6. A gas hose was connected to the Inlet on the Gas Dispersion Tube, and to one of the hose-barb ports on the Water Trap. A second hose was connected at the other hose-barb port on the Water Trap, and to the Needle Valve Outlet on the Gas Regulator at the pressurized CO<sub>2</sub> tank.
7. The Main Valve on the CO<sub>2</sub> tank was opened slightly. The Pressure adjusting Valve was opened until the pressure at the needle valve showed 50psi. The needle valve was slightly opened until gas bubbles were seen inside the Main Cell. The Gas flow was regulated to as high flow as possible, without having the solution splashing. The stirrer was set to 250rpm.
8. The solution was pre-saturated with CO<sub>2</sub> gas for at least 40 minutes to ensure no O<sub>2</sub> present and that a pH of 4-5 were achieved. This was checked with pH-paper strips.
9. The Reference Electrode was rinsed with distilled water before the #11-Bushing and O-Ring was slid on and inserted to the #11-port on the Reference Bridge Tube. When the tip of the Reference Electrode was observed to be fully submerged, the #11-Bushing on the Reference Electrode was tightened.
10. The Counter Electrode was rubbed with a wet paper to remove contaminations and rinsed with distilled water. The #7-Adapter and O-Ring was slid on the Counter Electrode, before being inserted into the #7-port on the Cell Top and secured into place by tightening the #7-Adapter.

11. The parts for the Working Electrode were checked for contamination and damage before being cleaned, assembled, and inserted to the #24/40 Centre Port on the Cell Top.
12. The stirring was lowered to 200rpm and the gas flow was lowered to a reasonable amount. Bubble accumulation on undesirable places were removed by gently tapping on the glassware.
13. After the Working Electrode was inserted, the Glass Frit Tip on the Reference Bridge Tube was adjusted to the right position, about 3-5 millimetres from the Metal Sample surface.
14. The seal on one of the available Ports on the Cell Top was taken off, and the Corrosion Inhibitor was added to the brine by using a pipette. If a hydrocarbon mix was used, it was injected after the Corrosion Inhibitor was added. This was done gently by using a long needle (100mm+) and syringe so that droplets from the hydrocarbon mix did not enter the brine solution. The seal was reattached afterwards.
15. The unused ports were left with the sealing on, and the Connection Clamps were properly attached to each Electrode. The distance between the Metal Sample surface and the Glass Frit Tip on Reference Bridge Tube was double checked.
16. The test was initiated as explained in **“3.2 – The Testing Sequence”**

During testing the electrodes was regularly checked visually for anything that may or may not be desired. This could be such as bubbles trapped between the metal surface and Glass frit Tip, extreme localized corrosion, or leakage.

After testing:

When all the desired tests were done, the equipment were disassembled and cleaned in the following procedure. Note that the hydrocarbon mix and/or corrosion inhibitor can stick to all surfaces that it is exposed to, thus acetone should be used for cleaning in most of the following steps!

1. The Connection Clamps were disconnected from each of the Electrodes.
2. The Main Valve at the gas tank was closed. The Pressure Adjusting Valve was closed. The Needle Valve was closed.

3. The hose from the Needle Valve to the Water Trap was disconnected at the Water Trap, followed by the hose from Water Trap to the Gas Dispersion Tube was disconnected and taken off.
4. The Reference Electrode was removed from the Reference Bridge tube and rinsed with distilled water.
8. The Reference Bridge Tube was gently taken out from the Ball Joint at the Cell Top and rinsed with distilled water inside and outside. All the parts on the Reference Bridge Tube were taken off and rinsed with distilled water. The Glass Frit Tip was thoroughly rinsed with distilled water multiple times.
5. The Counter Electrode were taken out of the Main Cell and rubbed with acetone to remove the added corrosion inhibitor and finished with rinsing of distilled water. All the parts on the Counter Electrode was taken off and rinsed with distilled water.
6. The Working Electrode was taken out and disassembled. All the parts were gently cleaned with acetone and rinsed with distilled water. The Metal Sample was cleaned with a brush and acetone.
7. The Main Cell was opened, and brine solution containing corrosion inhibitor and/or hydrocarbon mix were disposed into a waste container. The Ball Joint was disassembled, and all the compartments in the Main Cell was rubbed down with acetone and finally rinsed with distilled water.

## CHAPTER 4 – EXPERIMENTAL RESULTS AND DISCUSSION

To provide the most systematic presentation of the overall observed corrosion behaviours, it was evaluated to be reasonable that the corrosion rate data collected and presented in the following experimental result tables could be sorted and listed in an increasing order. Since this also made it more straightforward to perform a quantitative analysis of all the observed characteristics, this strategy was selected to be used in the following experimental results presented.

As the overall experimental results is mainly based on the Corrosion Rate parameter, the sub-parameters  $R_p$ ,  $i_{corr}$ ,  $E_{corr}$ , and OCP gathered in the LPR measurement have been excluded from this chapter. The experimental results for each of these parameters with their resulting data values can be found in *Appendix A – Detailed data results, Blank Testing* and *Appendix B – Detailed data results, CI's Testing*, in addition to the individual testing sequences that contained a high amount of deviation.

The blank test corrosion rate values used to create a baseline for graphical comparisons, were the 15 highest experimental results achieved and is noted as Blank in the following tables and graphs.

The experimental results for each individual corrosion inhibitors Imidazoline, Polymer, and Luvicap EG is presented through tabulated and graphical comparisons with the baseline corrosion rate, and calculated percent inhibition efficiency. The 15 lowest experimental results for each individual corrosion inhibitor are presented in the following tables and graphs. The single highest value collected from blank testing was used as  $X_0$  when the percent inhibition efficiency was calculated. This was to estimate the best inhibition efficiency relative to worst case scenario when no corrosion inhibitor was added.

The percent inhibition efficiency was calculated by using the following formula:

$$\% \eta = \left( \frac{X_0 - X_1}{X_0} \right) * 100$$

Where:

$\% \eta$  = Percent inhibition efficiency = %-Inhibition efficiency

$X_0$  = Corrosion rate without added corrosion inhibitor

$X_1$  = Corrosion rate with added corrosion inhibitor

## 4.1 – Experimental Results

### 4.1.1 – Corrosion Rate

The 15 highest experimental results achieved during blank testing is found in *Table 9* as Blank and were used as a baseline when evaluating the corrosion rate in both the absence and presence of 500ppm corrosion inhibitor, in addition to the 15 lowest experimental results achieved during corrosion inhibitor testing.

In *Appendix A – Detailed data results, blank testing*, each individual blank test performed with detailed experimental data result can be found. In *Appendix B – Detailed data results, CI's testing*, each individual corrosion inhibitor is presented in separated tables and graphs with comparison to the Blank test baseline, in addition to separated detailed experimental result data for each corrosion inhibitor testing.

The following experimental results are presented in unit millimetres per year (mm/year) for each individual LPR measurement performed (Test Number). To show the degree of confidence behind the achieved results the R<sup>2</sup> value can be seen in the following graphical illustration of the corrosion rate in *Figure 30*.

*Table 9: Numerical values of the measured corrosion rate in millimetres per year for the blank test, and when 500ppm of each CI was added in separated tests.*

Corrosion Rate – mm/year				
Test Number	Blank	Polymer	Imidazoline	Luvicap EG
0	0	0	0	0
1	0,8189	0,2114	0,05445	0,2809
2	0,9276	0,2326	0,06086	0,5759
3	1,079	0,3133	0,07443	0,7154
4	1,326	0,3506	0,1601	0,7517
5	1,329	0,3773	0,1624	0,779
6	1,333	0,4216	0,2414	0,8078
7	1,344	0,5682	0,3266	0,8611
8	1,393	0,5957	0,3769	0,885
9	1,591	0,6284	0,3797	0,9488
10	1,708	0,6285	0,3956	1,082
11	1,709	0,6487	0,4503	1,165
12	2,192	0,6924	0,4704	1,208
13	2,218	0,7084	0,506	1,215
14	2,366	0,8012	0,5673	1,353
15	2,743	0,8868	0,6223	1,359



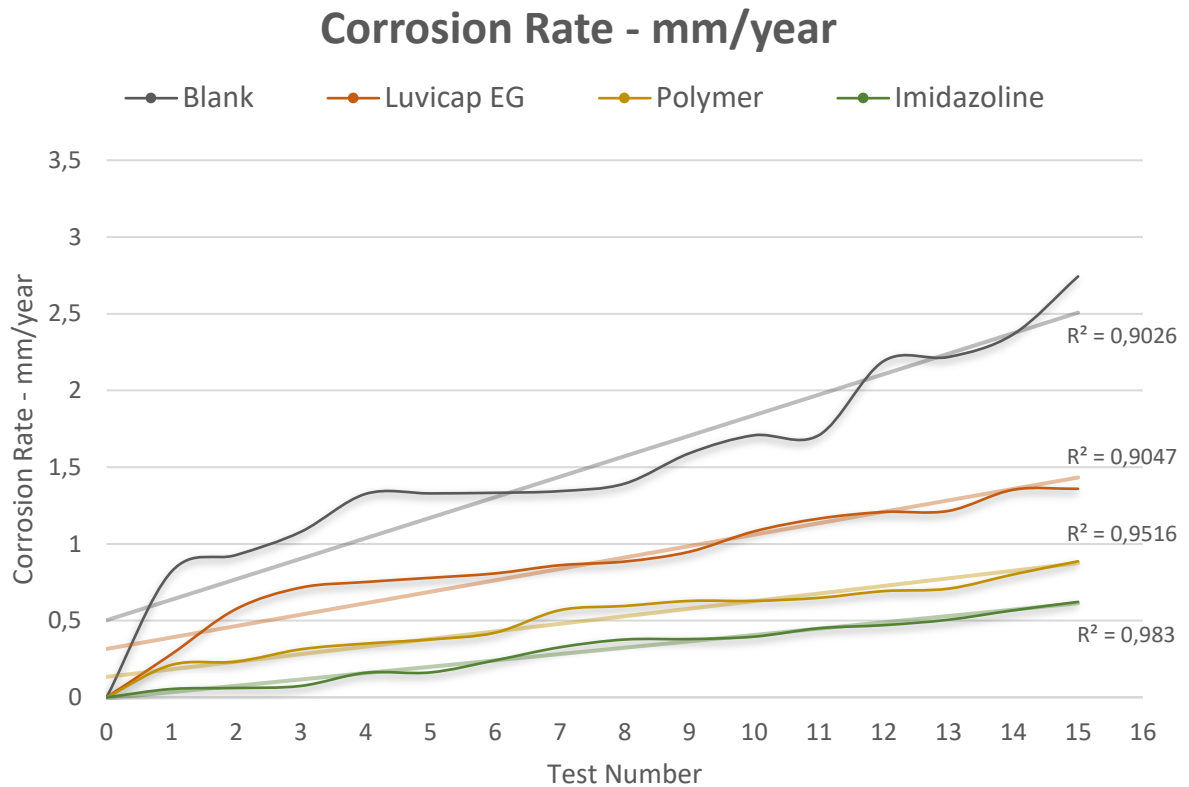


Figure 33: Graphical illustration of the corrosion rate for each LPR measurement performed, with the  $R^2$  value to show the degree of confidence.

By comparing the data listed in *Table 9* with the graphical illustration presented in *Figure 33*, the corrosion rate can be seen to remain at a relative low level through all the tests performed after the corrosion inhibitors was added.

The corrosion rate measured in the Blank seems to increase with a steady state, which may indicate that the corrosion rate would proceed towards a more severe region if further LPR measurements had been done.

The corrosion rate measured after 500ppm of Luvicap EG was added points towards a distinct positive impact on decreasing the corrosion rate when compared to Blank, but as the number of tests increased it showed a tendency to fail as the corrosion rate starts to increase.

The corrosion rate measured after 500ppm of Polymer was added can be seen to show a more significant decrease when comparing to the Blank and Luvicap EG, which can indicate that the Polymer is a relatively effective corrosion inhibitor with good performance.

The corrosion rate measured after 500ppm of Imidazoline was added can be seen to have the most distinct impact as it has the best effect towards lowering the corrosion rate. This can indicate that the Imidazoline is the most effective corrosion inhibitor with the best performance when comparing to the Blank, Polymer, and Luvicap EG.

#### 4.1.2 – Inhibition Efficiency

The highest corrosion rate achieved during blank testing is presented in *Table 10* as Test Number 15 = 2,743mm/year, which was used as  $X_0$  when percent inhibition efficiency ( $\% \eta$ ) was calculated.

The %-Inhibition Efficiency was calculated for each individual corrosion inhibitor test number in *Table 10* and can be found in *Table 10* with a graphical illustration *Figure 34*.

*Table 10: The calculated percent inhibition relative to Blank = 2,743mm/year for each individual corrosion inhibitor test number in Table 10.*

Test Number	%Inhibition Efficiency		
	Polymer	Imidazoline	Luvicap EG
0	100 %	100 %	100 %
1	92 %	98 %	90 %
2	92 %	98 %	79 %
3	89 %	97 %	74 %
4	87 %	94 %	73 %
5	86 %	94 %	72 %
6	85 %	91 %	71 %
7	79 %	88 %	69 %
8	78 %	86 %	68 %
9	77 %	86 %	65 %
10	77 %	86 %	61 %
11	76 %	84 %	58 %
12	75 %	83 %	56 %
13	74 %	82 %	56 %
14	71 %	79 %	51 %
15	68 %	77 %	50 %

## %-Inhibition Efficiency

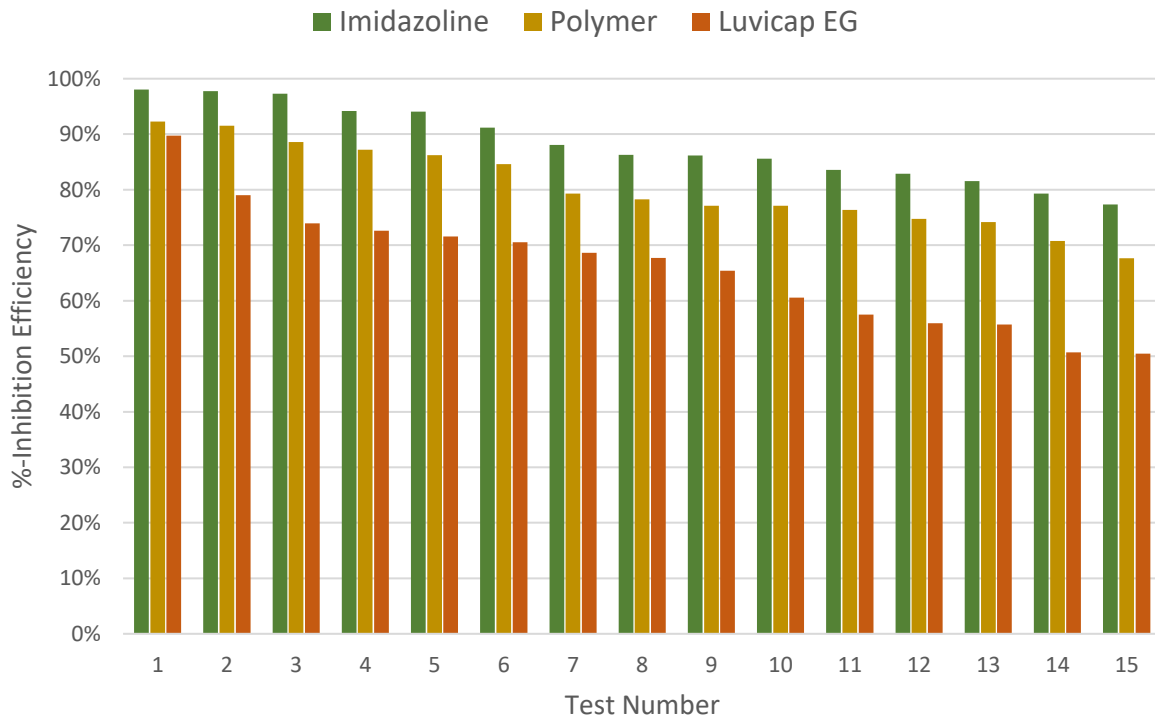


*Figure 34: Graphically illustration of the calculated percent inhibition relative to Blank = 2,743mm/year for each individual corrosion inhibitor test number in Table 10.*

When comparing the tabulated values in *Table 10* with the graphical illustration in *Figure 34*, the overall %-inhibition efficiency seems to decrease for every test performed. With the Imidazoline decreasing in a slower pace compared to Polymer and Luvicap EG, it may indicate that the Imidazoline has the best %-inhibition efficiency and performance. As the Luvicap EG can be observed to have the steepest decrease when comparing to Polymer and Imidazoline, it can indicate a poor %-inhibition efficiency and corrosion inhibitor performance. Since the Polymer can be observed to have a steady decrease in %-inhibition efficiency, it does not have an equally steep decrease as compared to Luvicap EG. This can indicate that the Polymer has a relatively good %-inhibition efficiency with good performance.

The average %-Inhibition Efficiency and standard deviation (SD) of each corrosion inhibitors can be found in *Table 11* below, with a graphical presentation in *Figure 35*.

Table 11: Calculated average %-Inhibition Efficiency and standard deviation (%) of the tested CI.

	Average %-Inhibition Efficiency	SD
<b>Imidazoline</b>	88 %	7 %
<b>Polymer</b>	80 %	8 %
<b>Luvicap EG</b>	66 %	11 %

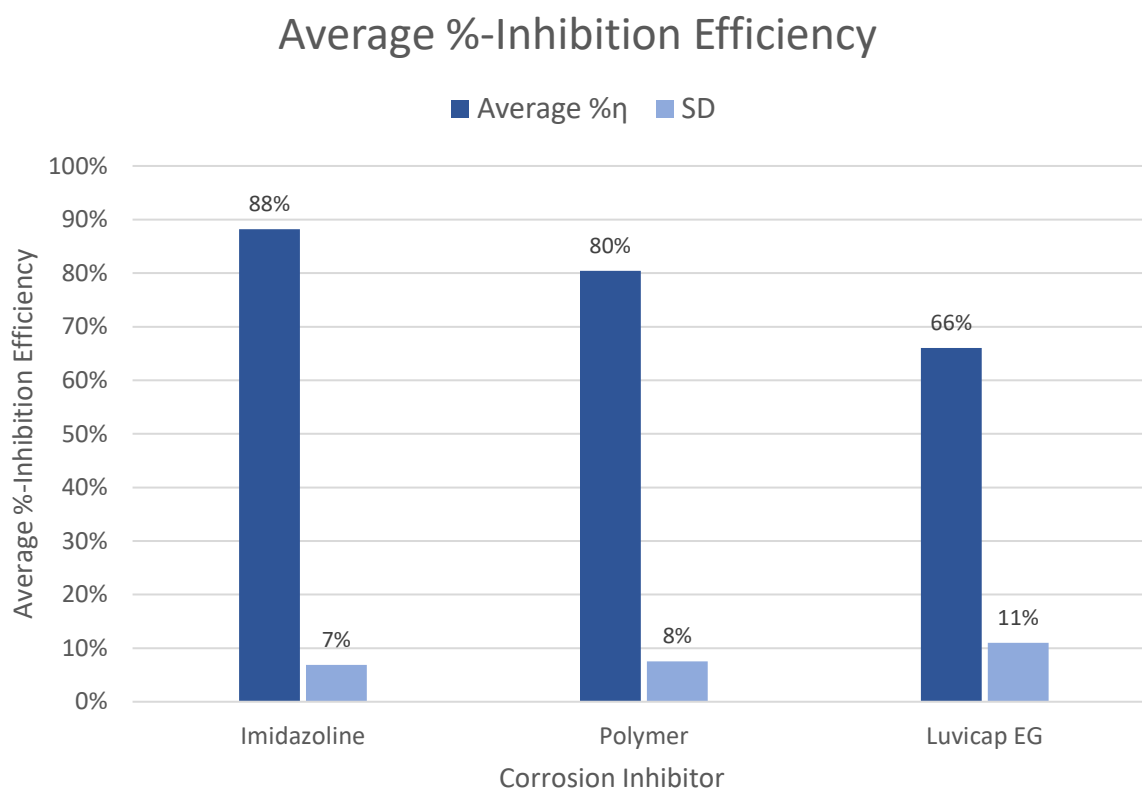


Figure 35: Graphically illustration of the average percent inhibition ( $\% \eta$ ) of each corrosion inhibitor analysed.

The average %-inhibition efficiency in Table 12 and graphically in Figure 35 may indicate that Imidazoline shows the best performance with an average %-inhibition efficiency of 88%. Since the Polymer shows an average %-inhibition efficiency of 80%, it can point towards a relatively good performance when comparing to Imidazoline. As Luvicap EG shows an average %-inhibition efficiency of 66% it seems to have a poor performance when comparing to Imidazoline and Polymer.

The percent standard deviation (SD) was lower for Imidazoline and Polymer compared to the SD of Luvicap EG. This can be because of the number of LPR measurements performed on Luvicap EG was

lower than the number of LPR measurements performed on Imidazoline and Polymer. With a higher number of LPR measurements performed, a more distinct trend in the collected data with a smaller amount of deviation was observed.

#### 4.1.3 – Effect of adding Hydrocarbon Mix

The experimental results of how the addition of hydrocarbon mix (H.C.) to a brine solution containing either 500ppm Imidazoline or 500ppm Polymer affected the corrosion inhibitor performance when comparing the corrosion rate can be seen numerically in *Table 12* and graphically in *Figure 36*.

*Table 12: The effect of adding hydrocarbon to a brine solution containing either 500ppm Imidazoline or 500ppm Polymer when comparing corrosion rate values achieved in LPR measurements.*

Test number	Corrosion rate – mm/year			
	Imidazoline		Polymer	
	Without H.C. added	With H.C. added	Without H.C. added	With H.C. added
0	0	0	0	0
1	0,054	0,454	0,211	0,714
2	0,061	0,556	0,233	0,741
3	0,074	0,582	0,313	1,154
4	0,160	0,585	0,351	1,312
5	0,162	0,600	0,377	1,398

## Corrosion inhibitor performance when added H.C.

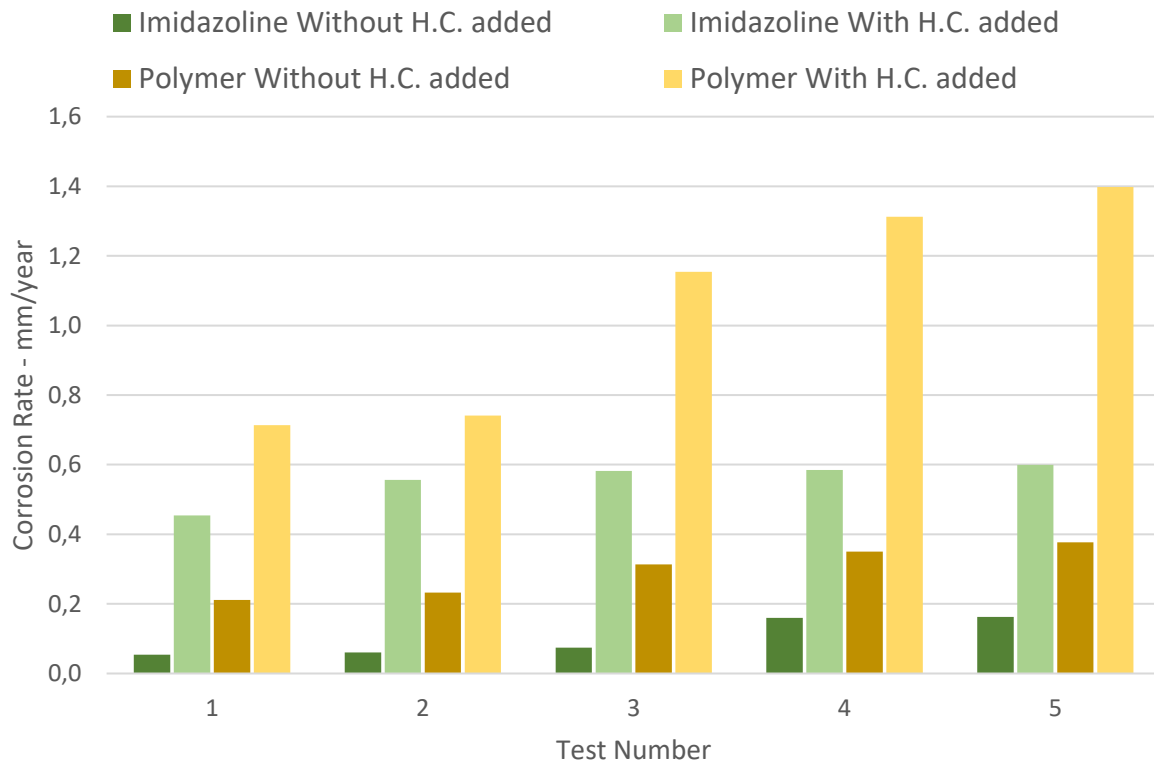


*Figure 36: Graphical illustration of the effect of adding hydrocarbon to a brine solution containing either 500ppm Imidazoline or 500ppm Polymer when comparing corrosion rate values achieved in LPR measurements.*

When observing *Table 13* and *Figure 36*, the presence of a hydrocarbon mix can point towards the that it has a high impact on the corrosion inhibitor performance. It was also observed that the colours in the solution caused by the presence of corrosion inhibitors faded. These observations can point towards that the corrosion inhibitors diffuses into the hydrocarbon phase in a different degree that may be dependent on the molecular structure and chemical behaviour, which furthermore makes the Metal Sample surface being more exposed to the corrosive environment.

### 4.1.4 – Effect of adding Oxygen Scavenger

The oxygen scavenger compound added where a mix of two chemicals: 50ppm sodium dithionite ( $\text{Na}_2\text{S}_2\text{O}_4$ ) and 5ppm cobalt dichloride hexahydrate ( $\text{CoCl}_2 \cdot 6\text{H}_2\text{O}$ ) relative to 800ml brine solution.

By adding an oxygen scavenger (O<sub>2</sub>-Scavenger) to the test solution followed by adding 500ppm Imidazoline before performing LPR measurements, the experimental results after LPR measurement can indicate that the corrosion rate was lowered by a small degree as presented in *Table 14*. The preparations and testing procedure were otherwise equal to the one presented in *Chapter 4*. A graphical illustration of *Table 13* is presented in *Figure 37*.

*Table 13: The effect of adding oxygen scavenger (O<sub>2</sub>-Scavenger) on the corrosion rate when 500ppm Imidazoline is present in the solution.*

Test Number	Imidazoline - Corrosion Rate - mm/year	
	Without O <sub>2</sub> -Scavenger	With O <sub>2</sub> -Scavenger
0	0	0
1	0,054	0,042
2	0,061	0,075
3	0,074	0,203
4	0,160	0,104
5	0,162	0,119
6	0,241	0,204

### The impact of adding O<sub>2</sub>-scavenger to solution containing 500ppm Imidazoline

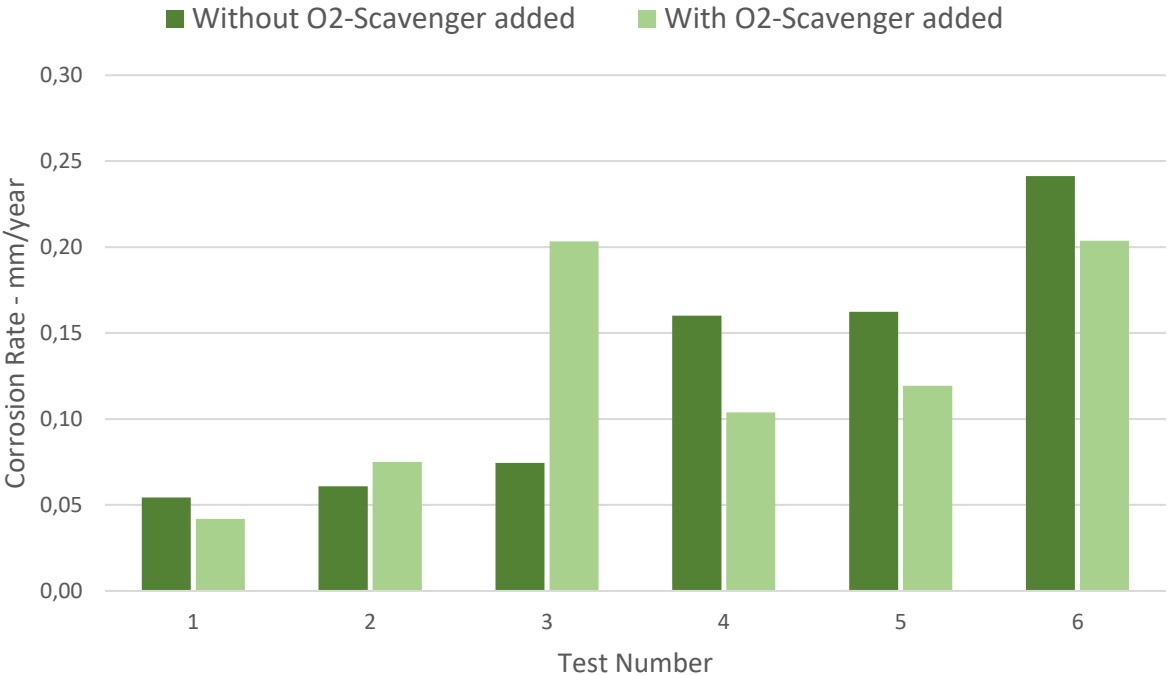


*Figure 37: A graphical illustration of the impact added O<sub>2</sub>-Scavenger to brine solution with 500ppm Imidazoline has on the corrosion rate measurement.*

An additional observation was also that when opening the collected data results in Gamry Echem Analyst, it seems to be more centred with less deviation between each data points. As presented in *Table 13* the corrosion rate was also lowered with a certain amount in Test Number 1 and 4-6 but had a opposite effect in Test Number 2 and 3. This can point towards that this situation needs to be further investigated before making a final conclusion on the impact the added O<sub>2</sub>-Scavenger has on the overall corrosion rate.

#### 4.1.5 – Effect of adding CO<sub>2</sub> gas

The effect of adding CO<sub>2</sub> gas was mainly studied on only one metal sample, with some of the collected corrosion rate data in *Table 14* accompanied with a graphical illustration in *Figure 38*. This data collection was not used when the Blank baseline was made or when corrosion inhibitors was analysed, as the Metal Sample was used multiple times under various circumstances to collect knowledge on the equipment and testing procedure, which resulted in a high amount of damage to the metal sample surface.

*Table 14: The impact on corrosion rate when CO<sub>2</sub> gas was added to the brine solution.*

<b>Corrosion Rate - mm/year</b>		
<b>Test Nr</b>	<b>Brine only</b>	<b>Brine and CO<sub>2</sub> gas added</b>
1	0,113	1,757
2	0,279	1,840
3	0,414	2,006



## Impact on corrosion rate when added CO<sub>2</sub> gas

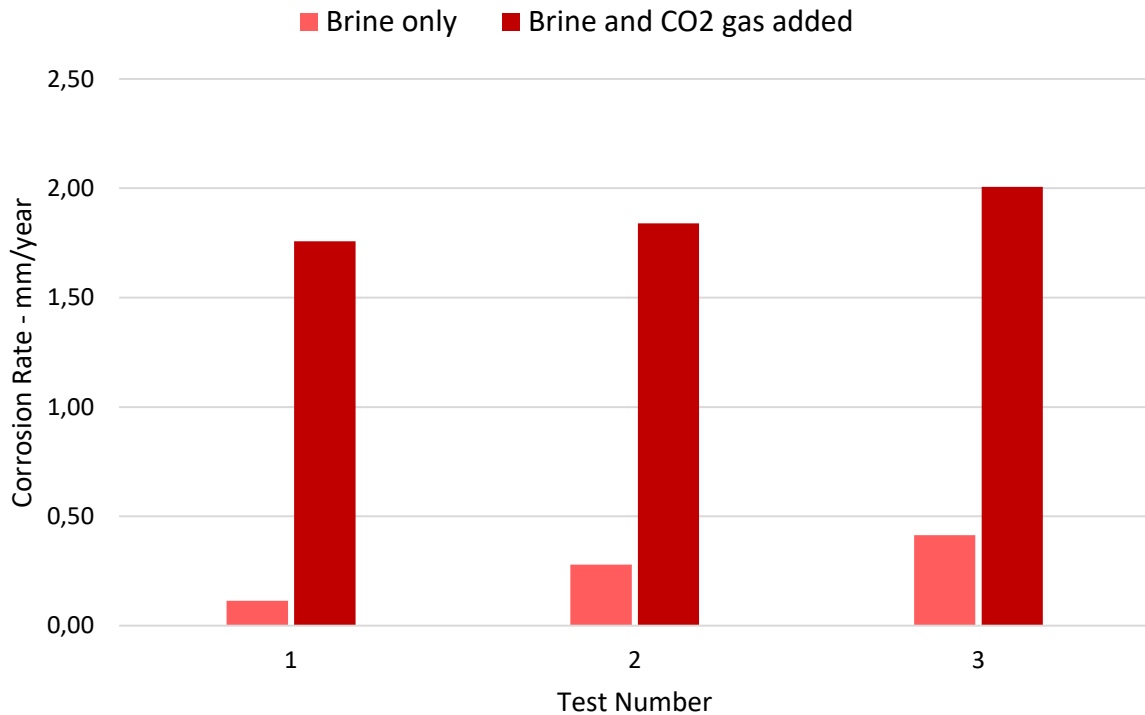


Figure 38: Graphical illustration of the impact added CO<sub>2</sub> gas have on the corrosion rate.

As seen in *Table 14* and *Figure 38*, the presence of CO<sub>2</sub> gas in the brine solution can have a high impact as the experimental results presented shows a 5 to 10 times increase in the corrosion rate.

### 4.1.6 – Leak Observation

Since a high amount of time was put into observing the corrosion behaviour of C1018 Mild Steel and gaining confidence around the resulting data, failure pointers was also encountered along the way.

In *Table 15* detailed experimental results is presented, which provides indications that leakage in the Working Electrode has occurred. The plot observed in the Gamry Echem Analyst when leak occurred, can be found in *Appendix C* as *Picture B-1* and *Picture B-2*.

Table 15: Data results that can provide indication of leak in the Working Electrode.

	No leak	Leak
OCP (V)	-0,5193	-0,25402

<b>E<sub>corr</sub> (mV)</b>	-518,4	-261
<b>I<sub>corr</sub> (A/cm<sup>2</sup>)</b>	2,36E-04	1,06E-06
<b>R<sub>p</sub> (Ω*cm<sup>2</sup>)</b>	110,2	24670
<b>Corrosion rate (mm/year)</b>	2,743	0,01226

As seen in *Table 15*, a high deviation in-between each of the presented parameters.

Since the Metal Sample's used for corrosion testing was consistently C1018 Mild Steel with a specific composition, a good amount of confidence was gained when evaluating the corrosion behaviour of this specific metal species. Because of the threaded rod holding the metal sample was of stainless steel, it was known from earlier experience that one of its properties is to hold a strong resistance towards corrosion.

In *Table 15* the extremely high R<sub>p</sub> value was the first to be observed, as it presents itself to be more than 200 times higher when leak was observed compared to the results when no leak occurred. This could be an indication that the performed measurements were done on the stainless-steel rod instead of the metal sample. Since the OCP value also was observed to hold an unusual low potential when compared to the OCP potential were no leak was observed, this can also indicate that the measurements were performed on another type of metal.

Since the E<sub>corr</sub> value is the corrosion potential and OCP value is the equilibrium potential, they should hold more or less the same potential as long as the metal sample is stable [34]. Since the observations in *Table 15* shows a high deviation when comparing the resulting data, this also points toward that leak has occurred. As I<sub>corr</sub> provides information on how much current is produced on the specific metal sample area during the polarization process, a high amount of deviation in the current such as presented in *Table 15* can give a good indication if leakage is suspected.

Lastly, in *Table 15* the corrosion rate was observed to be extremely low when leak was observed. When comparing the corrosion rate achieved when leak was observed to the measured corrosion rate in corrosion inhibitor LPR measurements, the corrosion rate achieved when leak occurred is lower than what was achieved when 500ppm Imidazoline. This can also indicate an unrealistic low corrosion rate was measured, as the leak was observed when no CI was added, and the brine was pre-saturated with CO<sub>2</sub> gas.

## 4.3 – Overall Discussion

Since most of the individual experimental results was discussed in the same sub-chapters they were presented in, the following discussion is more on the overall achieved experimental results and experience. As there were many different situations investigated, some was more in the focus than others.

- When performing the LPR measurement a high deviation between the resulting data for many tests performed was observed when varying the input values for each of the different parameters. This can be because of the fact that each of the parameters affect the measurement in very specific ways, making a consistent value for the parameter probably necessary when replicating tests is desired [32].
- When lowering the stirring below 200rpm it was observed that the resulting data collection had less deviation between each data sampling. This can indicate that lowering the flow kinetics provides a more static bulk solution surrounding the metal sample surface area, which further gives a more accurate data sampling. When testing with stirring higher than 200rpm a much higher deviation between each data point collection was observed. Overall, this can point towards that the kinetics may have a high influence on the corrosion behaviour as other researchers has concluded with [11], [14], [55]. It was reflected that there could also be a probability that an increase in the flow kinetics could make it difficult for FFCI to function at its best, as the generated film-formation is more prone to break as the flow increases [2].
- Creating a baseline was found to be challenging as the first 14 blank tests resulted in a significant lower corrosion rate when compared to the last 15 blank tests, which can be seen in the detailed data results in *Appendix A*. When taking account for the environmental conditions used in this thesis and comparing to what other researchers have achieved with other environmental conditions, such as higher temperatures, the 15 highest achieved corrosion rate values could be the most plausible representative [3], [4], [53], [56]. This could point towards that further blank testing could have been necessary in order to achieve a more representative baseline.
- Challenges around the reproductivity was experienced, as the data results collected from replicated tests performed on separated days sometimes did not correlate between each other. This can be because of the replicated environmental conditions or the metal sample

surface morphology did not correlate properly, which furthermore has been suggested to have a high influence on the overall corrosion behaviour [2], [11], [13], [16], [18], [19], [22].

- Occasional patches of localized corrosion were observed to appear before tests was initiated but disappeared when test was initiated. The frequency it appeared and disappeared in was also observed to be more rapid during the first tests and decreased as the number of tests performed continued. At one point, the appearing/disappearing frequency seemed to reach a limit as the localized corrosion suddenly became a more uniform corrosion, with a rapid decrease in the corrosion rate which can be observed in the *Appendix A – Blank Sample 1 – Sequence 2*. Because of the observed rapid decrease in corrosion rate when the uniform corrosion layer appeared, the uniform corrosion layer can seem to behave as a corrosion inhibitor itself. As other researchers have suggested that this can be true due to some corrosion compound can form semi-protective films on the metal surface, this may have had a contribution in the challenge of accomplishing a representative base line during blank testing [3], [13], [53].
- After observing the low corrosion rate on Blank Sample 2 presented in *Appendix A*, the metal sample was water sanded. This reviled deep scratches on the metal sample surface area, which may also be a reason as to why the corrosion rate was observed to be low.
- Dissolving Imidazoline into the brine solution was observed to be challenging as it was experienced that the solution became almost instantaneous cloudy white with poor visually effect the moment it was inserted, which did not improve when stirring was increased. By consulting the supervisor, it was suggested that this can possibly be because of the Imidazoline concentration was over the critical micelle concentration (CMC), which further can indicate that the surfactant molecules formed micelles instead of dissolving into separated surfactant molecules [57]. As the visual effect was very poor with a high risk of unnoticed bubble accumulations, leaks or localized corrosion, the resulting experimental data evaluation was solely based on the confidence gained by replicating the test multiple times.
- As the exact Tafel constants ( $\beta_a$  and  $\beta_c$ ) were not explored in this thesis it can probably have an influence the experimental results in a uncertain degree, even though they were evaluated to be sufficient [32].

- An undesired amount of foam was observed when performing tests with addition of corrosion inhibitors (CI's). By consulting supervisor, it was noted that this appears to be a known problem when using CI's and KHI's. Further investigation to find a solution for this problem was not performed but could be advisable to do.
- When adding an oxygen scavenger compound to a brine solution containing Imidazoline, it was observed that the collected data results appeared to be more centred when presented in the Gamry Echem Analyst. The corrosion rate was also observed to be lowered with a certain degree in some of the tests performed but showed an opposite effect in other tests performed. This can indicate that could have been some traces of O<sub>2</sub> left in the solution, even though the solution was pre-saturated with CO<sub>2</sub> gas, as oxygen has been suggested to increase the corrosion rate [12].
- As the testing methods and procedures were put together by looking at what other researchers have done, guidance from experienced corrosion engineer\* and supervisor, there is still room for improvement.
- When exploring other possible testing procedures such as a sequential testing with lower time in-between each individual test, a smaller amount of deviation between each individual test was observed. Since this was explored when a higher amount of knowledge was achieved, the time limitation made further investigation not possible.
- As the experience on this specific electrochemical measurement and testing method was humble to begin with but slowly increased with the high amount of research and user experience, other analysing strategies and testing methods would have been explored earlier. This could be such as exploring different statistical analysis strategies (T-testing, chi-squared test, normal distribution), exploring other possible test sequences (more frequently testing, higher/lower time in-between), investigating the Tafel plot and how the  $\beta_a$  and  $\beta_c$  influences the experimental results, investigating the impact of brine solution with other compositions, study the impact of temperature and pH on the corrosion behaviour, and other metal samples with different metal compositions.

## CHAPTER 5 – CONCLUSION AND FURTHER RECOMMENDATIONS

The goal was to make a manual containing an assembling procedure for the Gamry MultiPort Electrochemical Cell Kit equipment that could be used for performing Bubble Testing, how to perform corrosion testing through LPR measurement by using Gamry Framework, and how analyse the experimental results by using Gamry Echem Analyst. The corrosion rate was investigated and analysed in the absence and presence of corrosion inhibitor, and collected data was compared to evaluate the corrosion inhibitor performance.

When investigating the corrosion behaviour and observing how the corrosion inhibitors greatly reduced the corrosion rate, it can be clear that the usage of corrosion inhibitors for combating CO<sub>2</sub> corrosion is a highly effective strategy.

### 5.1 – Conclusion

By evaluating the collected experience and knowledge some general conclusions could be drawn, which is listed below:

- The Gamry MultiPort Electrochemical Cell Kit was experienced to be a very user-friendly equipment with many possibilities.
- The Gamry Framework was seen to have a broad spectrum of different testing methods available which makes it possible to explore and perform a high variety of testing techniques.
- The LPR measurement method was seen to provide a high amount of data in a short period of time.
- The Bubble Testing method can make it possible to simulate many environmental conditions in a small scale.

### 5.2 – Further Recommendations

Through the making of this manual it was observed that the probability of further optimization and deeper understanding could be necessary within some regions, which is listed below:

- Investigate the  $R_p/E_c$  testing method, as this was mentioned by co-supervisor to be a more long-term testing method which performs the LPR measurement in a selected time interval over a given timespan. Since the LPR measurements performed in this thesis was initiated manually with a consistent time-range, the  $R_p/E_c$  measuring method can be a more effective analysing strategy.
- Further testing on the impact of adding oxygen scavenger to the test solution, as the collected results can point towards a positive impact on the resulting data collection when the oxygen scavenger was added.
- Deeper investigation in the CMC when testing CI's, as this could be a crucial factor towards the analysing process of CI's performance.
- Investigation of the effect brine solution has on the corrosion rate, as this has been suggested to have an impact on the degree of corrosion rate [16], [19].
- Further investigation in the number of tests needed to make a solid conclusion. This could be such as a higher intensity of LPR measurement by performing more tests under an overall longer time span, or more frequently testing with lower time interval between within the same time span.
- Since a vast number of factors has been suggested that can influence the corrosion behaviour such as temperature, kinetics, and pH, these factors should be further investigated when analysing the corrosion behaviour and corrosion inhibitor performance.

## REFERENCES

- [1] M. Iannuzzi, A. Barnoush, og R. Johnsen, «Materials and corrosion trends in offshore and subsea oil and gas production», *Npj Mater. Degrad.*, bd. 1, nr. 1, s. 2, des. 2017, doi: 10.1038/s41529-017-0003-4.
- [2] B. Guo, X. Liu, og X. Tan, *Petroleum production engineering*, 2nd ed. Cambridge, MA: Gulf Professional Pub, 2017.
- [3] H. Mohamed, H. El-Lateef, V. Abbasov, L. Aliyeva, og T. Ismayilov, «Corrosion Protection of Steel Pipelines Against CO<sub>2</sub> Corrosion-A Review», *Chem J*, bd. 2, jan. 2012, [Online]. Tilgjengelig på: [https://www.researchgate.net/publication/267557833\\_Corrosion\\_Protection\\_of\\_Steel\\_Pipelines\\_Against\\_CO\\_2\\_Corrosion-A\\_Review](https://www.researchgate.net/publication/267557833_Corrosion_Protection_of_Steel_Pipelines_Against_CO_2_Corrosion-A_Review)
- [4] V. M. Abbasov, H. M. Abd El-Lateef, L. I. Aliyeva, E. E. Qasimov, I. T. Ismayilov, og M. M. Khalaf, «A study of the corrosion inhibition of mild steel C1018 in CO<sub>2</sub>-saturated brine using some novel surfactants based on corn oil», *Egypt. J. Pet.*, bd. 22, nr. 4, s. 451–470, des. 2013, doi: 10.1016/j.ejpe.2013.11.002.
- [5] M. B. Kermani og D. Harrop, «The Impact of Corrosion on Oil and Gas Industry», *SPE Prod. Facil.*, bd. 11, nr. 03, s. 186–190, aug. 1996, doi: 10.2118/29784-PA.
- [6] N. C. Boye, *Kjemi og miljølære*. Oslo: Gyldendal, 2017.
- [7] «Corrosion | Boundless Chemistry». <https://courses.lumenlearning.com/boundless-chemistry/chapter/corrosion/> (åpnet mai 07, 2021).
- [8] N. A. Says, «Galvanic Corrosion of Steel and Other Metals», *AZoM.com*, mar. 11, 2015. <https://www.azom.com/article.aspx?ArticleID=11833> (åpnet mai 07, 2021).
- [9] G. Rayner-Canham og T. Overton, *Descriptive inorganic chemistry*, Sixth edition. New York: Macmillan Higher Education, 2014.
- [10] «What is Sweet Corrosion? - Definition from Corrosionpedia», *Corrosionpedia*. <http://www.corrosionpedia.com/definition/1434/sweet-corrosion> (åpnet jun. 12, 2021).
- [11] T. E. Perez, «Corrosion in the Oil and Gas Industry: An Increasing Challenge for Materials», *JOM*, bd. 65, nr. 8, s. 1033–1042, aug. 2013, doi: 10.1007/s11837-013-0675-3.
- [12] V. S. Saji og S. A. Umoren, Red., *Corrosion Inhibitors in the Oil and Gas Industry*, 1. utg. Wiley, 2020. doi: 10.1002/9783527822140.
- [13] M. A. Kelland, *Production Chemicals for the Oil and Gas Industry*, 0 utg. CRC Press, 2014. doi: 10.1201/b16648.
- [14] A. H. Alamri, «Localized corrosion and mitigation approach of steel materials used in oil and gas pipelines – An overview», *Eng. Fail. Anal.*, bd. 116, s. 104735, okt. 2020, doi: 10.1016/j.engfailanal.2020.104735.
- [15] «gas/oil ratio (GOR) | Oilfield Glossary». <https://glossary.oilfield.slb.com/en/terms/g/gas-oil-ratio> (åpnet jun. 08, 2021).
- [16] H. Sørensen, K. S. Pedersen, og P. L. Christensen, «Modeling of gas solubility in brine», *Org. Geochem.*, bd. 33, nr. 6, s. 635–642, jun. 2002, doi: 10.1016/S0146-6380(02)00022-0.
- [17] G. Schmitt og M. Horstemeier, «Fundamental Aspects of CO<sub>2</sub> Metal Loss Corrosion - Part II: Influence of Different Parameters on CO<sub>2</sub> Corrosion Mechanisms», presentert på CORROSION 2006, mar. 2006. Åpnet: jun. 12, 2021. [Online]. Tilgjengelig på: <https://onepetro.org/NACECORR/proceedings/CORR06/All-CORR06/NACE-06112/118113>



- [18] M. B. Kermani og European Federation of Corrosion, Red., *A working party report on CO2 corrosion control in oil and gas production: design considerations*. London: Institute of Materials, 1997.
- [19] J. Han, J. W. Carey, og J. Zhang, «Effect of sodium chloride on corrosion of mild steel in CO<sub>2</sub>-saturated brines», *J. Appl. Electrochem.*, bd. 41, nr. 6, s. 741–749, jun. 2011, doi: 10.1007/s10800-011-0290-3.
- [20] M. Osman, *Chemistry*, Custom Book Edition. Pearson Education, 2011.
- [21] C. G. og A. F., «Corrosion Inhibitors – Principles, Mechanisms and Applications», i *Developments in Corrosion Protection*, M. Aliofkhaezai, Red. InTech, 2014. doi: 10.5772/57255.
- [22] K. Kousar *mfl.*, «Corrosion inhibition of carbon steel in hydrochloric acid: Elucidating the performance of an imidazoline-based surfactant», *Corros. Sci.*, bd. 180, s. 109195, mar. 2021, doi: 10.1016/j.corsci.2020.109195.
- [23] P. B. Raja og M. G. Sethuraman, «Natural products as corrosion inhibitor for metals in corrosive media — A review», *Mater. Lett.*, bd. 62, nr. 1, s. 113–116, jan. 2008, doi: 10.1016/j.matlet.2007.04.079.
- [24] S. Energy, «Corrosion Problems on Oil and Gas Industries», *SFAS ENERGY*, feb. 18, 2021. <https://www.sfasenergy.com/post/corrosion-issues-on-oil-and-gas-industries> (åpnet mai 27, 2021).
- [25] B. J. Usman og S. A. Ali, «Carbon Dioxide Corrosion Inhibitors: A review», *Arab. J. Sci. Eng.*, bd. 43, nr. 1, s. 1–22, jan. 2018, doi: 10.1007/s13369-017-2949-5.
- [26] S. Kesavan, J. S. Selvaraj, S. Seethalakshmi, Y. Queiros, A. Gessie, og N. Scanarotti, «Development of a Concentrated Corrosion Inhibitor Compatible with Produced Water Brine and Scale Inhibitor», jun. 2020. Åpnet: nov. 06, 2021. [Online]. Tilgjengelig på: <https://onepetro.org/NACECORR/proceedings/CORR20/All-CORR20/NACE-2020-14668/446044>
- [27] A. N. Frumkin Institute of Physical Chemistry and Electrochemistry, Russian Academy of Sciences, Leninskii pr. 31, Moscow, 119071 Russian Federation, N. N. Andreev, N. G. Anufriev, A. N. Frumkin Institute of Physical Chemistry and Electrochemistry, Russian Academy of Sciences, Leninskii pr. 31, Moscow, 119071 Russian Federation, I. S. Sivokon, og OJSC Transenergostroi, Derbenevskaya nab. 7, bldg. 10, Moscow, 115114 Russian Federation, «Laboratory assessment of corrosion inhibitors effectiveness at oilfield pipelines of West Siberian region. III. Bubble test», *Int. J. Corros. Scale Inhib.*, bd. 2, nr. 1, s. 017–029, 2013, doi: 10.17675/2305-6894-2013-2-1-017-029.
- [28] W. S. Tait, *An introduction to electrochemical corrosion testing for practicing engineers and scientists*. Racine, Wisc: PairODocs Publ, 1994.
- [29] «Linear Polarization Resistance monitoring». [Online]. Tilgjengelig på: <https://www.alspi.com/lprintro.htm>
- [30] «What is an Open Circuit Potential? - Definition from Corrosionpedia», *Corrosionpedia*. <http://www.corrosionpedia.com/definition/834/open-circuit-potential-ocp> (åpnet jun. 12, 2021).
- [31] «Potentiostat/Galvanostat Electrochemical Instrument Basics». <https://www.gamry.com/application-notes/instrumentation/potentiostat-fundamentals/> (åpnet mai 10, 2021).
- [32] «Polarization Resistance Tutorial». <https://www.gamry.com/application-notes/corrosion-coatings/corrosion-techniques-polarization-resistance/> (åpnet mai 10, 2021).
- [33] «Analyzing Cyclic Voltammetry at a Microdisk Electrode with Simulation», *COMSOL Multiphysics*. <https://www.comsol.com/blogs/analyzing-cyclic-voltammetry-at-a-microdisk-electrode-with-simulation/> (åpnet jun. 12, 2021).
- [34] «Getting started with electrochemical corrosion measurement». Gamry Instruments, Application Notes. [Online]. Tilgjengelig på: <https://www.gamry.com/application-notes/corrosion-coatings/basics-of-electrochemical-corrosion-measurements/>
- [35] Gamry Instruments, *Electrochemical Corrosion Rate Measurements*, (2021). Åpnet: jun. 01, 2021. [Online Video]. Tilgjengelig på: <https://www.youtube.com/watch?v=z3JjcDncEJc>

- [36] «Corrosion Assessment: 8 Corrosion Tests That Help Engineers», *Corrosionpedia*.  
<https://www.corrosionpedia.com/corrosion-assessment-8-corrosion-tests-that-help-engineers-mitigate-corrosion/2/1389> (åpnet jun. 08, 2021).
- [37] «Multiport Cell Kit Operator's Manual», s. 30.
- [38] «EchemAnalystSoftwareManual(1).pdf», s. 42.
- [39] Teaser PRO, *MultiPort Corrosion Cell Kit*, (jan. 04, 2018). Åpnet: mai 10, 2021. [Online Video].  
 Tilgjengelig på: <https://www.youtube.com/watch?v=umeF1JF9fKA&list=PLCFa0I6k8s-UyrFL2zbZ8JbPpbno4USv3&index=3>
- [40] Teaser PRO, *Webinar Live Demo Calculating Corrosion Rates with LPR and EIS*, (aug. 13, 2020). Åpnet: mai 10, 2021. [Online Video]. Tilgjengelig på:  
<https://www.youtube.com/watch?v=OJAardWD6DI&list=PLCFa0I6k8s-UyrFL2zbZ8JbPpbno4USv3&index=4>
- [41] «Comparison of Corrosion Rate Calculated by EFM, LPR, and EIS».  
<https://www.gamry.com/application-notes/corrosion-coatings/corrosion-rate-efm-of-iron/> (åpnet mai 10, 2021).
- [42] «Reference Electrodes Influence Electrochemical Measurements».  
<https://www.gamry.com/application-notes/instrumentation/reference-electrodes/> (åpnet mai 10, 2021).
- [43] «communication with producer through e-mails».
- [44] Gamry Instruments, «Gamry MultiPort Electrochemical Cell Kit, Parts». <https://orders.gamry.com/sj-28-male-to-7-ace-thread-adapter.html>
- [45] «Silver/Silver Chloride Electrode». <https://orders.gamry.com/electrodes-and-accessories/reference-electrode/silversilver-chloride-reference-electrode.html> (åpnet mai 19, 2021).
- [46] «Electrochemistry on the Bench and in the Field», *Sigma-Aldrich*.  
<https://www.sigmaaldrich.com/technical-documents/articles/technology-spotlights/electrochemistry-on-the-bench-and-in-the-field.html> (åpnet mai 19, 2021).
- [47] «GA - AGA Pro 200/300 fra Gassarmatur AS».  
[http://www.gassarmatur.no/norsk/produkter/AGA\\_Pro.php](http://www.gassarmatur.no/norsk/produkter/AGA_Pro.php) (åpnet mai 10, 2021).
- [48] «Two,Three,Four Electrode System Gamry 4-Probe Potentiostats».  
<https://www.gamry.com/application-notes/instrumentation/two-three-four-electrode-experiments/> (åpnet mai 19, 2021).
- [49] «LPR selecting», [Online]. Tilgjengelig på:  
[https://www.google.com/url?sa=i&url=http%3A%2F%2Fwww.csun.edu%2F~bavarian%2FCourses%2FMSE%2520227%2FLabs%2FGamry\\_instructions-Sept\\_2015\\_Reiner.pdf&psig=AOvVaw3VHjtq4ak-MoY8DwIU2Mm0&ust=1620811422754000&source=images&cd=vfe&ved=0CA0QjhxqFwoTCIC-kZ6nwfACFQAAAAAdAAAAABAm](https://www.google.com/url?sa=i&url=http%3A%2F%2Fwww.csun.edu%2F~bavarian%2FCourses%2FMSE%2520227%2FLabs%2FGamry_instructions-Sept_2015_Reiner.pdf&psig=AOvVaw3VHjtq4ak-MoY8DwIU2Mm0&ust=1620811422754000&source=images&cd=vfe&ved=0CA0QjhxqFwoTCIC-kZ6nwfACFQAAAAAdAAAAABAm)
- [50] «Gamry Framework Software: Basic Explanation of Overloads».  
<https://www.gamry.com/support/technical-support/getting-started-with-gamry-software/basic-explanation-of-overloads/> (åpnet mai 11, 2021).
- [51] «Reference Electrode Care Overview». <https://www.gamry.com/support/technical-support/frequently-asked-questions/reference-electrode-care-overview/> (åpnet mai 11, 2021).
- [52] «Porous Glass Frit Glass-Care of your Porous Glass Tips», *Electrochemistry Resources*, aug. 12, 2014.  
<https://electrochemistryresources.com/porous-glass-frits/> (åpnet jun. 13, 2021).
- [53] L. Sanders, X. Hu, E. Mavredaki, V. Eroini, R. Barker, og A. Neville, «Assessment of combined scale/corrosion inhibitors – A combined jar test/bubble cell», *J. Pet. Sci. Eng.*, bd. 118, s. 126–139, jun. 2014, doi: 10.1016/j.petrol.2014.04.008.

- [54] R. Sandoval-Jabalera, E. Arias-del Campo, J. G. Chacón-Nava, J. M. Malo-Tamayo, og A. Martínez-Villafane, «Corrosion Behaviour of 1018, 410 and 800 Steels in Synthetic Wastewater»; *Port. Electrochimica Acta*, bd. 24, nr. 4, s. 393–404, 2006, doi: 10.4152/pea.200604393.
- [55] Y. Zhu, M. L. Free, R. Woollam, og W. Durnie, «A review of surfactants as corrosion inhibitors and associated modeling», *Prog. Mater. Sci.*, bd. 90, s. 159–223, okt. 2017, doi: 10.1016/j.pmatsci.2017.07.006.
- [56] H. Thomson *mfl.*, «Development of New Laboratory Test Methods for Measuring Top of the Line Corrosion and Assessing Corrosion Inhibitor Performance», i *Day 2 Tue, May 10, 2016*, Aberdeen, Scotland, UK, mai 2016, s. D022S008R003. doi: 10.2118/179940-MS.
- [57] S. Laurén, «What is critical micelle concentration?» <https://www.biolinscientific.com/blog/what-is-critical-micelle-concentration> (åpnet mai 25, 2021).

## APPENDIX A – DETAILED DATA RESULTS, BLANK TESTING

The following data results was collected from blank testing performed on 3 different metal samples which is presented as Blank Sample 1, Blank Sample 2, and Blank Sample 3. Each of these metal samples had the same chemical composition, which can be seen in the certificate presented in *Appendix C – Picture A*. This was done to collect a high amount of data, since both high and low corrosion rates was observed.

### Blank Sample 1

Sequence 1					
Test number	OCP (V)	E <sub>corr</sub> (mV)	I <sub>corr</sub> (A/cm <sup>2</sup> )	R <sub>p</sub> (Ω*cm <sup>2</sup> )	Corrosion Rate (mm/year)
1	-0,6369	-639,9	1,158E-04	225	1,344
2	-0,5525	-551,2	1,142E-04	228,2	1,326
3	-0,5176	-517,3	2,038E-04	127,8	2,366
4	-0,5193	-518,4	2,363E-04	228,2	2,743
5	-0,5337	-533	1,911E-04	136,3	2,218
Sequence 2					
Test number	OCP (V)	E <sub>corr</sub> (mV)	I <sub>corr</sub> (A/cm <sup>2</sup> )	R <sub>p</sub> (Ω*cm <sup>2</sup> )	Corrosion Rate (mm/year)
1	-0,6017	-611,6	1,89E-04	137,9	2,192
2	-0,6151	-611,4	9,30E-05	280,2	1,079
3	-0,6084	-609,2	7,06E-05	369,3	0,8189
4	-0,6137	-612	4,84E-05	538,8	0,5613
5	-0,6119	-611,6	5,90E-05	442	0,6843

### Blank Sample 2

Sequence 1					
Test number	OCP (V)	E <sub>corr</sub> (mV)	I <sub>corr</sub> (A/cm <sup>2</sup> )	R <sub>p</sub> (Ω*cm <sup>2</sup> )	Corrosion Rate (mm/year)
1	-0,5928	-593,1	4,766E-05	546,7	0,5532
2	-0,6036	-601,6	4,239E-05	614,7	0,492
3	-0,6188	-606	4,559E-05	571,5	0,5292
4	-0,6157	-614,3	4,559E-05	571,5	0,4838
5	-0,6206	-622,3	4,435E-05	587,4	0,5148
Sequence 2					
Test number	OCP (V)	E <sub>corr</sub> (mV)	I <sub>corr</sub> (A/cm <sup>2</sup> )	R <sub>p</sub> (Ω*cm <sup>2</sup> )	Corrosion Rate (mm/year)

1	-0,5849	-583	5,408E-05	481,7	0,6278
2	-0,6007	-600	4,024E-05	647,4	0,4671
3	-0,6079	-607,9	3,524E-05	739,4	0,409
4	-0,6080	-606,2	5,670E-05	459,5	0,6582
5	-0,6166	-616,6	5,020E-05	519	0,5827
6	-0,6236	-623,2	7,991E-05	326	0,9276
7	-0,6326	-633,1	5,995E-05	434,6	0,6959

Blank Sample 3

Sequence 1					
Test number	OCP (V)	E <sub>corr</sub> (mV)	I <sub>corr</sub> (A/cm <sup>2</sup> )	R <sub>p</sub> (Ω*cm <sup>2</sup> )	Corrosion Rate (mm/year)
1	-0,6090	-610,2	1,145E-04	227,5	1,329
2	-0,6119	-610,4	1,200E-04	217,1	1,393
3	-0,6175	-616,6	1,473E-04	176,9	1,709
4	-0,6260	-623,9	1,148E-04	226,9	1,333
5	-0,6409	-623,9	1,471E-04	177,1	1,708
6	-0,6475	-648,5	1,371E-04	190,1	1,591

Table A-1: All the collected corrosion rate values from Blank Sample 1, 2, and 3 listed in increasing order

Test Nr.	Corrosion Rate (mm/year)
0	0
1	0,409
2	0,4671
3	0,4838
4	0,492
5	0,5148
6	0,5292
7	0,5532
8	0,5613
9	0,5827
10	0,6278
11	0,6367
12	0,6582
13	0,6843
14	0,6959
15	0,8189
16	0,9276
17	1,079
18	1,326
19	1,329
20	1,333
21	1,344
22	1,393
23	1,591

24	1,708
25	1,709
26	2,192
27	2,218
28	2,366
29	2,743

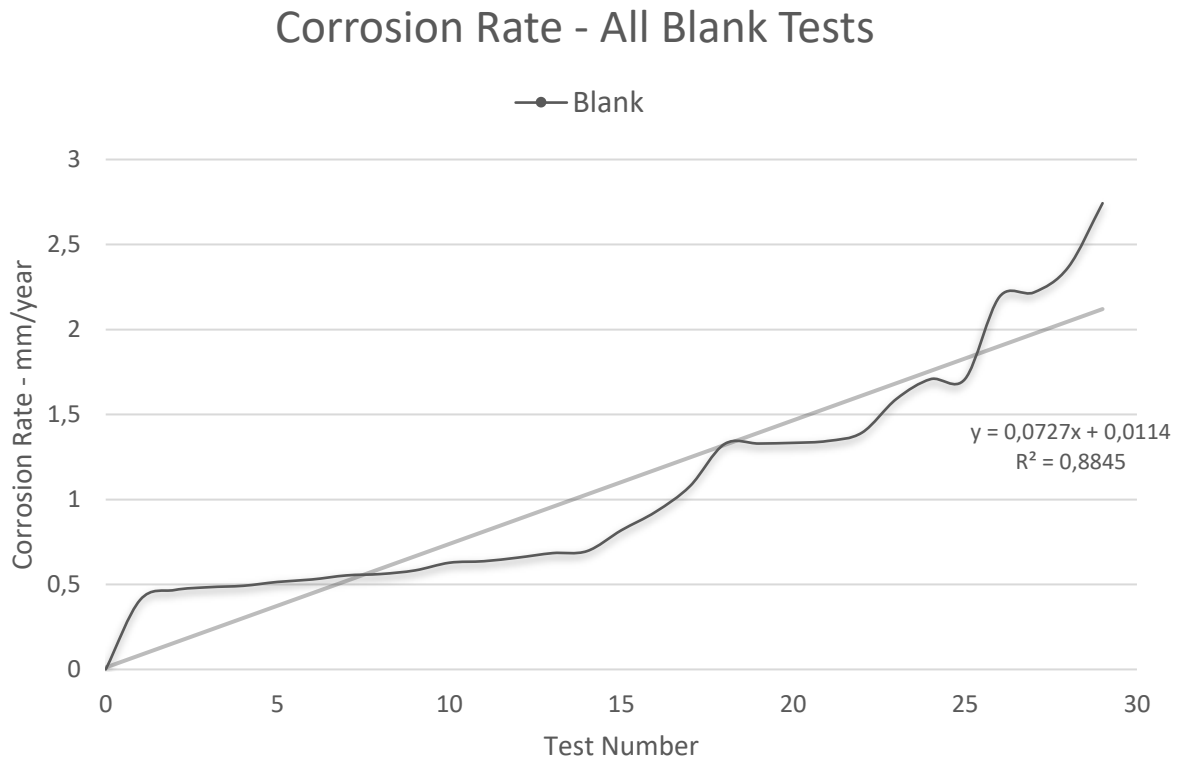


Figure A-1: Graph of estimated corrosion rate trend based on corrosion rate values in Table A.

Table A-2: The detailed LPR measurement experimental data results of the 15 highest Blank tests used when computing a Blank test baseline.

Detailed data from the selected data used in blank testing					
Test Nr.	OCP (V)	$E_{corr}$ (mV)	$I_{corr}$ (A/cm <sup>2</sup> )	$R_p$ (Ω*cm <sup>2</sup> )	Corrosion Rate (mm/year)
0	0	0	0	0	0
1	-0,608	-609,2	7,06E-05	369,3	0,819
2	-0,624	-623,2	7,991E-05	326,0	0,928
3	-0,615	-611,4	9,30E-05	280,2	1,079

4	-0,552	-551,2	1,142E-04	228,2	1,326
5	-0,609	-610,2	1,145E-04	227,5	1,329
6	-0,626	-623,9	1,148E-04	226,9	1,333
7	-0,637	-639,9	1,158E-04	225,0	1,344
8	-0,612	-610,4	1,200E-04	217,1	1,393
9	-0,648	-648,5	1,371E-04	190,1	1,591
10	-0,641	-623,9	1,471E-04	177,1	1,708
11	-0,617	-616,6	1,473E-04	176,9	1,709
12	-0,602	-611,6	1,89E-04	137,9	2,192
13	-0,534	-533	1,911E-04	136,3	2,218
14	-0,518	-517,3	2,038E-04	127,8	2,366
15	-0,519	-518,4	2,363E-04	110,2	2,743

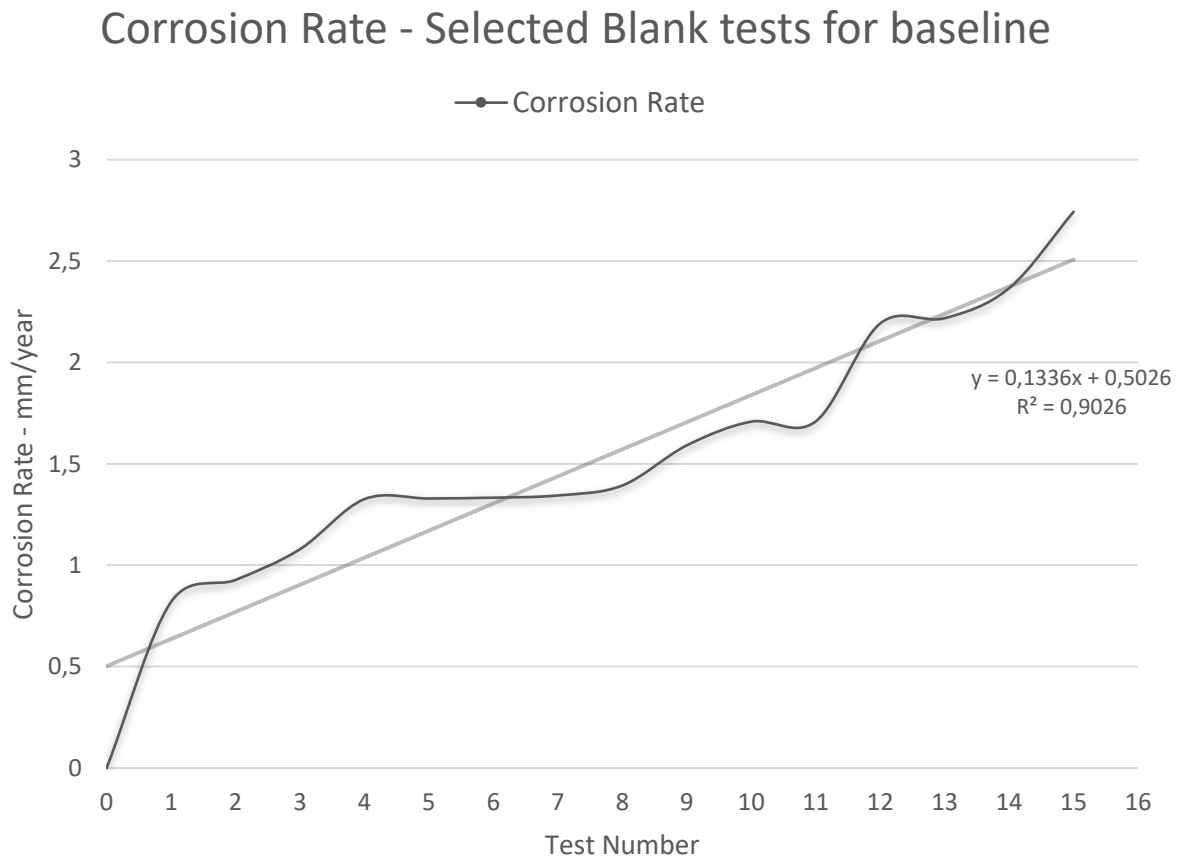


Figure A-2: Graph of estimated corrosion rate trend based on corrosion rate values in Table B.

## APPENDIX B – DETAILED DATA RESULTS, CI'S TESTING

Each of the following test sequence was performed on metal samples that was not used in blank testing. This was because some of the metal samples used during the blank testing was observed to get highly corroded which made it difficult to evaluate if the corrosion could interfere with the CI's testing data.

### Imidazoline, 500ppm

Sequence 1					
Test number	OCP (V)	E <sub>corr</sub> (mV)	I <sub>corr</sub> (A/cm <sup>2</sup> )	R <sub>p</sub> (Ω*cm <sup>2</sup> )	Corr. Rate (mm/year)
1	-0,5064	-498,6	6,94E-06	4063	0,07443
2	-0,4816	-481,4	3,88E-05	672	0,4503
3	-0,4590	-456,6	4,05E-05	642,9	0,4704
4	-0,4381	-437,9	3,41E-05	764,5	0,3956
5	-0,4342	-434,5	3,25E-05	802,4	0,3769
Sequence 2					
Test number	OCP (V)	E <sub>corr</sub> (mV)	I <sub>corr</sub> (A/cm <sup>2</sup> )	R <sub>p</sub> (Ω*cm <sup>2</sup> )	Corr. Rate (mm/year)
1	-0,5356	-529,4	4,96E-06	5554	0,05445
2	-0,5278	-526,9	1,38E-05	1889	0,1601
3	-0,5198	-520,1	3,27E-05	796,5	0,3797
4	-0,5181	-516,4	4,89E-05	533,1	0,5673
5	-0,5105	-508,8	5,36E-05	486	0,6223
Sequence 3					
Test number	OCP (V)	E <sub>corr</sub> (mV)	I <sub>corr</sub> (A/cm <sup>2</sup> )	R <sub>p</sub> (Ω*cm <sup>2</sup> )	Corr. Rate (mm/year)
1	-0,5197	-508,8	5,24E-06	4969	0,06086
2	-0,5108	-513	1,40E-05	1863	0,1624
3	-0,5290	-529,6	2,08E-05	1253	0,2414
4	-0,5401	-539,4	2,81E-05	926	0,3266
5	-0,5438	-545,2	4,36E-05	597,7	0,506

Table B-1: Corrosion Rate comparison of blank test and 500ppm Imidazoline added.

Corrosion Rate – mm/year		
Test Number	Blank	Imidazoline
0	0	0
1	0,8189	0,05445
2	0,9276	0,06086
3	1,079	0,07443
4	1,326	0,1601



5	1,329	0,1624
6	1,333	0,2414
7	1,344	0,3266
8	1,393	0,3769
9	1,591	0,3797
10	1,708	0,3956
11	1,709	0,4503
12	2,192	0,4704
13	2,218	0,506
14	2,366	0,5673
15	2,743	0,6223

### Corrosion Rate - Imidazoline

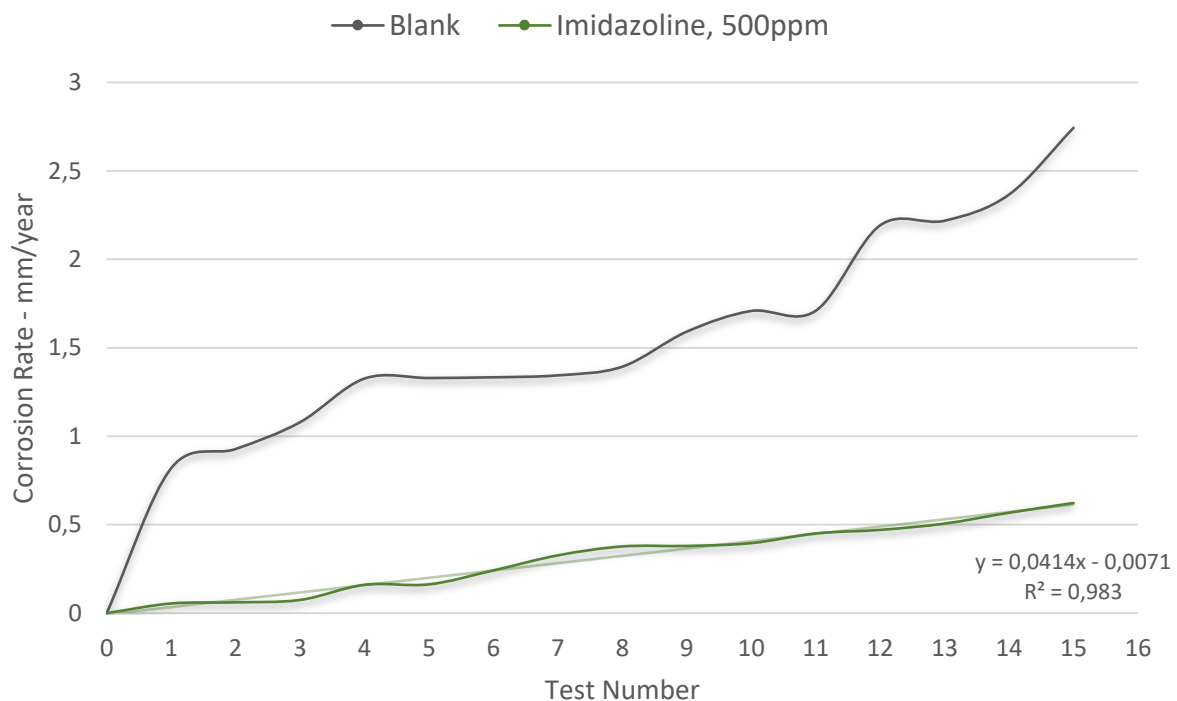


Figure B-1: Graphical illustration of the Corrosion Rate compared to blank test and 500ppm Imidazoline added.

Polymer (JP-PMA(DBAPA)NVCm-75(A)), 500ppm

**Sequence 1**

Test number	OCP (V)	E <sub>corr</sub> (mV)	I <sub>corr</sub> (A/cm <sup>2</sup> )	R <sub>p</sub> (Ω*cm <sup>2</sup> )	Corr. Rate (mm/year)
1	-0,6162	-615,1	9,34E-05	279	1,084
2	-0,6319	-632,2	8,57E-05	304	0,9947
3	-0,6250	-623,7	5,42E-05	481,1	0,6285
4	-0,6196	-622,1	5,97E-05	436,8	0,6924
5	-0,6075	-610,8	7,66E-05	340,2	0,8889
<b>Sequence 2</b>					
Test number	OCP (V)	E <sub>corr</sub> (mV)	I <sub>corr</sub> (A/cm <sup>2</sup> )	R <sub>p</sub> (Ω*cm <sup>2</sup> )	Corr. Rate (mm/year)
1	-0,5828	-579,9	2,00E-05	1300	0,2326
2	-0,5865	-586,8	3,25E-05	801,5	0,3773
3	-0,5952	-590,2	1,82E-05	1431	0,2114
4	-0,5800	-586,5	2,70E-05	965,4	0,3133
5	-0,5749	-582,7	5,59E-05	466,2	0,6487
6	-0,5860	-585,1	4,87E-05	532,3	0,5682
7	-0,5940	-596,9	5,13E-05	507,7	0,5957
8	-0,5973	-597,5	6,10E-05	426,9	0,7084
9	-0,5975	-598,7	6,90E-05	377,4	0,8012
<b>Sequence 3</b>					
Test number	OCP (V)	E <sub>corr</sub> (mV)	I <sub>corr</sub> (A/cm <sup>2</sup> )	R <sub>p</sub> (Ω*cm <sup>2</sup> )	Corr. Rate (mm/year)
1	-0,6148	-619,4	3,63E-05	717,4	0,4216
2	-0,6164	-612	3,02E-05	862,6	0,3506
3	-0,6117	-610,1	5,41E-05	481,2	0,6284
4	-0,6111	-610,4	7,47E-05	348,9	0,8868
5	-0,6078	-608,8	7,67E-05	339,9	0,8897
6	-0,6063	-606,8	8,54E-05	305,1	0,9913

Table B-2: Corrosion Rate comparison of blank test and 500ppm Polymer added.

<b>Corrosion Rate – mm/year</b>		
Test Number	Blank	Polymer
0	0	0
1	0,8189	0,2114
2	0,9276	0,2326
3	1,079	0,3133
4	1,326	0,3506
5	1,329	0,3773
6	1,333	0,4216
7	1,344	0,5682
8	1,393	0,5957
9	1,591	0,6284
10	1,708	0,6285

11	1,709	0,6487
12	2,192	0,6924
13	2,218	0,7084
14	2,366	0,8012
15	2,743	0,8868

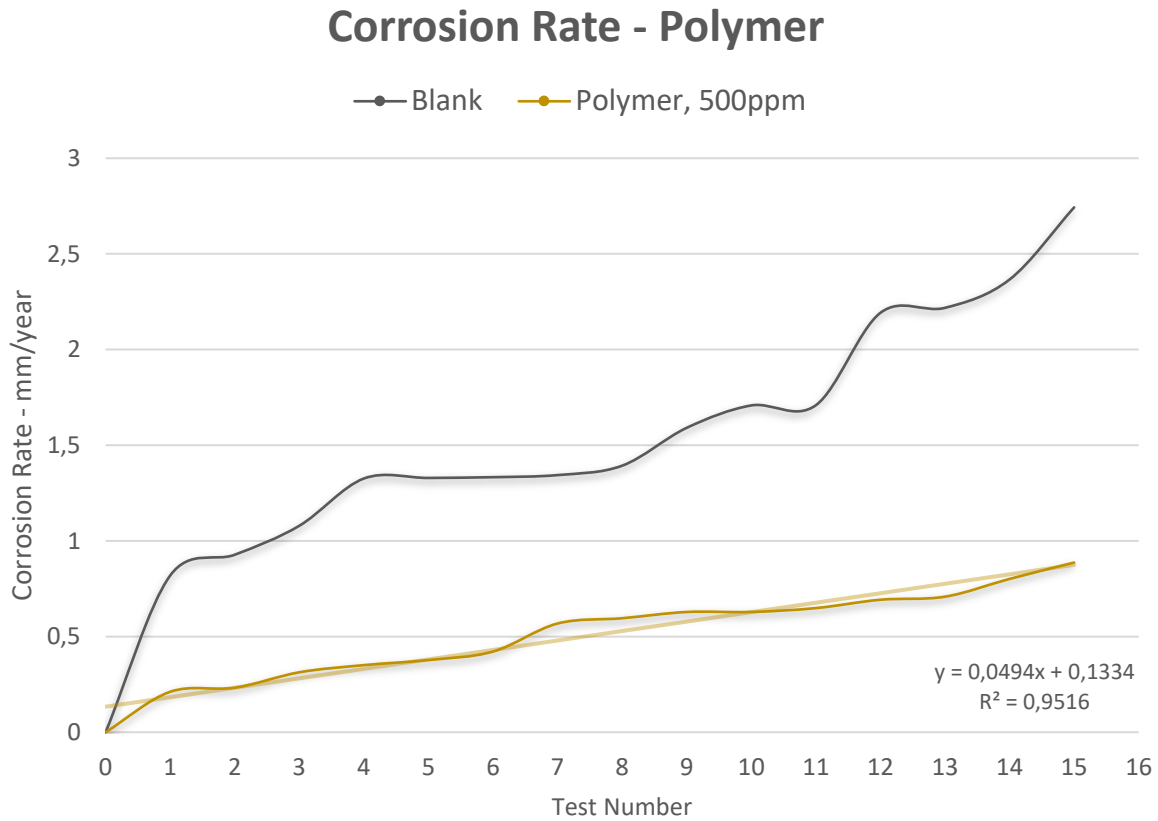


Figure B-2: Graphical illustration of the Corrosion Rate compared to blank test and 500ppm Polymer added.

Luvicap EG, 500ppm

Sequence 1					
Test number	OCP (V)	E <sub>corr</sub> (mV)	I <sub>corr</sub> (A/cm <sup>2</sup> )	R <sub>p</sub> (Ω*cm <sup>2</sup> )	Corr. Rate (mm/year)
1	-0,5865	-583,2	6,48E-05	402,3	0,7517
2	-0,5855	-582,5	6,16E-05	422,8	0,7154
3	-0,5922	-590,2	7,42E-05	351,2	0,8611
4	-0,6025	-602,6	7,62E-05	341,7	0,885
5	-0,5848	-587,6	6,71E-05	388,2	0,779

6	-0,5675	-566,4	1,00E-04	259,5	1,165
7	-0,5606	-561,2	1,05E-04	249	1,215
8	-0,5450	-542,9	9,32E-05	279,6	1,082
<b>Sequence 2</b>					
Test number	OCP (V)	E <sub>corr</sub> (mV)	I <sub>corr</sub> (A/cm <sup>2</sup> )	R <sub>p</sub> (Ω*cm <sup>2</sup> )	Corr. Rate (mm/year)
1	-0,5727	-572	2,42E-05	1077	0,2809
2	-0,5713	-568,7	4,96E-05	525,1	0,5759
3	-0,5729	-573,5	6,96E-05	374,4	0,8078
4	-0,5809	-577,8	8,17E-05	318,7	0,9488
5	-0,5862	-585,4	1,04E-04	250,4	1,208
6	-0,5896	-590,7	1,17E-04	223,5	1,353
7	-0,5974	-596,3	1,17E-04	222,5	1,359

Table B-3: Corrosion Rate comparison of blank test and 500ppm Luvicap EG added.

Corrosion Rate – mm/year		
Test Number	Blank	Luvicap EG
0	0	0
1	0,8189	0,2809
2	0,9276	0,5759
3	1,079	0,7154
4	1,326	0,7517
5	1,329	0,779
6	1,333	0,8078
7	1,344	0,8611
8	1,393	0,885
9	1,591	0,9488
10	1,708	1,082
11	1,709	1,165
12	2,192	1,208
13	2,218	1,215
14	2,366	1,353
15	2,743	1,359

## Corrosion Rate - Luvicap EG

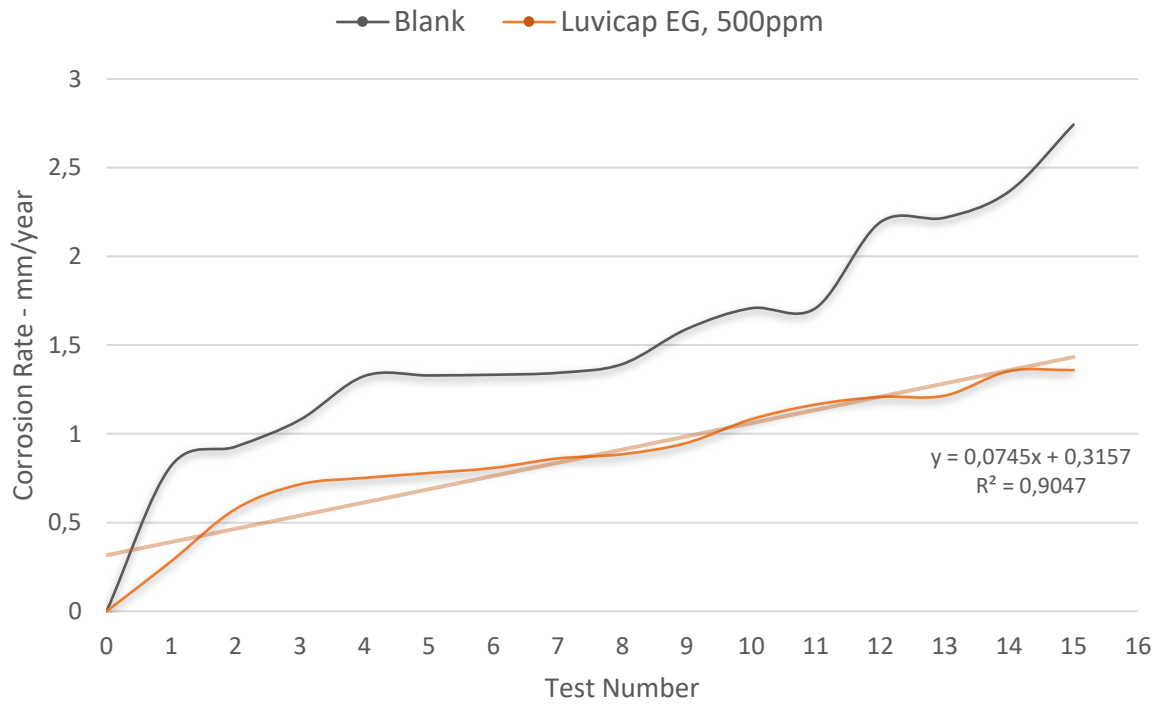


Figure B-3: Graphical illustration of the Corrosion Rate compared to blank test and 500ppm Polymer added.

# APPENDIX C – ADDITIONAL PICTURES

Additional pictures that either illustrates or contains information can be found in the given Appendix.

## **European Corrosion Supplies**

10 Meadowmill Estate  
Kidderminster  
Worcs DY10 1HH  
United Kingdom  
Tel: +44 1562 549200  
e-mail: eurocorrosion@btconnect.com



Customer:	Universitetet i Stavanger
Order No:	312100217
Part No:	
Description:	CYLINDER, PATTERN 3-48
Material:	C1018
Serial Nos:	n/a

## CERTIFICATE OF COMPLIANCE DIN 50049 3.1B

European Corrosion IMT No: B180  
Material: C1018 BAR ACENTA  
Specification: AISI / SAE 1018  
G10180  
Manufacturer: Acenta Steel  
Manufacturer's Trade Name: n/a  
Manufacturer's Cast No: 150800

### Chemical Composition (%):

Ag:	H:	Pb:
Al:	Mg:	S: 0.025
As:	Mn: 0.78	Sb:
C: 0.18	Mo:	Si: 0.20
Co:	N:	Sn:
Cr:	Nb:	Ti:
Cu:	Ni:	W:
Fe:	P: 0.025	Zn:
Other:		

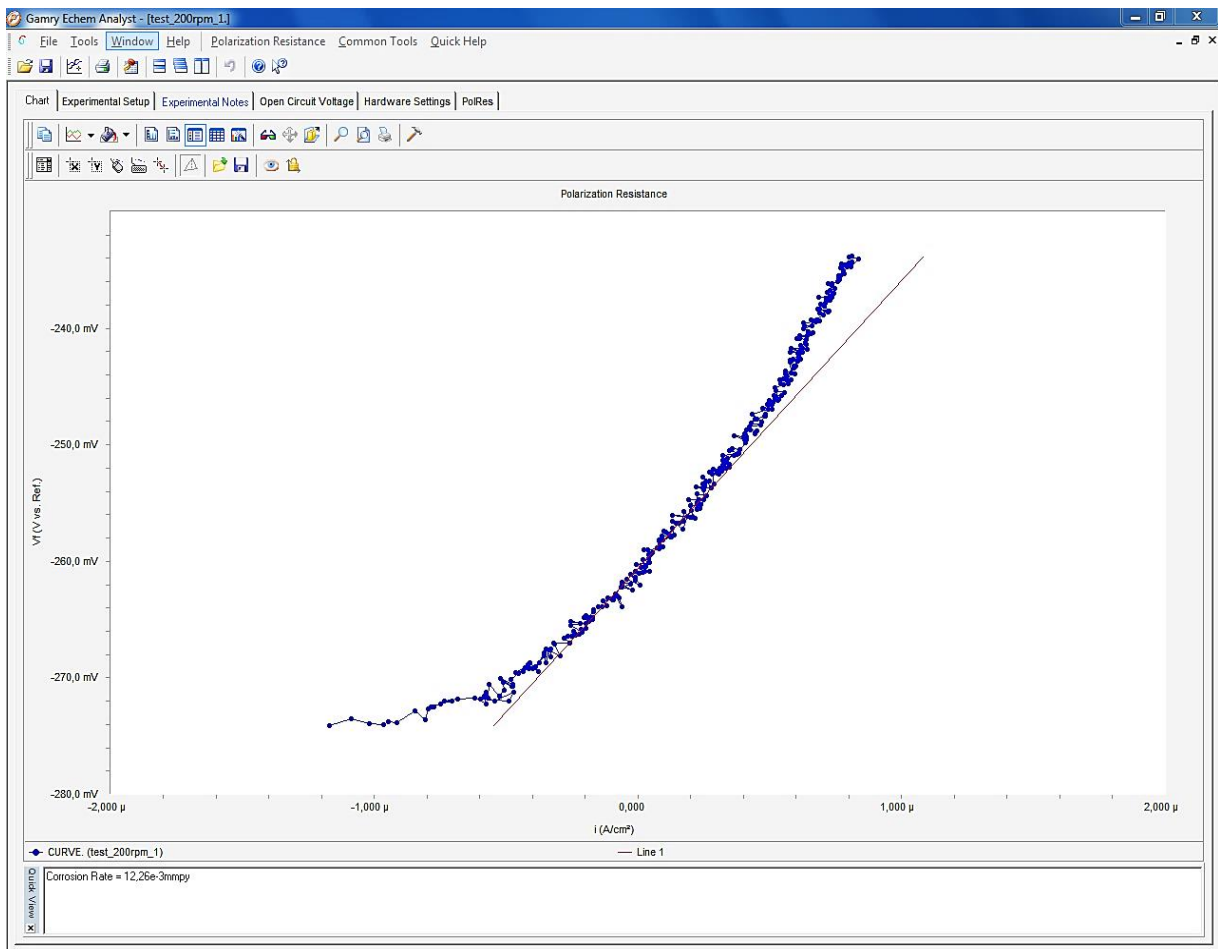
### Mechanical Properties

### Remarks:

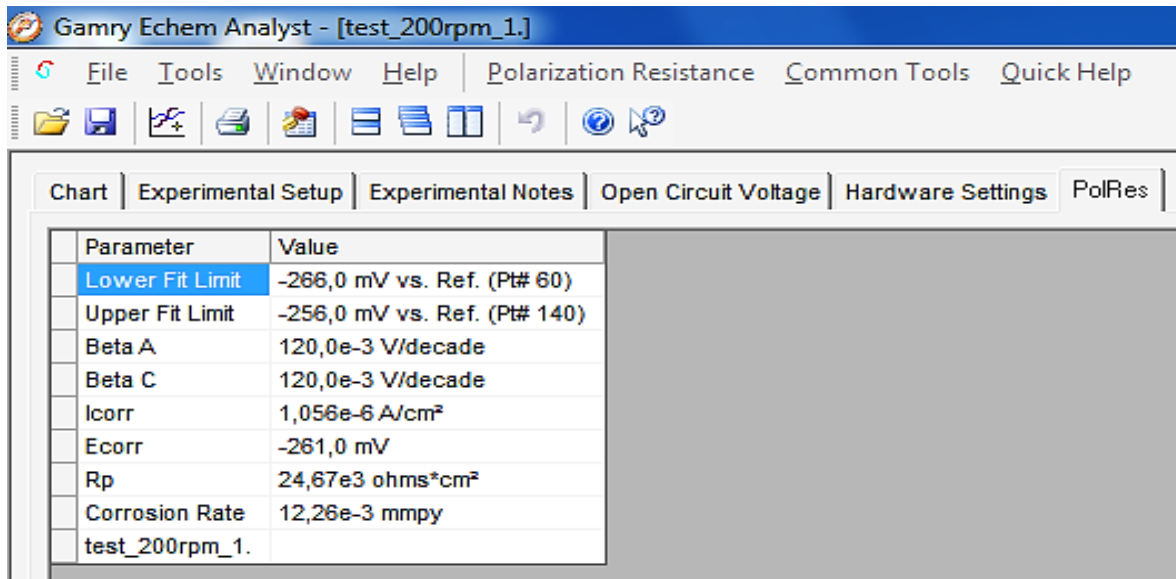
We hereby certify that specimens supplied are manufactured from the above material. The details are correct to the best of our knowledge and belief.

19-MAR-2021

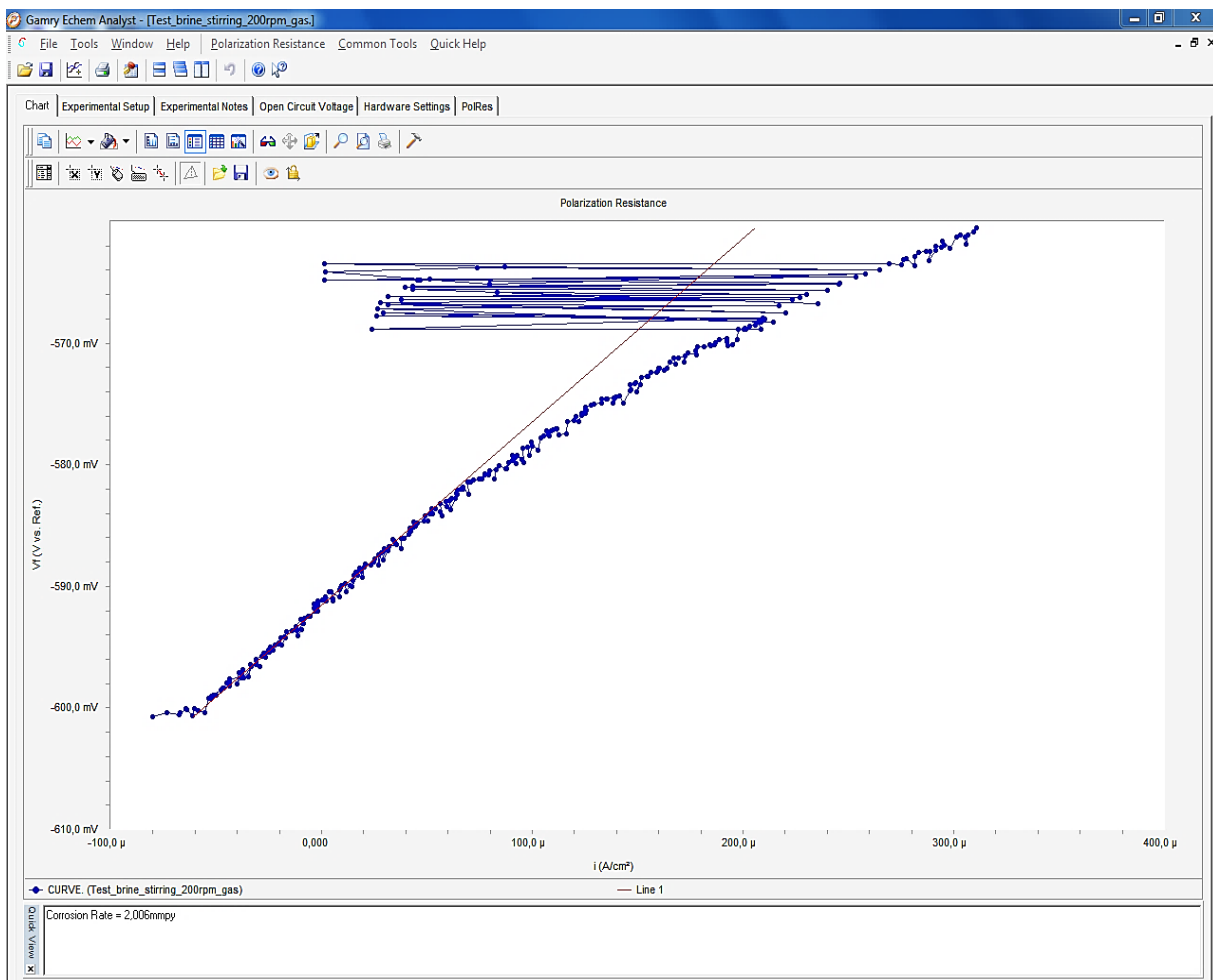
*Picture A: The certificate of the Metal Samples used for corrosion testing, which followed with the packaging.*



*Picture B-1: A screenshot of how the resulting LPR measurement data plot was presented when a leakage was detected at the laboratory. Note the steep slope and low corrosion rate.*

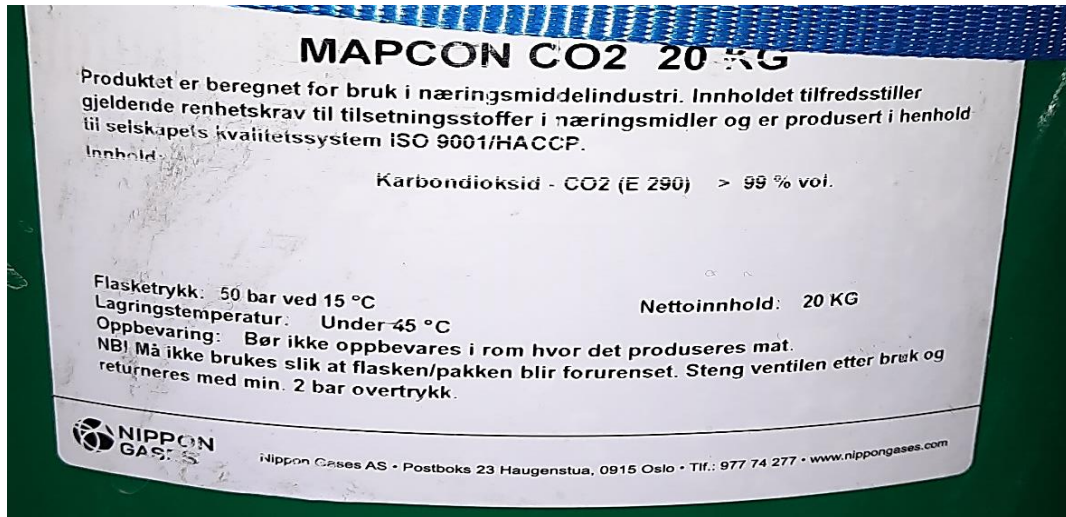


Picture B-2: A screenshot of how the numerically resulting data presented itself when a leakage was detected at the laboratory.

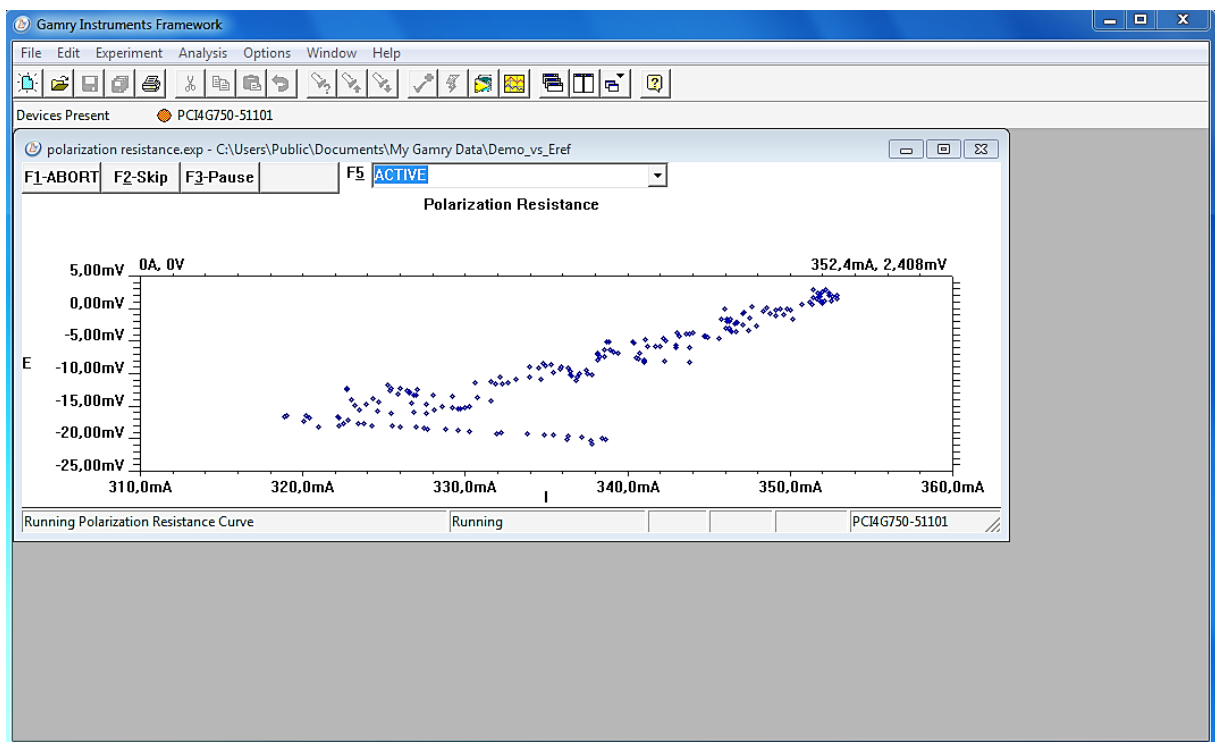




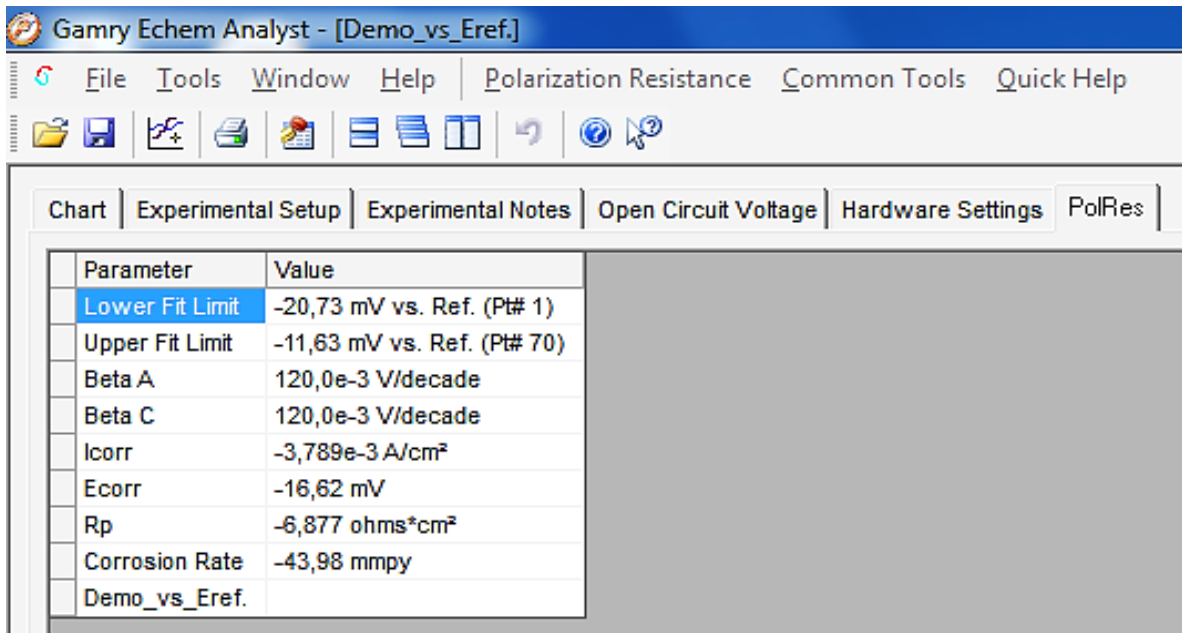
Picture C: A screenshot of how the resulting data plot was presented when overloads occurred in a LPR measurement, performed at the UiS laboratory. Note the abnormal data sampling at the end of the plot.



Picture D: Specifications of the  $\text{CO}_2$  gas used in this thesis.



Picture E-1: How the LPR measurement plot looks like when “vs.  $E_{ref}$ ” is selected as a reference point.



Parameter	Value
Lower Fit Limit	-20,73 mV vs. Ref. (Pt# 1)
Upper Fit Limit	-11,63 mV vs. Ref. (Pt# 70)
Beta A	120,0e-3 V/decade
Beta C	120,0e-3 V/decade
Icorr	-3,789e-3 A/cm <sup>2</sup>
Ecorr	-16,62 mV
Rp	-6,877 ohms*cm <sup>2</sup>
Corrosion Rate	-43,98 mmpy
Demo_vs_Eref.	

Picture E-2: How the LPR measurement data result looks like when “vs.  $E_{ref}$ ” is selected as a reference point.